Higher-Order Chemical Sensing

ARTICLE *in* CHEMICAL REVIEWS · MARCH 2008

Impact Factor: 46.57 · DOI: 10.1021/cr068116m · Source: PubMed

2 AUTHORS:

Andreas Hierlemann
ETH Zurich
288 PUBLICATIONS **4,779** CITATIONS
SEE PROFILE

Ricardo Gutierrez-Osuna
Texas A&M University
132 PUBLICATIONS **2,162** CITATIONS
SEE PROFILE

Higher-Order Chemical Sensing

Andreas Hierlemann*

ETH Zürich, Laboratory of Physical Electronics, Wolfgang-Pauli-Strasse 16, 8093 Zürich, Switzerland

Ricardo Gutierrez-Osuna

Texas A&M University, Department of Computer Science, College Station, Texas 77843-3112

Received April 3, 2007

Contents

* To whom correspondence should be addressed. Voice: +41 44 633 3494. Fax: +41 44 633 1054. E-mail: hierlema@phys.ethz.ch.

1. Introduction

Desired properties of a chemical sensor include high sensitivity, a large dynamic range, high selectivity or specificity to a target analyte, related low cross-sensitivity to interferents, perfect reversibility of the physicochemical detection or sensing process (short sensor recovery and response times), and long-term stability of the sensor and sensing material.[1−9] Unfortunately, a sensor exhibiting all these properties is a largely unrealizable ideal. Sensor sensitivity, selectivity, speed of response, and reversibility are determined by the thermodynamics and kinetics of sensor material/analyte interactions. In particular, high sensitivity and specificity on the one hand and perfect reversibility on the other hand impose contradictory constraints on the sensor design: high sensitivity and selectivity are typically associated with strong interactions, whereas perfect reversibility requires weak interactions. Consequently, it is necessary to compromise, and, in most cases, sensors showing partial selectivity to only some of the detected species are used to ensure reversibility. The output of an individual sensor consists of, e.g., a certain current value measured at a fixed potential or a resistance value of a certain material in response to a chemical stimulus.[1−9] This means that, usually, one feature per sensor is monitored at a time, preferably

10.1021/cr068116m CCC: $71.00
Published on Web 01/17/2008

Andreas Hierlemann received his diploma in chemistry in 1992 and the Ph.D. degree in physical chemistry in 1996 from the University of Tübingen, Germany. After working as a Postdoc at Texas A&M University, College Station, TX (1997), and Sandia National Laboratories, Albuquerque, NM (1998), he is currently associate professor at the Physical Electronics Laboratory at ETH Zurich in Switzerland. The focus of his research activities is on CMOS-based microsensors and interfacing CMOS electronics with electrogenic cells.

Ricardo Gutierrez-Osuna received a B.S. degree in Electrical Engineering from the Polytechnic University of Madrid, Spain, in 1992, and M.S. and Ph.D. degrees in Computer Engineering from North Carolina State University in 1995 and 1998, respectively. From 1998 to 2002, he served on the faculty at Wright State University. He is currently an associate professor of Computer Engineering at Texas A&M University. Dr. Gutierrez-Osuna is a recipient of the National Science Foundation Career Award for his research on machine olfaction with chemical sensors arrays. His research interests include pattern recognition, neuromorphic computation, chemical sensor arrays, and machine perception.

during an equilibrium-type or steady-state-type situation, in which a certain analyte concentration can unequivocally be correlated to the resulting sensor response. Individual sensors and the analysis of the respective individual signals or features, however, show limited selectivity performance in most practical applications, as mentioned above. Therefore, arrays of several sensors are commonly used, which effectively extends the "feature space". A feature space is an abstract space in which each sample (e.g., sensor measurement value) is represented as a point in *n*-dimensional space, whose dimension is determined by the number of features evaluated. Features are the individual measurable heuristic properties of the phenomena being observed, in our case, e.g., sensor measurement values. The acquired information is then processed using pattern recognition and multicomponent analysis tools.[10−12] Increasing the measurement or feature space dimensionality is an attractive approach to obtain a substantial improvement in analytical capabilities,[13,14] provided that the additional dimensions carry complementary information and provided that suitable data-analysis techniques are used, i.e., techniques to handle small numbers of samples.

The notion of "order" has been frequently used in instrumental analysis to categorize the dimensionality of the feature space and, consequently, the richness of the information obtained by a certain device or analytical instrument[15,16] and can, within certain limitations, also be applied to sensor or sensor array configurations.[17]

A zero-order device or sensor would be a single, more-or-less specific sensor. This sensor would be aimed at the detection of a certain target compound. However, it would not be possible to perform any reliable analyte quantification in the presence of interferents. Even worse, there would not be any evidence to let the operator know that the measurement had been influenced by interferents.

A first-order device is then a sensor array, the sensors of which differ in one domain, i.e., an array of identical transducers such as chemoresistors featuring different sensitive materials or layers or an array of chemoresistors featuring the same sensitive material but operated at different temperatures—provided that temperature has a distinct effect on the sensor selectivity. This is the case for, e.g., high-temperature metal-oxide-based sensors.[18−22] A prerequisite for the successful use of such first-order devices is the establishment of a calibration model that includes the signals of the species of interest and of all possible interferents. Then, multicomponent analysis and outlier detection will be possible, but any unexpected interferent will invariably upset the respective predictions. In other words, the calibration of a first-order array allows interferences to be detected but not to be compensated for.

This problem can be addressed by using second-order or higher-order sensor devices. These devices utilize analyte characteristics in at least two domains, which should be ideally orthogonal, or, inasmuch as possible, independent from each other (see section 6.2 for a definition of these terms). Under certain conditions, the calibration of second-order instruments allows the target analytes to be quantified even in the presence of unknown interferents; this property is commonly referred to as the "second-order advantage".[23] Additional potential benefits of second-order devices include the ability to perform calibration with a single mixture sample and recover the response profiles of the individual target analytes.[24]

Higher-order sensor devices can, according to a paper published by Göpel,[25] be generated by making use of various features to be exploited in chemical sensing. Though the estimated overall number of features may be overly optimistic (Figure 1), in particular with regard to "independent features", it may be interesting to briefly summarize the findings of this paper. The number of sensitive materials to convert a chemical into, e.g., electrical information is estimated to be on the order of 10^8, the number of suitable transducers (e.g., chemoresistor, microbalance, optical fiber, etc.) is estimated to be $\sim 10^1$, the number of transducer geometries (e.g., electrode distance, shape, etc.) is estimated to be on the order of 10^2, and the features that can be added through variation of modulation of external (e.g., gas switching strategies, use of filters, catalysts, etc.) and internal parameters (e.g., light frequency, operation temperature, bias voltage, etc.) is estimated to be on the order of 10^2. The distinctive way to modulate these parameters (e.g., stepwise, sinusoidal, ramp, etc.) is assumed to account for an additional

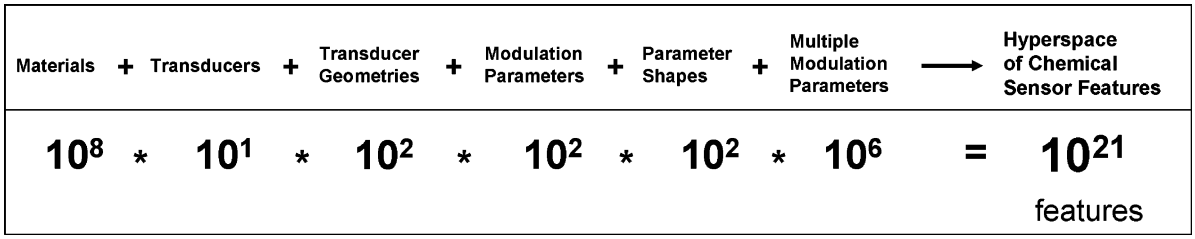

Figure 1. "Hyperspace" of chemical sensor features with more than 10^{21} independent features according to Göpel. Redrawn with persmission from ref 25. Copyright 1998 Elsevier.

10^2 features, and, finally, multiple modulations that can be performed simultaneously (e.g., simultaneous variation of bias voltage, temperature, and gas flow) are assumed to account for another 10^6 features. While the above considerations are of hypothetical nature, and the number of viable parameters and realizable variations will be massively lower, the exercise shows that a large variety of parameters is available that can be used to identify or quantify a specific analyte or complex mixture.

Higher-order (i.e., "hyphenated") instrumentation, such as the combination of gas chromatography (GC) and mass spectrometry (MS), is vastly used in modern laboratory analytical chemistry. Although the data-analysis methods applied to sensor and analytic-instrument data are mostly the same, there is no direct analogy between the preprocessing of a sample to separate it into multiple, less complex samples that are then characterized by an analytical method and the attempts to enhance the selectivity of a set of sensors by modulation of physical parameters. Yet, it is striking that higher-order methods are still uncommon in the field of chemical sensors. This holds particularly true, since the higher-order advantage may be important due to unpredictable changes in the sample matrix composition. This situation is arguably a consequence of the requirements for sensors or sensor systems, which include low costs, small physical size, and ease of use. The progress in micro- and nanotechnology, microelectronics, and in data-processing speed and capability will help to address many, if not all, of these issues:[26−30] rather complex and versatile microsensor and microanalysis systems operable directly through standard interfaces from a laptop or palmtop by means of standard software are already available, as will be also demonstrated in this article.

1.1. Integrated versus Discrete Sensor Arrays

In this context, we want to address the advantages and disadvantages of integrated or even monolithic multisensor arrays or systems versus the use of sets of discrete sensors and electronics, particularly, since both types of sensor arrays or systems will appear in the following sections. There is a number of aspects that have to be taken into account, which will be briefly discussed here.[31]

1.1.1. Materials and Fabrication Processes

For monolithic designs or integrated systems, the selection of materials is restricted to a few, e.g., CMOS-technology-related materials and CMOS-process-compatible materials, as well as to a set of specific fabrication steps[32] (CMOS technology, complementary-metal-oxide-semiconductor technology, is an industrial standard fabrication technology for integrated circuits on silicon microchips). High-temperature steps (e.g., >400 °C) can be detrimental to metallizations (metal oxidation, diffusion) and may alter semiconductor characteristics. For hybrid or discrete devices, any material, or the optimum sensor material, can be used, and a wealth of fabrication techniques is available.

1.1.2. Performance

Microsensors frequently also generate "microsignals", and perform pronouncedly better in monolithic designs owing to the fact that the signals can be conditioned at the site of generation (filters, amplifiers, etc.), e.g., by means of on-chip electronics, so that the influence of parasitic and crosstalk effects can be reduced.[33,34] On-chip analog-to-digital conversion is another feature that helps to generate a stable sensor output that can be easily transferred to off-chip units. For hybrid or discrete microsensors, it is sometimes very difficult to read out rather minute analog sensor signals.

1.1.3. Auxiliary Sensors/Smart Features

Temperature or flow sensors can be monolithically co-integrated with the chemical sensors on the same chip. Calibration, control, and signal processing functions as well as self-test features can be realized on-chip. For hybrid designs, additional devices and off-chip components are required.

1.1.4. Connectivity

The number of electrical connections prominently contributes to the overall system costs (failure probability and packaging costs). The monolithic implementation of, e.g., an array of gas sensors (see also later in this article) with multiplexer structures and interface units requires only a few connections.[33,34] A hybrid/discrete approach will require many more connections, since each sensor has to be individually addressed and since there are no interface units available on the sensor side.

1.1.5. Sensor Response Time

The response time of, e.g., a gas sensor array is, in most cases, determined by the volume of the measurement chamber and the flow rate (other relevant processes include also analyte diffusion or dissociation). Using the monolithic or integrated approach and a suitable packaging technique, such as flip-chip packaging, the volume of the measurement chamber can be kept very small as a consequence of a small-size, flat and planar sensor or sensor array. Therefore, parameter modulation, such as flow variations or dynamic protocols, can be easily realized. For hybrid or discrete arrays, the volume is dependent on sensor geometries and array arrangements.

1.1.6. Package

To package monolithic designs, microelectronics-derived packaging techniques can be modified and adapted, such as

flip-chip technology or simple epoxy-based packaging methods. Hybrid implementations require complex packages to reduce sensor interference (e.g., high-frequency acoustic-wave sensors), to minimize electric crosstalk, and to optimize the critical connections. This further complicates the already difficult task of chemical sensor packaging.

1.1.7. Summary

The main disadvantages of integrated or monolithic arrays or systems include the restriction in materials and the limited choice of fabrication processes and steps. On the other hand, integrated systems offer unprecedented advantages over hybrid or discrete arrays, especially with regard to signal quality, device performance, increased functionality, and available packaging solutions.[35] These advantages, in our opinion, clearly outweigh the drawbacks and limitations.[31] In the case of well-established physical sensors, such as acceleration and pressure sensors, a trend toward integrated monolithic solutions can be identified for large production volumes and severe cost restrictions.

1.2. Outline

The topic of this review is "higher-order devices", i.e., neither single sensors nor homogeneous transducer arrays featuring only different coatings will be treated any further. The latter constitute, according to the text in the introduction above, a first-order system, since analyte exposure generates a one-dimensional data vector (row or column). In some publications, an array of sensors with different coatings is referred to as a zero-order array,[9] with an array being itself a first-order device. We here prefer to use a categorization according to the data output format (0th order, single value; first order, vector; second order, matrix; third order, tensor; etc.).

We decided to apply a rather broad scope in this review in order to give the reader a comprehensive overview on strategies to increase the information that can be extracted from sensor systems or arrays. In section 2, devices consisting of arrays of identical transducers (with different coatings) will be described, for which an extension to a higher order has been realized by adding additional dimensions such as time (sensor dynamics and transients) or by varying internal and external operation parameters such as temperature modulation or the use of a catalyst for analyte decomposition. In this section, it will also be shown how different information, e.g., in the physical and chemical domains, can be extracted from an array of identical transducers. Section 3 focuses on different monolithic and discrete sensor arrays making use of more than one transduction principle. In section 4, we will briefly describe practical measurement and setup considerations for using multitransducer sensor arrays and for recording transients or applying parameter variations. Section 5 includes sensor-based complex microanalytical systems, consisting of preconcentration, separation, and detection stages. In section 6, we will discuss the relations between dimensionality, information, cross-selectivity, and redundancy, concepts that are important when dealing with higher-order sensor systems. Section 7 presents a review of two important data preprocessing procedures for chemosensors: baseline correction and scaling. Section 8 will be dedicated to methods for drift compensation. In section 9, we will review computational methods to extract information from transient and temperature-modulated responses of chemosensors. Section 10 is dedicated to multivariate calibration for higher-order sensing, with an emphasis on multiway and dynamical models. Section 11 will include methods to optimize arrays for specific applications, including sensor selection, feature selection, and optimization of temperature programs. This article will be concluded by a short summary and outlook.

Before embarking upon the subject of multisensor arrays, there is a last note on terminology. The term "electronic nose" has been very popular for more than a decade to describe multisensor and multitransducer arrays.[6,36,37] We believe, however, that this term can be very misleading for several reasons. Following a definition of Gardner and Bartlett, an "electronic nose" is "an instrument comprising an array of electronic chemical sensors with partial specificity and an appropriate pattern recognition system, capable of recognizing simple or complex odors".[6,36,37] The majority of such "electronic noses" may be capable of differentiating between analytes or analyte mixtures from the headspace of different foods or beverages, but, in most cases, the sensor response patterns cannot be directly correlated with human olfactory perception. Another more important point concerns the general applicability implied by the term "electronic nose". Most of the sensor systems perform well in certain key applications, but there are few systems, if any, that exhibit the enormously broad applicability spectrum, at once including the sensitivity and discriminating power of a human or animal nose. In addition, successful sensor systems have to be designed and optimized with the key application in mind to guide the selection of coatings, transduction mechanisms, etc. As yet, however, there is no universally applicable system that invariably provides satisfactory performance under all circumstances. Therefore, we will use this term sparingly and only in quotation marks. Similar considerations apply to "electronic tongues", ion-sensitive or lipid-film based sensors in liquid phase. An article on "electronic noses" by Weimar[38] is included in this issue.

2. Arrays and Systems Comprising Identical Transducers

In this section, we will treat arrays of identical transducers with, e.g., different coatings, for which an extension to a higher order has been realized by adding additional dimensions in the feature space. These additional dimensions may include time (sensor dynamics and transients), or the variation of internal and external sensor operation parameters (temperature variation, use of a catalyst for analyte decomposition). It will also be shown how information in the physical and chemical domains can be extracted from microarrays and microsystems. A short glance at differential or ratiometric methods concludes this section.

2.1. Parameter Variations

Following Göpel and Weimar,[25,39] the parameters that can be varied during sensor operation include internal parameters, such as sensor temperature, electrode bias voltage, or measurement frequencies, and external parameters, such as the use of filters or catalysts to change the gas composition.

In looking at the literature, it is evident that one type of *internal* variation, the sensor operation temperature variation, is very popular in particular for conductometric metal-oxide-based sensors.[40] This development has been fueled by the appearance of microhotplates with low thermal mass,[41] which allow for millisecond-scale temperature variations, so that

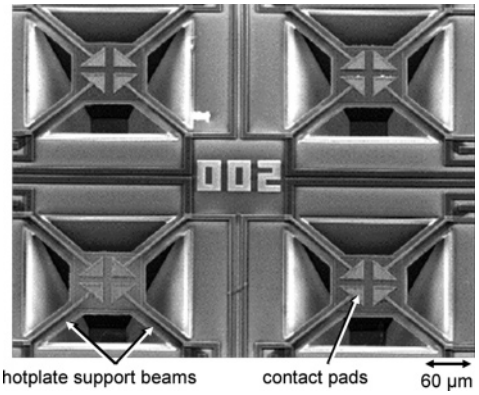

Figure 2. Scanning-electron micrograph of microhotplates. The suspended plates exhibit a polysilicon heater, an aluminum plane for homogeneous heat distribution, and electrodes for measuring the resistance of a semiconductor metal oxide. Reprinted with permission from ref 51. Copyright 1998 American Chemical Society.

the temperature variations are faster or on the same time scale as the chemical processes occurring during gas/metal-oxide interaction. This enables effective gas discrimination via the use of analyte-specific dedicated temperature profiles. More details on temperature-modulation strategies can be found in section 9.2 of this article, as well as in the articles by Benkstein and Semancik[42] and Nakamoto[43] in this issue.

A variety of hotplate structures has been used including membranes,[18,41,44−47] spiderlike structures[48−51] (see Figure 2), and bridgelike structures.[52] The most recent developments in temperature-variable microhotplates include standalone CMOS-based microsystems featuring temperature-control loops, transistor heaters, digital circuitry, and standard interfaces, which allow for the application of any arbitrary temperature profile to three differently coated hotplates via standard software and a USB interface.[53,54]

Besides microhotplate-based systems, there have been also static approaches to temperature variation using 38 metal-oxide sensor elements (the array features a noble metal doping gradient) on a 4×8 mm^2 bulk silicon substrate equipped with 4 meander heaters, which create temperature gradients between 3 and 7 °C per mm in the array area, producing a temperature difference of 50 °C over the array.[55−57] This system consumes up to 6 W at operation temperatures between 300 and 400 °C, which is 3−4 times the power consumption of microhotplate-based systems per detection spot or sensor.

The gas reactions at the metal-oxide surfaces and, hence, the sensor selectivity or sensitivity patterns, are highly depending on the operation temperature:[1,58−66] carbon monoxide is usually detected at lower operation temperatures using a tin-oxide-based sensitive layer, whereas higher temperatures are used for monitoring, e.g., methane. The variation of the operation temperature of a single sensor or a small set of sensors can lead to a degree of selectivity that would otherwise require arrays of fixed-temperature sensors and, thus, effectively extends the feature space of single sensors or small arrays.

With regard to static, fixed-temperature sensors, the fast temperature variation of microhotplates, which generates a large set of "virtual" sensors, is clearly preferable due to the almost infinite number of possible and target-analyte-specific temperature-variation profiles (sinusoidal, ramp, rectangular); the arbitrarily selectable temperature interval, within which the variations can be realized; and the massively lower instrumental complexity and overall power consumption.

A temperature-modulation example is shown in Figure 3,[47] which shows a sinusoidal modulation of the operation temperature of a single tin-oxide sensor between 200 and 400 °C that produces characteristic frequency-dependent resistance features. Resistance changes of the micromachined sensor upon exposure to CO, NO_2, and a mixture of CO and NO_2 in synthetic air at 50% relative humidity are displayed. By applying this temperature-modulation profile and by using fast Fourier transformation techniques for feature extraction and data evaluation, a single sensor could be used to qualitatively and quantitatively analyze a binary mixture.[47] The authors ascribe the possibility to differentiate between the two gases, CO and NO_2, to the different reaction kinetics of the two gases at the sensor surface and, in particular, to the presence of oxygen species at the surface at low temperature as a consequence of the fast temperature modulation. These surface oxygen species would not exist on the surface under equilibrium conditions at the lower temperatures in the cycling range (200 °C).[47]

Additionally, an example for *external* parameter variation will be given, which includes the use of a catalyst located upstream of the sensor array in the analyte gas inlet.[67−69] The noble metal catalyst is heated to different temperatures and decomposes (oxidizes) the incoming analyte molecules or promotes chemical reactions of those. The resulting reaction products are then detected by an array of, e.g., electrochemical sensors.[67−69] By varying the catalyst temperature, the sensor responses can be modified, and operation regimes can be optimized for the detection of specific target compounds. The catalysts included, e.g., rhodium or platinum filaments.[67−69] A test analyte pattern for 8 different electrochemical sensors (4 CO sensors, 2 hydrogen sulfide sensors, 1 sulfur dioxide sensor, and 1 nitrogen monoxide sensor) and 7 different catalyst temperature steps is shown in Figure 4.[67] The sensor-response patterns vary according to temperature and sensor type upon exposure to the 19 analytes. Again, the use of the catalyst generates virtual sensors and efficiently extends the feature space.

2.2. Dynamic Methods and Transient Signals

The sensor-signal evolution over time can be used to extend the feature space of a sensor array. The information content that can be extracted from a transient signal $f(t)$ is considerably higher than that from a steady-state signal f; whereas the steady-state signal is given by a single number f, the transient signal $f(t)$ provides a series of measurement values at discrete time intervals t. More detailed information on transient analysis can be found in section 9 of this article and also in the article by Nakamoto[43] in this review issue. An example of transient signals is displayed in Figure 5, which shows how the creation of exposure steps and transients of varying length can help to discriminate between methanol and ethanol using a polymer-coated capacitive device.[70]

It is noteworthy that the recording of transient signals stringently requires a dedicated gas manifold[70,71] (permanent gas flows, crossover valves, small dead volumes between valves and measurement chamber, and small-volume chamber; for more information, see section 4.1 of this article), so that the recorded dynamics represent the real sensor dynamics and not those of the manifold or of the gas exchange in the measurement chamber. The time required for a full exchange

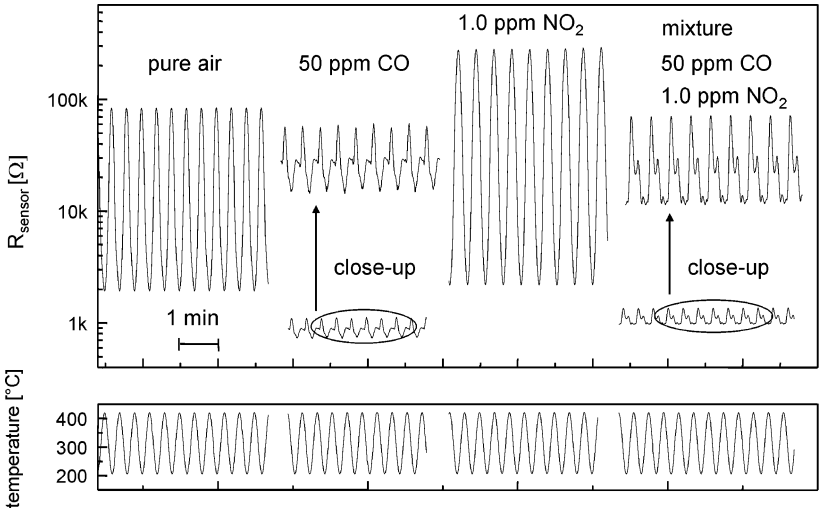

Figure 3. Sinusoidal modulation of the operation temperature of a tin oxide sensor between 200 and 400 °C (bottom) leads to characteristic frequency-dependent resistance features (upper part). Changes of the resistance (R sensor) of the micromachined sensor upon exposure to 50 ppm CO, 1 ppm NO_2, and a mixture of 50 ppm CO and 1 ppm NO_2 in synthetic air (50% relative humidity). Reprinted with permission from ref 47. Copyright 1997 Elsevier.

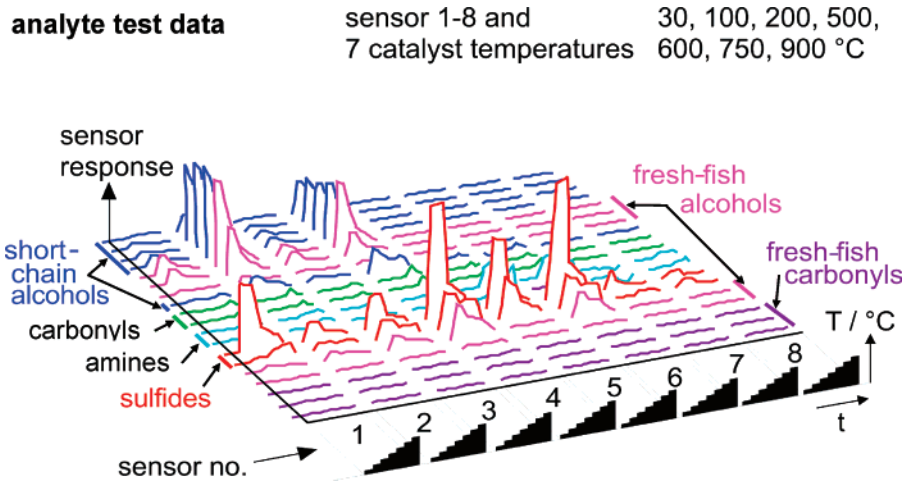

Figure 4. Analyte test data of a sensor array consisting of 8 electrochemical sensors detecting the analyte gas reaction products at 7 different catalyst temperatures (30, 100, 200, 500, 600, 750, 900 °C) of an upstream Pt filament. The analytes included a set of 10 alcohols, 2 ketones, ammonia, an amine, 2 sulfides, and 3 aldehydes, all of which are characteristic for fish freshness. Reprinted with permission from ref 67. Copyright 1994 Elsevier.

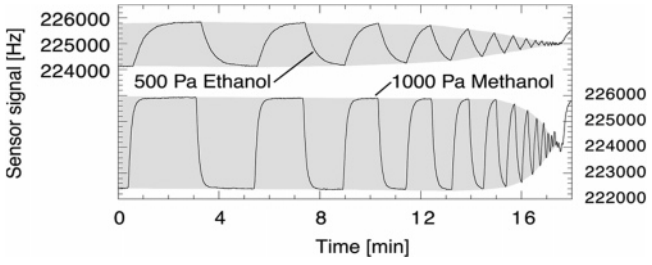

Figure 5. Sensor signals for a series of concentration steps of decreasing lengths from 160 down to 1 s. The capacitor was coated with a 4-μm-thick layer of poly(epichlorohydrin). The envelope of the response profile is highlighted in gray. It is analyte-specific and depends on the analyte absorption and desorption times in the respective polymer. Reprinted with permission from ref 70. Copyright 2006 American Chemical Society.

of the measurement chamber volume is often underestimated. A recording of the setup and manifold dynamics using sensors with very fast response times, e.g., sensors coated with very thin sensitive layers,[70] is, therefore, recommendable.

A wealth of parameters can be extracted from a sensor-signal-versus-time representation and can be used as input to multicomponent-analysis or pattern-recognition algorithms. These parameters can include simple parameters like pulse heights, derivatives, and integrals calculated directly from the response curves or coefficients estimated from different models of the transient response like polynomial functions, exponential functions, or autoregressive models that have been fitted to the response curves.[72]

For most types of sensors (metal oxides and polymer-based sensors), the respective response times to reach equilibrium state are on the order of tens of seconds. In general, there are two different mechanisms determining the transient sensor response upon a sharp analyte concentration increase or decrease:[73] (a) diffusion within the sensitive layer, whereat the diffusion processes in the measurement chamber should be significantly faster, and (b) surface or bulk reaction kinetics of the sensitive material. A nonlinear diffusion−reaction model for thick-film metal-oxide sensors has been proposed by Gardner,[73] and similar models have been used by other authors.[74−77] The sensors included, in most cases,

Taguchi-type thick-film sensors, and it was found that the response time is predominantly diffusion-limited (porous thick-film layer) and not reaction-limited.[73]

In many publications, polymer-based sensors are used, for which no reactions occur, so that bulk dissolution processes, i.e., analyte molecule diffusion into and out of the sensitive-material matrix, determine the transient characteristics.[71,78−80] Mass-sensitive devices, such as thickness-shear-mode resonators, have been used by several authors to identify, e.g., the aromas of alcohols,[80] a variety of organic volatiles,[71,79] or wine aroma compounds.[78] The polymeric layers are usually <1 μm thick.

The temporal or transient characteristics of sensor responses upon different analytes can also be induced by applying modulation techniques similar to the ones described in the preceding section on parameter variation: the exposure interval of the sensors to the analytes can be varied by actuating valves and by switching between analyte-loaded and pure carrier gas as displayed in Figure 5.[70] The sensor signals in Figure 5 are given in Hertz, since on-chip electronics convert the minute capacitive signals into the frequency domain.[81] A poly(epichlorohydrin)-coated (4 μm thickness) capacitive sensor has been used in these experiments, since measurements can be made very rapidly with this transducer (no extended gate time needed as for resonant sensors), and since the dynamic sensor signal neither relies on secondary effects like analyte-induced conductivity changes (conducting polymers) nor is influenced by accompanying effects such as analyte-induced film plasticization (acoustic-wave-based devices). Methanol and ethanol exposure steps of varying duration (from 160 s exposure duration down to 1 s exposure duration) were applied to the sensor. By applying long exposure intervals, all analytes reach absorption equilibrium and maximum signal amplitude, whereas for short intervals, this holds true only for fast-diffusing analytes. The sensor responses to methanol shown in Figure 5 reach saturation and sorption equilibria, even for relatively short exposure duration. For ethanol, which is a larger molecule with a smaller diffusion constant, the sensor signals do not reach equilibrium for medium or short exposure durations; as a result, the amplitude of the ethanol response begins to decrease much earlier in comparison to methanol. In conclusion, variations in the exposure interval can be used to facilitate the discrimination of analytes that belong to even the same homologous series.[70]

Additionally, modulation techniques to produce transients and to reveal the temporal sensor signal characteristics can be combined with any other parameter modulation in the preceding section, such as temperature modulations or the use of a catalyst.

2.3. Extracting Information in Different Domains

In this last subsection on arrays of identical transducers, we will detail examples on how to extract, e.g., physical sensor data such as temperature or magnitude of flow from chemical sensors in addition to the chemical information they provide. A very simple multipurpose sensor/actuator structure offering three sensor operation modes (temperature, conductivity, and amperometric measurements) and two actuator operation modes (local heating and pH gradient control) was proposed by Langereis et al.[82] and is displayed in Figure 6.

The temperature can be measured along two different resistive paths between pads A and B or between C and D. By short-circuiting A and B as well as C and D, an interdigitated structure for conductivity measurements results, as has been shown for various potassium nitrate concentrations. By short-circuiting all four pads (A−D), the resulting electrode can be used for amperometric measurements against an additional reference electrode in a two-electrode setup, as has been demonstrated for different hydrogen peroxide concentrations. The heating can be performed by applying a voltage between A and B, or C and D, and by using one of the meanders or both as resistive heaters. One meander can be used as a temperature sensor. Finally, by supplying a current to all four pads (A−D) against an additional counter electrode, the aqueous environment can be electrolyzed and the local pH can be either increased or decreased (production of protons or hydroxide ions), as has been demonstrated by a coulometric titration of an aqueous acetic acid solution.

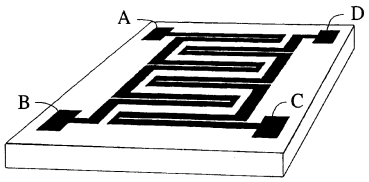

Figure 6. Sketch of the multipurpose sensor structure: temperature between pads A and B or C and D, conductivity between pads A, B and C, D, and amperometric working electrode with all pads (A−D) short-circuited against an additional reference electrode. Reprinted with permission from ref 82. Copyright 1998 Elsevier.

In another approach, multifunctional modules have been realized on the basis of an array of ion-sensitive field-effect transistors (ISFETs).[83−86] A schematic is shown in Figure 7.[86] The setup is arranged around a flow-through cell hosting a so-called "hybrid module" (2 ISFETs, 1 Pt-wire counter electrode, and 1 gold generator electrode), and an Ag/AgCl reference electrode, all connected to external measurement equipment. The ISFET sensors are either pH-ISFETs with sensitive Ta_2O_5 films (55−58 mV/pH-unit) or enzyme-modified ISFETs (penicillinase adsorbed on Ta_2O_5). The temperature is measured by a differential measurement of the two ISFETs operated at different working points. A flow-velocity measurement has been realized by using the generator electrode to electrochemically generate ions (H^+ ions, electrolysis) and by measuring the ion concentration downstream upon their arrival at one of the ISFETs (pH-ISFET). By placing the ion generator electrode between two ISFETs, the flow direction and flow velocity can be determined. If the solution is not pumped through the setup, the diffusion of generated ions away from the generator electrode can be measured, and diffusion coefficients can be determined. An extended version including two of the "hybrid chips" in series has been detailed by the same authors, and, in the same paper, the use of an ISFET as a liquid-level sensor has been described.[85]

The multiparameter detection systems as described above have been used to detect, besides the physical parameters (temperature, flow, and diffusion), potassium ion concentrations (limit of detection (LOD) = 5 μM) via valinomycin-containing poly(vinyl chloride) (PVC) membranes on the Ta_2O_5 gates[85] and pH changes, since also the penicillin sensor (LOD = 5 μM) detected the concentration of H^+ ions resulting from an enzymatic penicillin hydrolysis.[83−86] Examples for other enzyme-based ISFETs are given by the same authors.[87] An open question that remains is, whether or not the concept of using chemosensors with their well-known drift- and stability problems for measuring physical param-

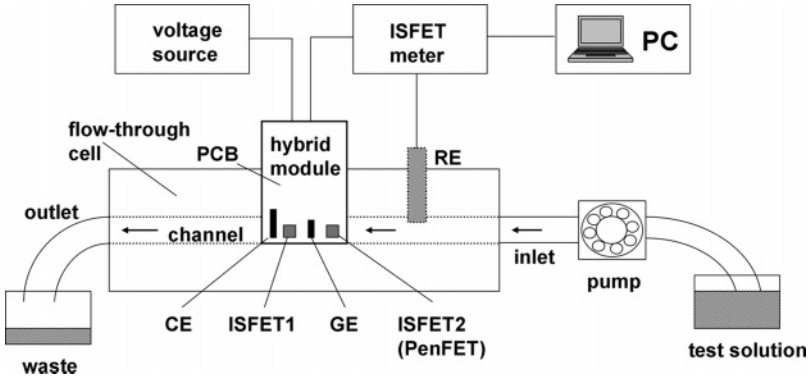

Figure 7. Schematic of a multiparameter detection system with a hybrid module in a flow-through setup: PCB, printed circuit board; GE, generator electrode; CE, counter electrode; ISFET, ion-sensitive field-effect transistor; PenFET, penecillinase-modified ISFET; RE, reference electrode; PC, personal computer. Redrawn with permission from ref 86. Copyright 2003 Elsevier.

eters (temperature, flow, and liquid level) will prove itself in the long run, in particular, since rather simple fully integrated temperature/flow units are commercially available. As will be seen later in this review, the co-integration of temperature sensors has been realized with the aim to enhance the reliability of the chemical sensor signals.[81,88]

3. Arrays and Systems Comprising Different Transducers

In this section, different monolithic and discrete sensor arrays making use of more than one transduction principle will be detailed. The information gained from the different transducers should be as orthogonal or complementary as possible (see discussion in section 6.2), i.e., different analyte-induced changes in the properties of the coating materials, such as resistivity and work function changes, or different properties of the analyte molecules themselves, such as dielectric coefficients and mass, should be exploited. The application of different transduction principles for monitoring changes in the same or in highly correlated physical properties upon analyte dosage will not provide significantly more information than applying only one transducer. In this section, several multisensor arrays will be presented, which include discrete transducers and fully integrated complex microsystems. We have categorized the different systems with regard to the thermodynamic phase (gas and liquid) they are operating in and then subcategorized them according to the types of sensitive materials.

3.1. Metal- and Metal-Oxide-Based Gas Sensors

In the case of metal-oxide-based sensors, several approaches have been made to extract more than only resistance/conductance or impedance values. A rather obvious possibility is to monitor gas-reaction-induced temperature changes on the heated stage of the metal-oxide-coated sensor. The reaction of, e.g., CO, methane, or alcohols at heated metal-oxide surfaces featuring catalytic metals such as Pd or Pt leads to changes in the heat budget, which either increase or decrease the temperature of the heated structure.[89−91]

To explain the occurring temperature effects, all processes involved in the gas interaction process and contributing to heat budget changes have to be considered: adsorption, dissociation, surface reaction, and desorption of the products. The particular thermal gas signature is dependent on these different contributions. CO was found to provide negative

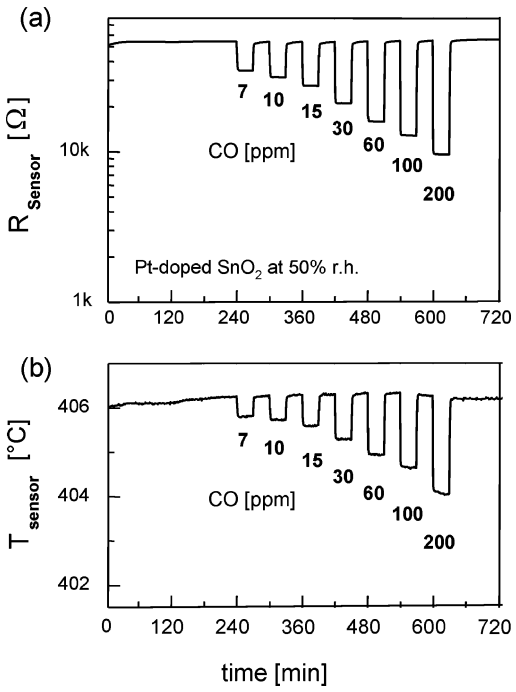

Figure 8. Simultaneously recorded sensor temperature and resistance traces upon dosage of CO at concentrations between 7 and 200 ppm to a Pt-doped tin oxide sensor at 50% relative humidity. Reprinted with permission from ref 91. Copyright 1999 Elsevier.

calorimetric signals (temperature decrease) upon surface reaction with Pt- or Pd-doped tin oxide, though the oxidation reaction and formation of CO_2 is generally exothermic.[54,90,91] Exemplary resistance changes (resistance decreases) and simultaneously recorded temperature changes (temperature decreases) are displayed in Figure 8.[91] The thermal signature can also be recorded for temperature-controlled microhotplate devices by monitoring the changes in the heating power (or in the source-gate voltage in the case of using a heating transistor[54]) for maintaining a preset temperature.

The recording of work function data and catalytic activity in addition to the metal-oxide resistance has been reported on by several authors.[92−94] A setup schematic for such measurements is shown in Figure 9 for the example of tin oxide.[94] It includes a two-electrode resistance arrangement (Taguchi-type sensor), a Kelvin probe for the work function measurements (Kelvin probe relies on the displacement of one of the two surfaces in a periodic oscillation so that a sinusoidal current is produced, which is proportional to the

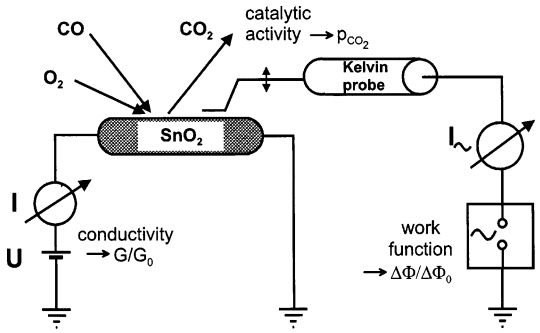

Figure 9. Setup schematic for measurements of conductance, change in work function, and catalytic activity of tin-oxide-based sensors. The catalytic activity is assessed by measuring the concentration of the formed CO_2 via spectroscopy or electrochemical sensors. Reprinted with permission from ref 94. Copyright 1990 Elsevier.

work function difference between the two surfaces), and spectroscopic methods or electrochemical sensors to, e.g., detect the concentration of CO_2 formed through the catalytic reaction of CO at the tin-oxide-sensor surface.

Since the setup and experimental efforts are quite substantial, this combination of methods has been used prevailingly to reveal details of surface reactions and sensor mechanisms for, e.g., CO.[93] Conductivity or impedance measurements provide information on band bending effects and/or changes in the relative position of the Fermi level; the work function measurements additionally provide information on electron affinities. By conducting both types of measurements simultaneously, the different contributions to the overall work function and resistance characteristics can be sorted out, and mechanistic details of the surface and interface reactions can be revealed. Specific signatures for different gases like CO, methane, hydrogen, and H_2S have been found and reported on by several authors.[92,94]

Because of the large cross-sensitivity of the metal oxides to water, differently doped metal-oxide sensors have been combined with a commercially available humidity sensor to yield a sensor system for more reliable carbon monoxide detection.[95] Simply implementing a commercially available humidity sensor, however, may not always be a good solution. Humidity sensors may not perform well over a wide dynamic range, and they may exhibit large cross-sensitivities to other analytes.

In an example of a metal-based gas sensor approach, catalytic palladium nickel metal resistors (thin-film metal resistors) have been combined with catalytic metal-gate field-effect transistors (FETs), FET-type heaters, and a temperature diode in a single-chip integrated system for the detection of hydrogen.[96,97] The FET can detect hydrogen already at rather low concentrations (0.0001−1%), whereas the resistor is aimed at measuring in the range of higher concentrations (up to 20%). The system can be utilized in a multitude of sensing applications, and the respective calibration models have been presented.[96]

3.2. Polymer-Based Gas Sensors

In analogy to the metal-oxide-based sensors above, different transduction principles have also been used for organic materials, such as conducting polymers, to elucidate sensing mechanisms. The question whether charge transfer or sorption characteristics drive the polymer−analyte interaction for the combination polypyrrole/methanol has been addressed by the simultaneous use of mass-sensitive thickness-shear-mode resonators, a Kelvin probe to measure work function changes, and UV/vis spectrophotometrical methods to monitor optical absorption characteristics.[98] Methanol transients have been investigated, and it has been found that analyte sorption is the driving force of the interaction.[98] The simultaneous use of two different transduction mechanisms, chemomechanical transduction by thickness-shear-mode resonators and chemoelectric transduction in conductometric measurements (resistance measurement over a 50 μm wide gap on one of the faces of the quartz crystal) has been shown for polypyrrole films.[99] Frequency decreases and resistance increases upon analyte sorption (various alcohols) have been observed.[99] An array of eight solid-state field-effect-transistor-based sensors for simultaneous potentiometric and impedance sensing in the gas phase using the conducting polymer polyaniline has been studied by Polk et al.[100] The sensor platform consisted of two different chips, a chemical-sensing chip (CSC), and an electronic service chip (ESC), with the latter intended to be flip-chip bonded to the center area of the sensor chip. Two different measurands, the work function and the impedance or resistance changes upon exposure of the polyaniline gate material to ammonia, have been simultaneously recorded, as is displayed in Figure 10.

More recently, arrays of discrete chemical sensors relying on optical fibers (silica optical fiber, 1310 nm wavelength) and thickness-shear-mode resonators (10 MHz, AT-cut, quartz) with carbon-nanotube-based sensitive materials deposited using Langmuir−Blodgett techniques have been used.[101,102] The authors find a significant improvement in the identification of the organic vapors (alcohols, acetone, toluene, and ethyl acetate) by combining the optical and mass-sensitive sensor responses.[101,102] Several authors have combined capacitive and mass-sensitive sensors to detect sulfur dioxide,[103] or capacitive, mass-sensitive, and calorimetric sensors (discrete devices[104−106] or integrated microsystems[81,88,107]) to detect a wide range of organic volatiles. An example of a polymer-based integrated microsystem in CMOS technology (complementary-metal-oxide-semiconductor technology; standard fabrication technology for microelectronics) is shown in Figure 11.

The single-chip gas-detection system comprises three polymer-coated transducers (capacitive, mass-sensitive, and calorimetric) that record changes upon analyte absorption. The absorption of the analyte in the polymeric coating alters the physical properties of the polymer film, such as its mass or volume, which is detected by the mass-sensitive cantilever; it changes the composite dielectric constant as detected by the capacitive transducer, or a certain amount of heat is generated during the absorption process (heat of analyte condensation or vaporization), which can be detected by the Seebeck-effect-based calorimetric transducer (aluminum−polysilicon thermopile). The three different transducers require different operation conditions, the mass-sensitive and the capacitive sensors rely on steady-state signals during sorption equilibria, whereas the calorimetric sensor needs sharp concentration gradients and a switching mechanism, since it only produces a signal upon sudden concentration changes (no signal at equilibrium state). A strategy to deal with these different operation requirements will be presented in section 4.2. The polymer-coated cantilever responds to any analyte dosing with frequency decreases (increasing oscillating mass), and the calorimetric sensor shows two transients per exposure, a positive one at the analyte

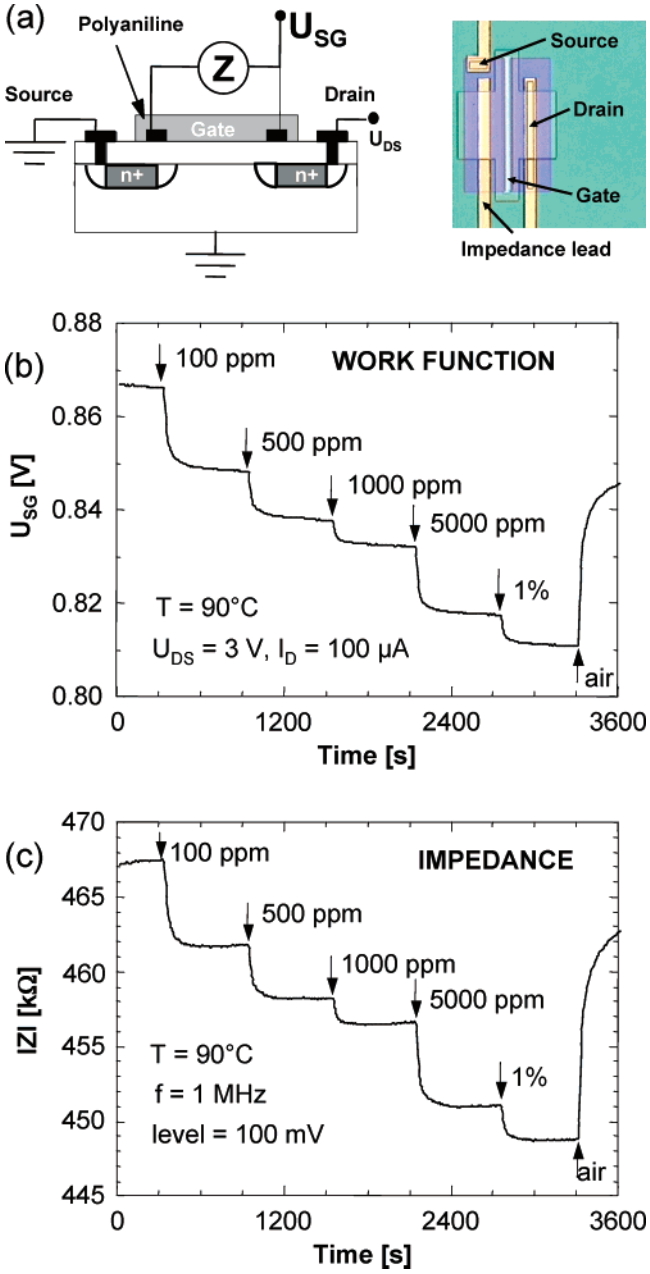

Figure 10. (a) Schematic of the transducer setup to perform impedance and work function measurements. Work function and impedance response of one of the eight sensor modules coated with polyaniline upon exposure to different concentrations of ammonia (100 ppm to 1%) at 22 °C. The graph in (b) shows the potentiometric response (FET gate voltage changes), whereas the graph in (c) shows the impedance response. Graphics kindly provided by Prof. Jiri Janata, GeorgiaTech, Atlanta, GA.

concentration onset (analyte condensation into the polymer matrix) and a negative one upon switching off the analyte (vaporization of the analyte). The responses of the capacitive sensor can, in the case of thick polymer layers (>1.2 μm, larger than half the periodicity of the electrodes), be tuned according to the ratio of the dielectric constants of analyte and polymer. If the dielectric constant of the polymer is lower than that of the analyte, the capacitance will be increased; if the polymer dielectric constant is larger than that of the analyte, the capacitance will be decreased.[108] This effect is shown in Figure 12 for two analytes featuring a larger (ethanol, 24.3) and smaller (toluene, 2.36) dielectric coefficient than that of the sorptive polymer (4.8) and has been

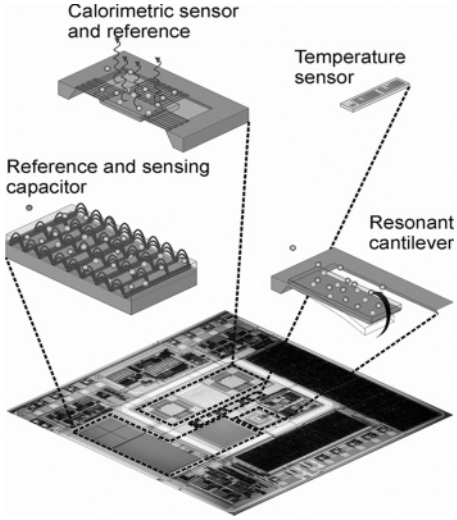

Figure 11. Micrograph of the single-chip CMOS gas sensor microsystem. The three different transducers (capacitive, mass-sensitive, and calorimetric) and the additional temperature sensor are marked. The driving and signal-conditioning circuitry of the different sensors and the digital interface are integrated on chip. The total size of the chip is 7 × 7 mm^2. Reprinted with permission from ref 107. Copyright 2006 American Chemical Society.

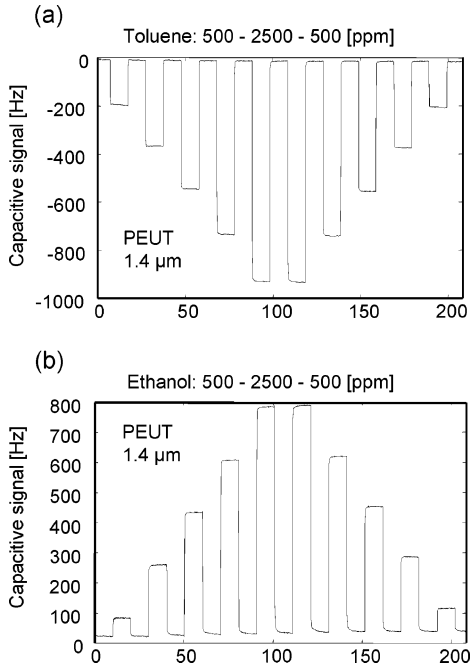

Figure 12. Sensor responses of capacitive sensors coated with a 1.4-μm-thick poly(etherurethane) layer (PEUT) upon exposure to various concentrations of ethanol and toluene. The analyte concentrations included 500−2500 ppm, up and down. The dielectric coefficient of ethanol (24.3) is larger than that of PEUT (4.8), so that positive capacitance changes occur upon ethanol dosage, and the dielectric coefficient of toluene (2.36) is lower, producing negative signals.

previously detailed and substantiated by simulations.[109] It offers the possibility to pick polymers according to their dielectric properties in order to differentiate selected analytes. Moreover, a blinding-out of selected analytes (same dielectric coefficient as that of the polymer) and the use of polymer blends is possible. Another parameter that allows fine-tuning is the layer thickness,[108] as the relative thickness of the polymer layer with respect to the extension of the electric

field lines is decisive for the observed capacitance changes, as will be shown in section 3.3.

All three transducer responses are simultaneously used to characterize the analyte or analyte mixture. Methanol, e.g., provides comparably low signals on mass-sensitive transducers because of its high saturation vapor pressure and low molecular mass. On the other hand, methanol has a dielectric constant of 33 and provides rather high signal intensities on capacitors. Drastic changes in the thermovoltages on the thermopiles are, e.g., measured upon exposure to chlorinated hydrocarbons, which have a low dielectric constant and, thus, provide only low signal intensity on capacitors. The simultaneous probing and recording of changes in different polymer properties upon gas exposure produces additional dimensions in the feature space and provides more comprehensive and complementary information about the analyte or the analyte mixture at hand. Since physisorption processes of organic volatiles in polymers are strongly temperature-dependent, a temperature sensor has to be integrated in such a system to enable reliable quantitative measurements. As a rule of thumb, a temperature increase of 10 °C decreases the fraction of analyte molecules absorbed into the polymer by ~50%, which results in a drastic sensor signal reduction. The temperature sensor in the microsystem exhibits an accuracy of 0.1 K at operation temperatures between −40 and 120 °C. The sensor front-end circuitry that has been integrated on the chip includes all the sensor-specific driving circuitry and signal-conditioning circuitry. The analog/digital conversion is done on-chip as well. This leads to achieving a unique signal-to-noise ratio, since noisy connections are avoided, and since a robust digital signal is generated on-chip and then transmitted to off-chip units.[33,110]

The sensor system has been used to demonstrate that the different transducers indeed provide complementary information on the various organic volatiles and that this information can be used for an analyte characterization according to the respective physical properties.[107] The sensitivity values for a set of analytes and polymers have been evaluated. These sensitivity values have been normalized with regard to the partition coefficients (divided by the partition coefficients) so that all thermodynamic effects related to analyte absorption were accounted for and that the characteristics of the different transducers should then become clearly visible.[107] The partition coefficient is a dimensionless thermodynamic equilibrium constant and is characteristic for a given volatile/polymer combination; it is inversely proportional to the saturation vapor pressure or proportional to the boiling temperature and vaporization enthalpy.[111]

A selection of normalized sensitivity values is shown in Figure 13. The normalization of the sensitivity values with respect to the partition coefficient allows the detection or transduction process to be split into two parts (a) the absorption or partitioning, which is the same for all transducers for a given polymer, and (b) the transducer-specific part, which includes the measurand detected by the respective transducer such as sorption heat (calorimetric), molecular mass (mass-sensitive), and dielectric properties (capacitive).[107] For a selected set of analytes, the characteristic properties of which are sufficiently different, there should be a systematic order in the normalized sensitivity values with respect to the transducer-specific measurand. This is obviously the case and is clearly demonstrated in Figure 13 for any given polymer: The order in the normalized sensitivity values of the calorimeter approximately reflects the

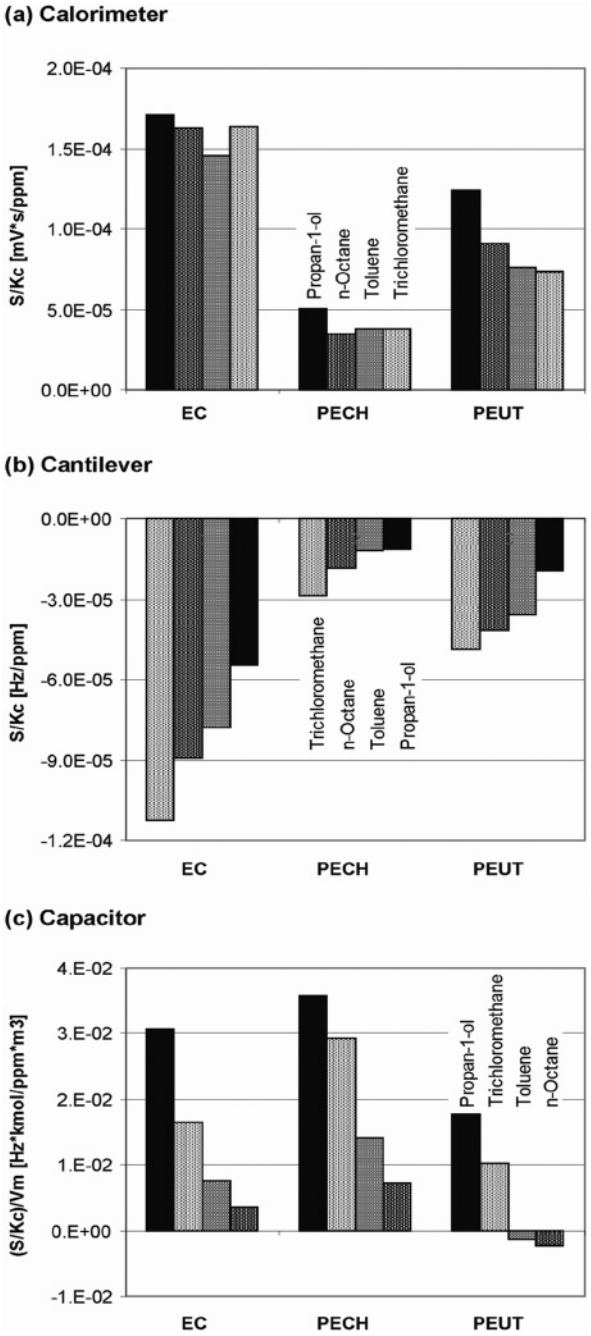

Figure 13. Bar graphs representing *normalized sensitivity* values at 30 °C. Four different analytes (*n*-octane, toluene, propan-1-ol, and trichloromethane) were detected with three different polymers (ethyl cellulose, EC; poly(epichlorohydrin), PECH; and poly(etherurethane), PEUT). The analytes have been ordered with regard to the decisive molecular property for the respective transducer: (a) decreasing heat of vaporization for the calorimeter, (b) decreasing molecular weight for the cantilever, and (c) decreasing analyte dielectric coefficient for the capacitor Reprinted with permission from ref 107. Copyright 2006 American Chemical Society.

vaporization heat of the respective analytes (propan-1-ol, 48.4 kJ/mol; *n*-octane, 41.6 kJ/mol; toluene, 38.0 kJ/mol; and trichloromethane, 31.5 kJ/mol), the order in the cantilever values is according to the analyte molecular mass (trichloromethane, 119.38 g/mol; *n*-octane, 114.23 g/mol; toluene, 92.14 g/mol; and propan-1-ol, 60.10 g/mol), and the order of the capacitive values reflects the analyte dielectric properties or dielectric coefficients (propan-1-ol, 20.45; trichloromethane, 4.81; toluene, 2.38; and *n*-octane, 1.95).

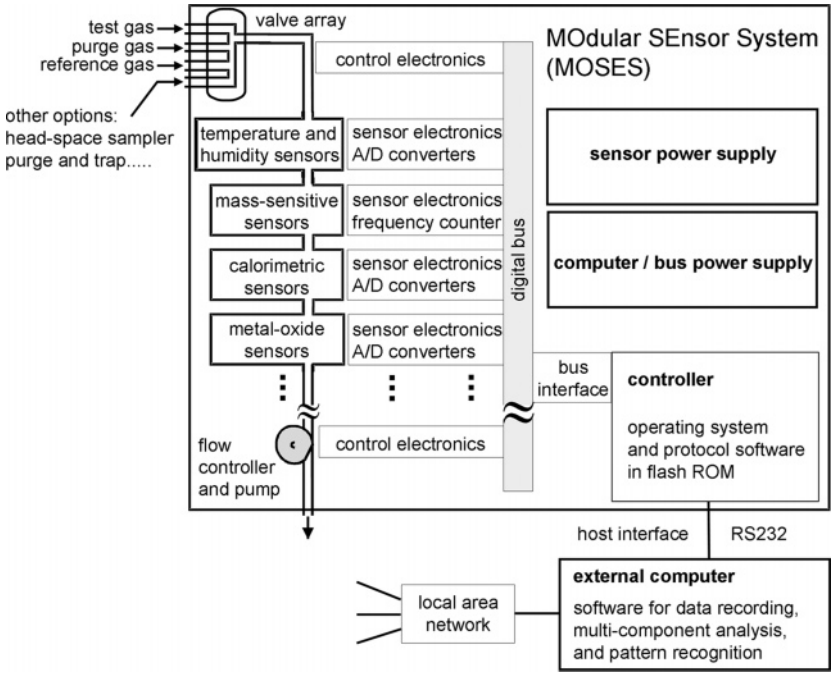

Figure 14. System schematic of the modular sensor system (MOSES): independent sensor modules (mass-sensitive, calorimetric, conductometric, temperature, and humidity) and gas intake and sampling units communicate via a digital bus with the overall system controller. Several alternative gas intake units such as a headspace sampler or a purge-and-trap system can be chosen. The system can be extended by additional modules. Redrawn with permission from ref 119. Copyright 1998 American Chemical Society.

The simultaneous recording from the different transducers causes a unique response pattern for each volatile compound. Because of their fundamentally different transduction principles, the sensors do (within experimental error) indeed respond to the diverse physical properties of the analytes, such as the molecular weight, the dielectric constant, and the heat of vaporization, so that they provide orthogonal information on a given analyte. To what extent the different responses are then also independent in the feature space, however, cannot be determined a priori (see also the respective discussion in section 6.2).

Finally, combinations of the above-mentioned different transducers (mass-sensitive and optical[112,113] or calorimetric[114]) coated with chiral receptors (e.g., cyclodextrins or amino-acid-derived compounds) dissolved in or bound to polymers have been successfully used to discriminate enantiomers.

3.3. Gas Sensor Arrays Relying on Different Transducer and Sensitive-Material Types

Modular sensor systems including different types of polymer-based transducers, metal-oxide-based transducers, noble-metal-gate field-effect transistors, and electrochemical cells have been used as "electronic noses" by different groups to, e.g., qualitatively determine the quality of paper or packaging materials,[115,116] to identify odors and flavors,[116,117] or to assess food products.[118] Please note that a more detailed article on the concept and performances of "electronic noses" is included in this issue.[38]

Holmberg et al. used an array of 10 noble-metal-gate CHEMFET devices (Pd, Ir, and Pt as gate metals) operated between 150 and 190 °C, 4 metal-oxide base conductometric sensors (Taguchi sensors), and an infrared-based carbon dioxide sensor to differentiate various types of cardboard papers.[115] An examination of the sensor correlation matrix revealed that many sensor responses were strongly correlated and that a subset of 7 sensors (5 CHEMFETs and 2 conductometric sensors) or, after data preprocessing, even of only 4 sensors (2 CHEMFETs and 2 conductometric sensors) showed the best discrimination performance. The authors concluded that the success in their application critically depended on the way of gathering the samples, the selection of sensors, and the data-preprocessing method.[115] Data-preprocessing strategies will be covered in detail in section 7.

The concept of a modular sensor system (MOSES) featuring an open architecture and the possibility to add new sensor modules was introduced at the University of Tübingen in the late 1990s.[119] A schematic of this system is displayed in Figure 14.

Arrays of different discrete transducers are located in the respective sensor modules (mass-sensitive, electrochemical, calorimetric, and conductometric modules), which, along with temperature and humidity sensors and gas intake and sampling units, communicate via a digital bus with the overall system controller. The system can be extended by additional modules or modified in any arbitrary way to accommodate the sensors and sampling units needed for a specific application.[119] According to the authors, the modularity offers the best prospects to select sensors and features from a potentially large variety and to optimize the individual sensors or components of the system. Moreover, it provides great flexibility in the feature selection for specific applications: The information content of each feature can be analyzed with due regard to the application at hand, and the total number of features can then be optimized and reduced accordingly (for more details about feature extraction issues, see section 11 of this review).

In most applications, a metal-oxide-based chemoresistor array (8 sensors), operated at temperatures between 200 and 500 °C, and a polymer-based 30 MHz thickness-shear-mode resonator array (8 sensors), operated at room temperature,

have been used. The polymer-based sensors are more stable in the long term and show less drift in comparison to the metal-oxide sensors. Moreover, metal-oxide-based and polymer-based sensors show considerable differences in the response time: the thickness-shear-mode resonators reach equilibrium values 10−15 s after the dosing of the respective analyte, whereas metal-oxide-based chemoresistors need at least 60−90 s, with both transients being slower.[116] While this feature could be used to advantage as described in section 2.2, in most cases only the equilibrium signals or response maxima were evaluated. Principal-component analysis plots of an application example are shown in Figure 15.[117] Principal-component analysis (PCA) is an orthogonal linear transformation method that arranges the data in a new coordinate system such that the greatest variance by any projection of the data comes to lie on the first coordinate (called the first principal component), the second greatest variance comes to lie on the second coordinate, and so on.[10−12] The new coordinates are orthogonal to each other. PCA can be used for dimensionality reduction in a data set by retaining those characteristics of the data set that contribute most to its variance.[10−12]

Figure 15 shows the results of investigations on an artificially rancidized vegetable oil. To have reproducible and defined sample composition, a vegetable oil was contaminated with 100 ppm of different aldehydes (pentan-1-al, hexan-1-al, heptan-1-al, octan-1-al, and nonan-1-al), since aldehydes have been identified as the key components causing rancid taste and smell of degraded edible oils. Figure 15 shows three principal-component analysis (PCA) plots for only the set of metal-oxide-based sensors (MOX), for only the set of thickness-shear-mode resonators (TSMRs), and for a combination of both sets. The added different aldehydes are indicated; "blank" means that the oil is in its original state and has not been manipulated. The metal-oxide-based sensors provide a discrimination of most oils according to the added aldehydes, but the noncontaminated oil and the nonan-1-al-contaminated oil cannot be differentiated. The polymer-based TSMRs cannot really discriminate the short-chain (C5−C7) aldehydes. However, the use of both arrays simultaneously leads to a clear separation and relatively small scattering within the different clusters.[117]

Other examples investigated with the same array configuration, and with an additional electrochemical module in selected cases, include textile materials,[117] odors of plastic materials, coffees, olive oils, whiskey, and tobacco samples.[116] In all cases detailed above, and in many other cases, the data analysis of sensor-array or "electronic-nose" data is limited to the drawing of PCA plots, which might be sufficient for easy problems or problems with a small data set, where the advantage of using a multitransducer array is rather large and obvious. PCA plots are not very representative for higher-dimensional measurement or feature spaces, simply because all the data are projected onto a two-dimensional plane irrespective of the original dimensionality. Thus, multitransducer arrays may also be beneficial even if this is not immediately apparent from the respective PCA plots. The important criterion is that a quantitative indicator of the array performance, such as the test set error for some classifiers, is lowered.[118] Feature selection and the selection of good or optimized sensor subsets for a given application, in this case, the analysis of cured meat products (salami, ham, corned beef, salmon, roast beef, and different packaging materials), has been performed using an extended MOSES array (7 polymer-based sensors, 8 metal-oxide-based sensors, and 4 electrochemical cells).[118] The findings of the authors include

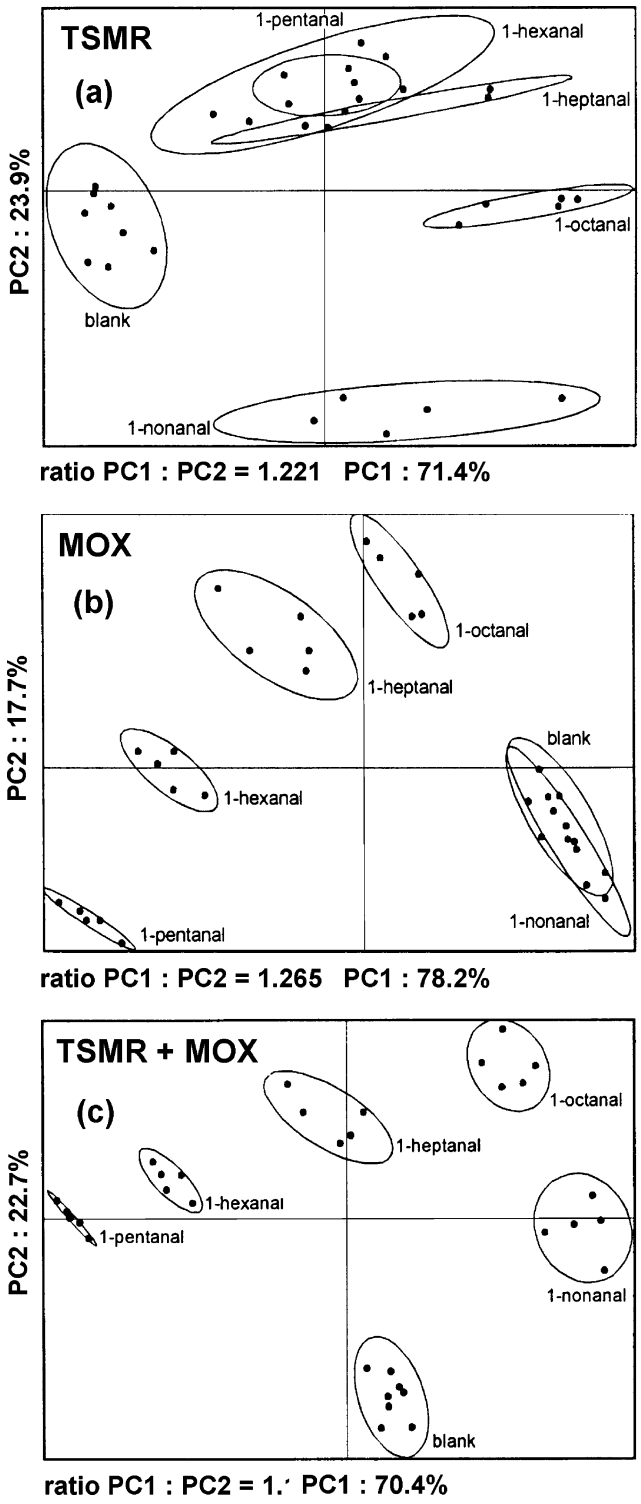

Figure 15. Principal-component-analysis (PCA) plots showing the first two principal components, PC1 and PC2. Discrimination of homologous aldehydes (100 ppm) added to a vegetable oil matrix using (a) eight polymer-based thickness-shear-mode resonators (TSMR), (b) eight metal-oxide-based sensors (MOX), or (c) a combination of both arrays. The PCA plot of the MOX sensors (b) shows an overlap of the clusters of nonan-1-al contamination and the pure oil. In the case of the TSMRs (a), the clusters of the low-molecular-weight aldehydes (pentan-1-al to heptan-1-al) overlap. Only by using both arrays simultaneously, all different contaminated oils and the pure oil can be discriminated. Reprinted with permission from ref 117. Copyright 2000 Elsevier.

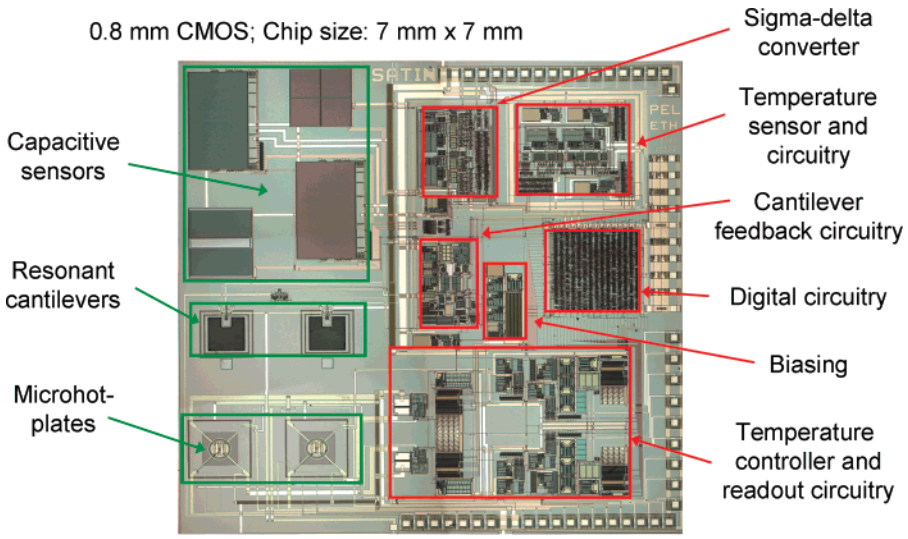

Figure 16. Monolithic multitransducer system including four polymer-based sensors relying on two capacitive and two gravimetric transducers, two metal-oxide-based conductometric sensors on temperature-controlled microhotplates (temperature modulation possible), the respective driving and signal processing electronics, and a digital communication interface. Reprinted with permission from ref 122. Copyright 2007 Elsevier.

that (i) subsets of selected sensors perform better than the whole array in most of the applications (test set error lowered by ~25%), (ii) selected sensors from different classes (different transducer types) show significantly better performance than sensors selected only from a single class, and (iii) subsets that outperform the whole array may be as small as only two different sensors, such as one TSMR and one electrochemical cell.[118] Several modular multitransducer systems based on discrete sensors are commercially available (see, e.g., refs 120 and 121). More details on feature selection can be found in section 11.2.

A monolithically integrated multitransducer array in CMOS technology for the detection of organic and inorganic gases has been recently presented.[122] The system comprises two polymer-based sensor arrays based on capacitive and gravimetric transducers (magnetically actuated cantilevers[123]), a temperature sensor, a metal-oxide sensor array located on microhotplates (thermal time constant ~20 ms with metal-oxide coating), the respective driving and signal processing electronics, and a digital communication interface (Figure 16). The chip has been fabricated in industrial 0.8 μm, CMOS technology with subsequent post-CMOS micromachining. The system has been developed in the framework of a "toolbox strategy" relying on microelectronics standard technology (CMOS), which was identified as the most promising platform technology to achieve major progress.[124,125] The toolbox strategy was chosen as a consequence of the fact that the sensor market is strongly fragmented and that there exist a large variety of applications with different specifications and sensor requirements. The components of the toolbox, such as transducers, sensor modules, and circuit modules, can be developed one by one. Thereafter, specific components that meet the respective applications needs can be selected and assembled into a customized system.

The simultaneous detection of organic and inorganic target analytes with the single-chip multitransducer system has been demonstrated in ref 122. Different organic volatiles have been discriminated according to their dielectric properties and molecular mass in analogy to the results presented in the context of Figures 12 and 13 in the preceding section. Another application possibility concerns the detection of carbon monoxide (CO) or other inorganic gases on a background of changing humidity or alcohol content. For this scenario, the microhotplates and the capacitive sensor, which acts in this case as a humidity or alcohol sensor, have been used.[122]

The microhotplates can be covered with any metal oxide and can be temperature-modulated using any arbitrary waveform. The magnetically actuated cantilevers (Lorentz force[123]) can be used to monitor organic volatiles or interferents. Because of its high dielectric coefficient, humidity will have a major impact on any organic-volatile measurement of the capacitor. However, there is a possibility to measure organic volatiles with capacitive transducers even on a background of humidity or changing relative humidity. This method relies on the use of two differently thick polymer coatings on two identical capacitor structures and has been detailed previously:[108] The signal difference of two capacitors with different layer thicknesses in the range of 0.8−4 μm is almost insensitive to water but retains sensitivity to low-dielectric-constant analytes like toluene or *n*-octane. Such differential or ratiometric methods have also been used, e.g., for conducting polymers,[126,127] and constitute a very useful approach in dealing with interferents, cross-sensitivities, or low signal levels. It is very often more effective to purposefully select or deselect sensors or to use signal ratios or differential values instead of increasing the array size or the transducer diversity. In summary, this system offers great flexibility and can be used for various applications. The respective system configuration can be selected, and all parameters (sensor selection, differential or single sensor signal measurement, and temperature modulation of the hotplates) can be varied and set by means of standard software on a computer communicating with the digital control circuitry on the chip.[122]

At the end of this section on multitransducer systems and "electronic noses", it is noteworthy that a shortcoming of many multisensor-array or electronic-nose papers, besides the predominant use of PCA score plots, is that the qualitative sensor results are not scientifically explained or substantiated by a thorough chemical gas-phase or headspace composition analysis, so that it is not clear, which compounds or which chemical effects lead to a discrimination of the different samples. A more detailed analysis of the contributions of

the different sensors, and of the underlying surface reactions and physicochemistry of the different types of sensors, would be desirable. Varying humidity or alcohol content, e.g., may be more effective in changing the sensor array response to different food, perfume, or wine samples than the presence of aroma or odor components at very low concentration levels, which still are perceivable in human olfaction, but which are no more detectable using chemical sensors. Moreover, sample-to-sample variability, sample deterioration, and the strong influence of the sample preparation and sampling procedure on the sensor results, in particular for natural products, are often underestimated, and the corresponding information is missing in many papers. Information on sampling methods and how these influence sensor array results can be found in dedicated papers.[128,129]

There are also a number of multitransducer sensor systems, besides the already mentioned MOSES II sytem,[130] commercially available, such as the GDA 2 (electrochemical cells, metal-oxide sensors, ion-mobility spectrometer, and photoionization detector) from Airsense Analytics,[131] the FOX 4000 (metal-oxide sensors and polymer-based sensors: thickness-shear-mode resonators, conducting polymers) and the RQ Box from Alpha M.O.S,[132] the Hazmatcad Plus (surface-acoustic-wave devices and electrochemical cells) and the CW Sentry 3G (surface-acoustic-wave devices and electrochemical sensor array) from Microsensor Systems,[133] or microanalytics-based systems from RAE Systems.[134]

3.4. Liquid-Phase Chemo- and Biosensors

A liquid-phase chemical microanalysis system aimed at applications in liquid-phase chromatography has been developed by Norlin et al.[135] The system includes a multisensor chip, a micromachined flow-through cell, and optical fiber interfaces to monitor pressure, flow rate, temperature, conductivity, UV-absorption, and fluorescence. A schematic of the microanalysis system is shown in Figure 17a.[135]

The multisensor chip hosts integrated sensors for pressure, temperature, fluid flow, and conductivity; a flow-cell chip (silicon) defines the measurement chamber or liquid volume (5 μL) and features ports for the optical fibers to monitor fluorescence and UV-absorption. A close-up of the sensor structures is shown in Figure 17b.[135] The substrate of the sensor chip is quartz. The temperature sensor is a simple Pt thermoresistor. The pressure sensor consists of a closed cavity under a polysilicon membrane; the pressure-induced strain in the membrane is measured with piezoresistors (doped polysilicon). For conductivity measurements, planar Pt electrodes (size: 500 μm $\times$ 1000 μm; 400 μm gap) are used. The principle of the fluid-flow sensor is to locally heat the fluid with a heating resistor (polysilicon) and to measure the temperature difference between two points up- and downstream from the heater using aluminum/polysilicon thermopiles (thermoelectric or Seebeck effect). Two laterally connected optical fibers enable UV light to be introduced into and collected from the liquid volume (path length = 9 mm). The fluorescence measurements are performed by using a bundle of seven optical fibers connected laterally to the chamber or from below. The excitation light from a laser diode (wavelength = 630 nm) is guided through the central fiber, and the six outer fibers transmit the fluorescent signal back to a photodetector. Initial results for the pressure sensor, the thermistor, and the flow sensor have been shown as well as conductivity measurements for NaCl solutions with concentrations between 0.001 and 1 mol/L and UV absorption signals for relative acetone contents between 0.1 and 1%.[135]

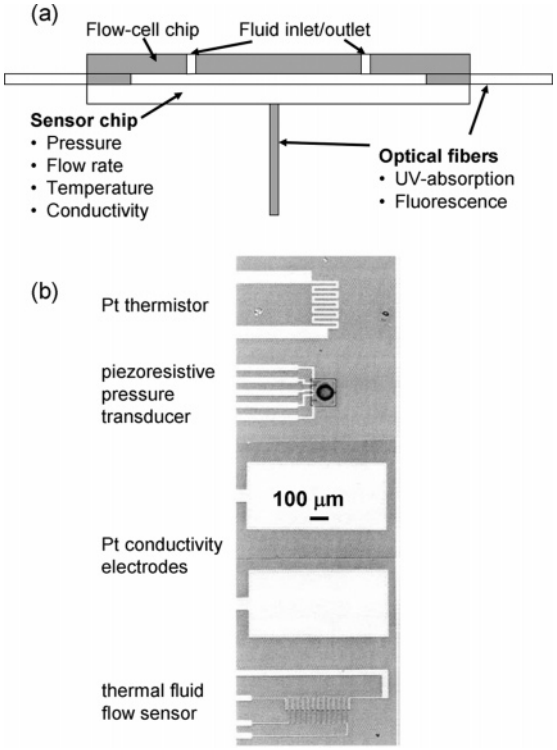

Figure 17. (a) Schematic of the microanalysis system including a multisensor chip, a micromachined flow-through cell, and optical fiber interfaces. (b) Micrographs of the different single sensors, the temperature sensor, the pressure sensor, the conductivity electrodes, and the thermoelectric flow sensor. Reprinted with permission from ref 135. Copyright 1998 Elsevier.

A similar array of sensors including three temperature sensors (microelectronic proportional-to-absolute-temperature sensors), three pressure sensors (thin-silicon-membrane gauge-type sensors with piezoresistive readout), two ISFETs (silicon nitride and silicon oxide ISFET with Pt counter-electrode to monitor pH), and some basic circuitry (multiplexer, differential measurement electronics for chemical sensors, and temperature compensation for pressure sensors) was realized on a CMOS chip and is intended to be part of a drug delivery microsystem.[136] The ISFET sensors were intended to control the pH value of the liquid to be delivered. Besides test results of the pressure and temperature sensors, the sensitivities of the ISFET sensors were determined to be 20−30 mV/pH for the silicon-oxide ISFET and 52 mV/pH for the silicon-nitride ISFET. A nonlinearity in the differential signal of both ISFETs was assessed to be due to the nonlinearity in the silicon-oxide ISFET.[136]

A multisensor array of discrete ISFETS, light-addressable potentiometric sensors (LAPS, *p*-silicon with SiO_2 and Ta_2O_5 on top), and miniaturized ion-selective electrodes (ISE, *p*-silicon, SiO_2, and metal electrode: 15 nm Ti, 30 nm Pt, and 250 nm Au) with a chalcogenide glass material ($CdSAgIAs_2S_3$) as the sensitive layer (200−1300 nm thickness) to detect heavy metal ions in aqueous solution was presented by Kloock et al.[137] The sensitive material was deposited on the transducer structures by means of pulsed laser deposition, and the three different transducers were then compared in their sensitivity to Cd^{2+} ions. The sensitivities of all three potentiometric transducers are in the range of 22−25 mV per decade Cd^{2+}, and the lower detection limit varied between 6×10^{-7} and 5.7×10^{-7} mol/L.[137] The different transducers may, according to the authors, be combined in a future handheld "electronic-tongue" system.

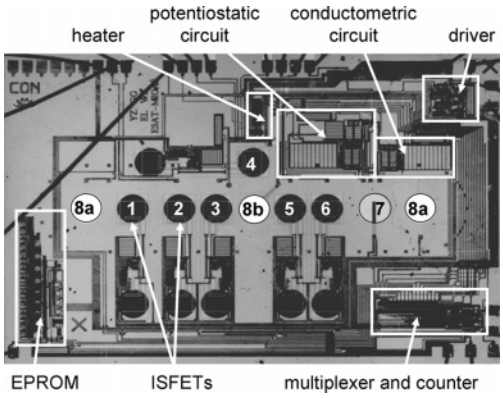

Figure 18. Micrograph of the CMOS multiparameter biochemical sensor chip, which includes 6 ISFETS (1−6), an (amperometric) oxygen sensor (7), and a conductometric sensor (8a,b). The on-chip circuitry includes an EPROM, a multiplexer and counter, a driver unit, a conductometric and potentiostatic circuit, and a heater. Reprinted with permission from ref 138. Copyright 2001 IEEE.

The benefit of using different transducers, however, is not obvious, since all three transducers provide very similar information. Significant differences exist in the transducer fabrication and signal readout complexity.

A biochemical microsensor system aimed at continuous monitoring of ions, dissolved gases, and biomolecules in liquid phase, such as blood, has been presented recently (Figure 18)[138] and is based on an earlier design by Gumbrecht et al.[139,140] The eight integrated chemical sensors comprise six ion-sensitive field-effect transistors (ISFETs = 1−6 in Figure 18), one oxygen sensor (7 in Figure 18) and one conductometric sensor (8a and 8b in Figure 18), all of which can be operated in parallel.[138] An Ag/AgCl reference electrode is also integrated on the CMOS chip to obviate the need for external references. The eight sensors can continuously monitor ions, dissolved gases, and biomolecules via enzymatic reactions that produce charged particles. A flow channel (polyimide) restricts the liquid-phase access to the sensor area.

The six ISFETs allow for direct contact of the electrolyte with the gate oxide. Either the gate oxide itself is pH-sensitive or the ISFET can be used as a "*Severinghaus*"-type pH-FET to measure dissolved carbon dioxide (detection of carbon dioxide via dissolution in water, formation of "carbonic acid", and monitoring of the pH change). The gate oxide can also be covered with different ion-selective membranes to achieve sensitivity to a range of target ions, such as potassium. All six ISFETs or only a subset can be used. The idea was to make a standard chip to reduce manufacturing costs and to then modify the chip with selective coatings according to user needs. The integrated amperometric sensor can be used as a *Clark*-type oxygen sensor, which is based on a two-step reduction of gaseous oxygen in aqueous solution via hydrogen peroxide to hydroxyl ions. The conductometric sensor consists of two parallel sensors (8a), which share one common electrode (8b). A sinusoidal ac potential is applied to the electrodes, and the current, which depends on the solution composition (concentration of charged particles or ions), is recorded. The full system has been produced in a 1.2 μm single-metal, single-poly CMOS process, and the chip size is 4.11 × 6.25 mm^2.[138] The chip, operated at 5 V, hosts all driving circuitry of the sensors such as ISFET buffer amplifiers, a potentiostatic setup for the amperometric sensor, and the circuitry necessary to perform a four-point conductometric measurement on-chip. In addition, the chip exhibits a temperature-control unit to keep the system temperature at a preset value (physiological conditions). This temperature-control unit includes a temperature sensor and a transistor heater. A single-bit EPROM (electrically programmable read-only memory) was implemented on-chip to make sure that the chip is used only once and then is disposed of, which is a crucial feature for medical applications.[138] First tests including amperometric oxygen measurements, the assessment of potassium concentrations with ISFETs (by directly connecting the ISFET buffer to a plotter), and conductometric measurements with a buffer solution have been performed.[138]

Disposable electrochemical multisensor systems for fast blood analysis are marketed by, e.g., companies like Abbott (formerly I-STAT).[141] Sodium, potassium, chloride, calcium, pH, and carbon dioxide are measured by ion-selective-electrode potentiometry. Concentrations are calculated from the measured potential through the Nernst equation. Urea is first hydrolyzed to ammonium ions in a reaction catalyzed by the enzyme urease. The ammonium ions are also monitored by means of an ion-selective electrode. Glucose is measured amperometrically. Oxidation of glucose, catalyzed by the enzyme glucose oxidase, produces hydrogen peroxide. The liberated hydrogen peroxide is oxidized at an electrode to produce an electric current, the intensity of which is proportional to the glucose concentration. Oxygen is also measured amperometrically. The oxygen sensor is similar to a conventional Clark-electrode. Oxygen permeates through a gas-permeable membrane from the blood sample into an internal electrolyte solution, where it is reduced at the cathode. The oxygen reduction current is proportional to the dissolved oxygen concentration. Hematocrit is determined conductometrically. The measured conductivity, after correction for electrolyte concentration, is related to the hematocrit.

3.5. Cell-Based Biosensors

Whole living cells can be used to sensitively detect the presence of certain chemicals in their environment.[142−148] The cell reacts upon exposure to a chemical in a cell-specific response, which can include changes in the cell electrical-activity pattern in the case of electroactive cells (neuronal cells and heart cells). The cellular responses can be monitored by a suitable set of different sensors, with the cell itself acting as a transducer and constituting a very sensitive and selective recognition system for different chemicals. It has to be noted that the cellular environment of living cells in in vitro situations differs considerably from their native environment in vivo.

An example of a multiparameter sensor chip to monitor the cell-culture temperature, the cell-metabolism products, the cell electrical activity, and the cell adhesion to the sensor surface has been developed by a group at the University of Rostock.[149−151a] The aim was to develop a sensor system that allows for the measurement of chemical or metabolic parameters as well as electrical signals with the same sensor chip.

The developed system, the concept of which is illustrated in Figure 19a, provides online monitoring of cellular reactions under well-controlled experimental conditions. The system includes cell-potential field-effect transistors (CPFET, sensitive gate areas of 6 × 1 μm^2) and palladium electrodes

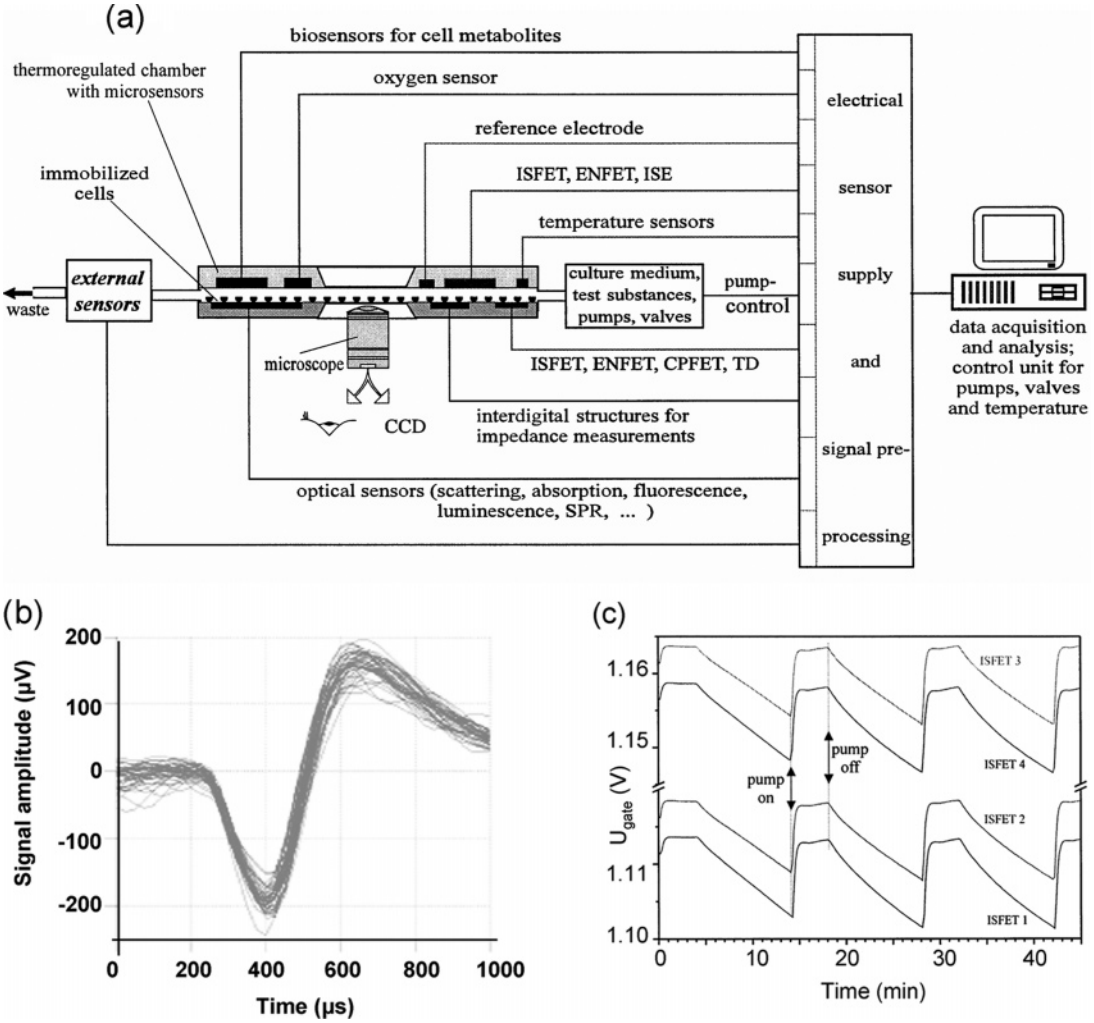

Figure 19. (a) Cell monitoring system concept: thermoregulated cell culture chamber with fluid handling system and different microsensors (ISFET, ion-selective field-effect transistor; ENFET, enzyme FET; ISE, ion-selective electrode; CPFET, cell potential FET; TD, temperature diode; CCD, charge-coupled device; SPR, surface plasmon resonance). Reprinted with permission from ref 142. Copyright 1999 Elsevier. (b) Extracellular recordings from one of the chip electrodes (~40 superimposed neuronal action potentials). Reprinted with permission from ref 149. Copyright 2002 University of Prague. (c) Extracellular acidification measurements in a neuronal network on a silicon chip as performed with ISFETs in a flow-through system. The acidification was measured during the time when the pump was off. When the pump was on, the medium was completely replaced with fresh medium. Output signal of four ISFETs on one sensor chip (ISFETs 1 and 2 with $U_{DS} = 0.2$ V and ISFETs 3 and 4 with $U_{DS} = 0.4$ V ; I_{DS} was 10 mA). The pump cycle was 5 min "pump on" and 10 min "pump off". During the pump-off period, the pH of the medium decreased significantly due to the acidification through the presence of the cells. In the pump-on period, fresh medium is pumped through the chamber. Reprinted with permission from ref 142. Copyright 1999 Elsevier.

(10 μm diameter) to measure the electrical cell activity as shown in Figure 19b,[149] a sensor to monitor the temperature of the cell culture, and ion-sensitive field effect transistors (ISFETs) to monitor the pH in the cellular microenvironment, recordings of which are shown in Figure 19c.[142] The ISFETs allow for monitoring local acidification and respiration in in vitro cell networks. The interdigitated electrodes are used to measure the cell adhesion by means of impedance measurements.[151,151a] The quality of the contact between the electrically active cells and the transducers is of pivotal importance for applications in basic and biomedical research. According to the authors, impedimetric measurements using interdigitated electrode structures have been found to provide information on the cell density and number, the cell adhesion, and the cellular morphology, since an ac current between the electrodes is influenced by the presence and structural properties of living cells growing on these electrode structures. More details on how different chemicals trigger cellular responses of prevailingly electrogenic cells can be found in the literature.[142−148,152]

4. Operational Considerations for Higher-Order Devices

4.1. Setup and Manifold Considerations

An often underestimated issue concerns the gas test setup and manifold for sensor measurements. The manifold for, e.g., any type of gas sensors relying on fast steep concentration gradients and interval analyte dosing (thermopile sensors), or for performing dynamic measurements and applying modulation techniques, has to be carefully designed, so that the dynamics of the transient sensor signal reflect the sensor-specific analyte diffusion and reaction characteristics rather than the gas flow dynamics of the setup and the measurement chamber. This means that all gas switching processes must be fast in comparison to the analyte-specific diffusion and reaction dynamics. To this end, a manifold and flow setup as shown in Figure 20 can be used. The most important features include a crossover flow architecture by use of a fast crossover 4-way valve, matched flow resistances of the

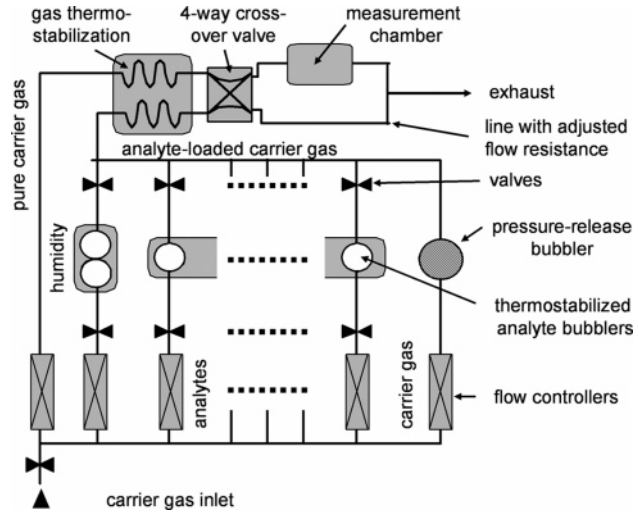

Figure 20. Schematic of the gas manifold as designed for fast transient signal recording.

two output gas lines of the 4-way valve, as well as a small tubing volume between the valve and the sensor measurement chamber.[70,71]

The crossover flow architecture implies that there are two input gas lines, one supplying pure carrier gas and the other supplying carrier gas with defined doses of the analyte, and two output gas lines, one leading to the measurement chamber and the other leading directly to the exhaust. This architecture offers the advantage that both input flows and both output flows are continuously flowing, and that the buildup time of a certain analyte concentration does not influence the dynamic sensor response. With the dosing line being routed to the exhaust (sensors exposed to pure carrier gas), the desired analyte concentration can be adjusted by means of flow controllers. After sufficient time for concentration stabilization, the crossover valve switches the dosing line to the sensors (carrier gas to the exhaust), which then experience a sudden steep concentration gradient. Using the crossover architecture, it is, hence, possible to rapidly switch between pure carrier gas and carrier gas containing a defined concentration of a certain analyte.

The valve must be very fast, e.g., a pneumatically driven 4-way crossover valve with a switching time of <0.5 s, which is commercially available.[70] The 4-way crossover gas switching functionality can also be obtained with a pair of appropriately connected 3-way valves, wired in parallel so that a single switch activates both valves simultaneously.[153] The fast switching of the valves may generate pressure waves in the direction of the measurement chamber but also backward in the direction of the supply lines and the flow-controllers. The system is open on the measurement-chamber side, and no effect on the sensor signal is usually observed. On the side of the flow controllers, additional measures have to be taken since pressure-wave-induced artifacts can otherwise be observed: flow controllers are very sensitive to pressure transients occurring either at their inlet or their outlet, so that an additional empty glass bubbler (large diameter and volume) has to be mounted in between the flow controller for the carrier gas in the dosing line to eliminate these artifacts (Figure 20). The glass bubbler acts as an expansion chamber or accumulator commonly used in pneumatic systems.

Moreover, when switching the 4-way valve, any pressure difference in the two output flow lines affects the gas flow

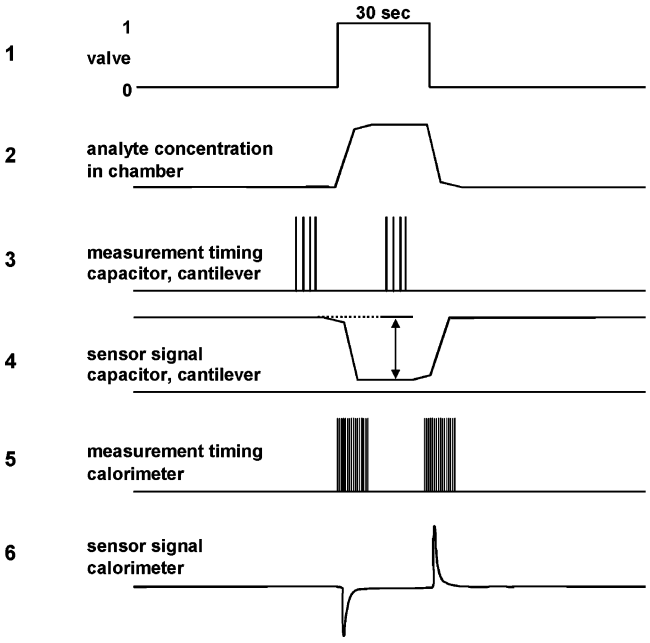

Figure 21. Operation mode as developed for micromachined multisensor chips: operation states of valves and corresponding gas concentrations in the chamber (lines 1−2), timing of the signal recording for the different transducers, and resulting sensor signals (lines 3−6). For details, see text.

dynamics and, consequently, influences the preset concentrations. Therefore, the output line without measurement chamber has to be designed to exhibit a flow resistance as similar as possible to that with the measurement chamber, and the two output lines of the 4-way valve should feed into the same exhaust line after the measurement chamber.

The overall gas volume between the valve and the sensors has to be minimized, taking into account the target overall gas flow. The time span between switching the valve and the moment, at which the gas reaches the sensor, should be as short as possible. The overall flow rate also may influence the dynamic sensor signals if it is rather low or may influence the operating temperature of high-temperature sensors if very high. The optimum flow rate for a given flow setup has to be assessed in prestudies.

4.2. Multitransducer Operation Example

Since multitransducer systems include different types of transducers that require different operation regimes, such as the recording of steady-state or transient signals, it is necessary to apply dedicated operation protocols, which enable reliable qualitative and quantitative measurements and allow for the extraction of a maximum of information. An example strategy will be described here that has been developed for the polymer-based multitransducer unit described in section 3.2 and that meets the operational requirements of the different transducers.

The signal baseline is established by purging with filtered ambient air or clean air from the gas manifold. The operation state of the valve and the resulting analyte concentration in the measurement chamber is displayed in Figure 21, which additionally shows the timing of the signal recording from the different transducers as well as prototypical sensor signals. The gas manifold that can be used to perform the respective measurements has been described in the previous section (4.1).

Line 1 is used to indicate the valve status. "0" represents the basic state of the valve, when pure carrier gas flows through the measurement chamber. In state "1", fractions of the carrier gas pass one or more vaporization units or bubblers, and analyte molecules are present in the gas stream: analyte-loaded gas is flowing over the sensors. In line 2, the corresponding analyte gas-phase concentrations are displayed. In the beginning of a measurement sequence, there is no analyte gas in the measurement chamber, which is purged with pure carrier gas. Baseline signals of the capacitive and mass-sensitive transducers are recorded, the measurement timing of which is displayed in line 3. The valve is then switched to the analyte line for, e.g., 30 s, which leads to an instantaneous analyte concentration increase since analyte-loaded gas is now flowing through the measurement chamber. Equilibrium state capacitive and mass-sensitive signals in analyte-loaded air are then recorded. The resulting sensor signals (mass changes or capacitance changes) are schematically shown in line 4.

The valve is then switched back to pure carrier gas, which generates a sharp decrease in analyte concentration. The last switching would not be necessary for the equilibrium-based sensors, but it is necessary to get the second calorimetric transient, as shown in line 6. As already described in section 3.2, the calorimetric sensor relies on transients and provides signals exclusively upon concentration changes. Therefore, the calorimetric recording has to be performed at high temporal resolution (1 kHz) in two short intervals covering both flanks of the concentration signal (line 2), i.e., at the maximum gradient of the analyte concentration. The two transient signals of the calorimetric transducer (positive upon analyte absorption, negative upon analyte desorption) are displayed in line 6. Usually, the areas of the respective peaks (absorption and desorption peaks) are integrated and then averaged to obtain the final value.

5. Sensor-Based Microanalytical Systems

In this section, we briefly describe more complex miniaturized analytical systems based on gas sensor arrays, which resemble most closely higher-order analytical instruments. The sensor arrays act as detector units in those systems. In most cases, preconcentration (see also the article of Grate et al. in this issue[154]) and/or separation stages have been combined with the sensor array for better analytical performance of the resulting system.[155−166] The preconcentration stages lower the detection limits for the sensors through enrichment of the target analytes in a sorptive matrix. After some time allowed for the analyte enrichment, a sharp heating pulse is applied to the sorptive material so that all the analyte molecules, which were absorbed during a user-defined time span, desorb at once. In this manner, considerably higher analyte concentrations hit the subsequent separation (micro-GC) and/or detection unit (sensor array).[156,157] The preconcentration stages can be classified into two groups: (i) dynamic headspace or purge-and-trap systems and (ii) solid-phase microextraction methods using fibers coated with absorbing materials.[167] Nanoporous carbon, sol−gels, ceramic matrices, polymers, and commercial packing materials are commonly used as absorption matrixes. In comparison to sensors without preconcentrators, improvements in the lower detection limit range between 1 and 3 orders of magnitude can be achieved, so that the lower ppb range (relevant for many applications) becomes accessible. Preconcentrators with commercial material such as Tenax TA have been used in conjunction with mass-sensitive Rayleigh surface-acoustic-wave devices to detect the BTX compounds (benzene, toluene, and xylene) in the low ppm and sub-ppm range,[161] or with thickness-shear-mode resonators (temperature of the preconcentrator was modulated) for apple and banana flavors.[164] A two-step preconcentrator to enrich organic volatiles and to remove water vapor from the sample air (first and second stages feature a hydrophobic coating, which enriches organic volatiles and which lets water pass) was used for analyzing exhaled air or human breath with the help of carbon-black/polymer-coated chemoresistors.[162] Low levels of organic volatiles in human breath could be detected.[162]

Several groups have used sensors as detectors at the end of standard desktop chromatographic units.[165,166] The use of bulky chromatographic units to boost the discrimination performance of small and cheap sensors, however, defeats the purpose of having small and portable units, in particular since the performance of the sensors is, in most cases, not superior to that of a standard flame-ionization detector (FID). It also has been proposed to combine a metal-oxide-based chemoresistor (zinc-oxide pellet) with a 80 mm long fused silica capillary to record diffusion-dependent sensor responses and to identify certain target analytes.[168]

Miniaturized gas chromatographic units were first presented in the late 1970s[169] and, then, in the mid-1990s.[170] In most cases, they have been realized as spirals (column lengths = 0.6−0.9 m; widths = 100−200 μm; and depths = 200−400 μm) micromachined into a planar silicon substrate (~1 cm^2) with a glass plate bonded to the silicon substrate to close the column (see Figure 22 and Figure 24). More recently, rather long (up to 3 m) square-type micromachined columns on 3.3 × 3.3 cm^2 dies have been presented.[160] Within this review, we will not give more details on micromachined gas chromatographic units but will describe two approaches to miniaturized, sensor-based, low-power microsystems potentially capable of comprehensive environmental vapor analysis.

A hybrid microsystem developed in a broad-based effort at the University of Michigan[155−157,159,160,163] contains the following components (Figure 22):[160] a sample inlet with particulate filter, an on-board calibration-vapor source, a multistage preconcentrator/focuser, a dual-column separation module with pressure- and temperature-programmed separation tuning, an array of microsensors for analyte recognition and quantification, and a pump and valves to direct the sample flow. MEMS (micro-electromechanical system) processing technologies have been used to fabricate the system with the ultimate goal of creating a fully operational micro-instrument that occupies only 1−2 cm^3, requires an average (battery) power of just a few mW per analysis, provides rapid determinations of mixtures of at least 30 vapors of arbitrary composition at low- or sub-part-per-billion (ppb) levels, has an embedded microcontroller, and can be remotely interrogated through an RF-MEMS (RF = radio frequency) wireless communication link.[160] The calibration-vapor source, shown in Figure 22a, is designed to generate calibrant vapor at a constant rate by passive diffusion from a liquid reservoir. Analysis of this ''internal standard'', along with vapors captured from the environment, provides the means to compensate for aging, drift, or other factors that might affect analytical performance. The calibration-vapor source is a 3-layer structure, whose base contains a deep porous-Si (PS) reservoir for retaining the volatile-liquid calibrant, a glass spacer layer with a central aperture that

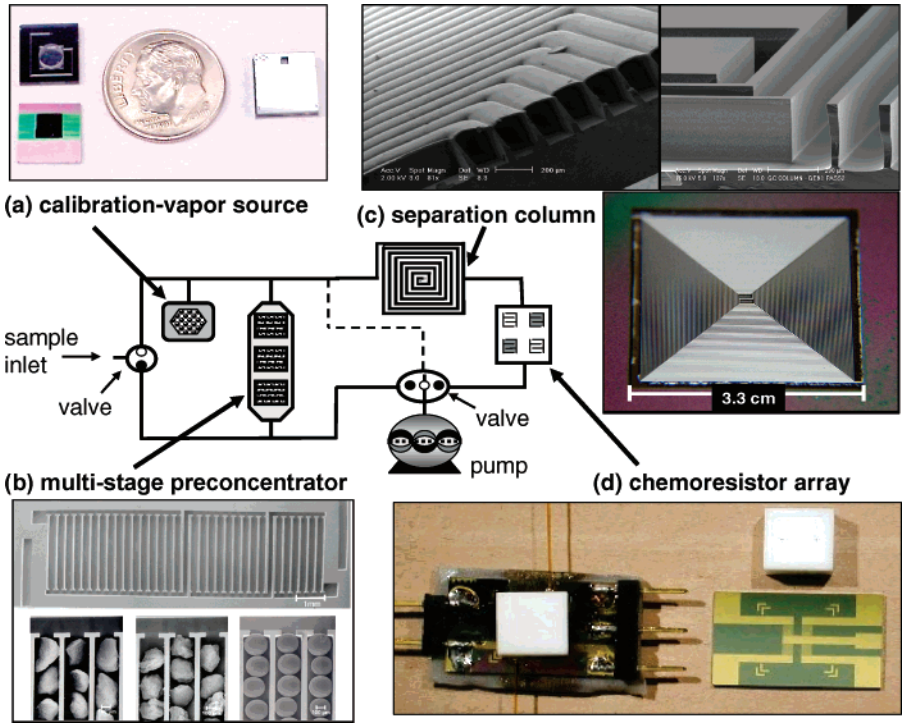

Figure 22. Schematic and components of the Michigan analytical microsystem: (a) calibration-vapor source before (left) and after (right) assembly; (b) 3-stage adsorbent micropreconcentrator prior to loading and sealing (top left), with close-up SEM images of each section loaded with adsorbents (lower left); (c) 3 m separation-column chip (lower right) with close-up views of the channel cross sections prior to (top right) and after (top left) sealing; (d) detector assembly with 4-chemiresistor-array chip (right), Macor lid (white square structure), and sealed detector with connecting capillaries mounted on a custom fixture (left). Reproduced with permission from ref 160. Copyright 2005 Royal Society of Chemistry.

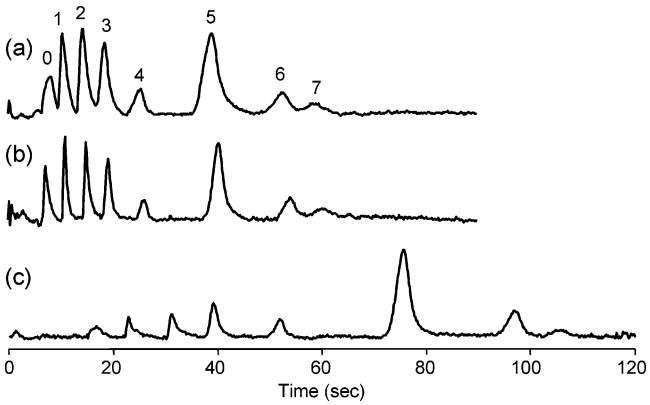

Figure 23. Seven-vapor chromatograms of the Au-6-phenoxyhexane-1-thiolate-coated chemiresistor showing the effect of micropreconcentrator-desorption and column-elution flow rates and flow-rate ratios on resolution and analysis time. For split-flow operation, a portion of the flow through the micropreconcentrator was diverted around the separation column: (a) no split flow, 1.3 mL/min; (b) 4:1 split ratio, 5.1 mL/min (micropreconcentrator)/1.3 mL/min (column); (c) 8:1 split ratio, 5.8 mL/min (micropreconcentrator)/0.75 mL/min (column). Vapors: 0, water; 1, toluene; 2, *n*-butyl acetate; 3, *m*-xylene; 4, *n*-nonane; 5, mesitylene; 6, *n*-decane; 7, octamethylcyclotetrasiloxane. Reproduced with permission from ref 160. Copyright 2005 Royal Society of Chemistry.

defines the headspace region, and a Si cap that contains an etched diffusion channel and exit port.

The three-stage micropreconcentrator (Figure 22b) is designed to capture organic vapors quantitatively and to thermally desorb them into a much smaller volume, thereby increasing the effective concentration to facilitate detection as well as providing a sharp injection plug to facilitate high-speed chromatographic separations.[156,157] The preconcentrator is manually packed with porous, carbon-based adsorbents (total mass $\approx$ 5 mg) in order to increase the specific surface area. Adsorbents are loaded through a stencil mask to maintain segregated sections of each material.

As can be seen in Figure 22c, a large single-substrate column was used, which consisted of a convolved square-spiral silicon channel (150 μm wide, 240 μm deep, and 3 m long) on a square die, 3.3 cm on a side, capped with an anodically bonded Pyrex glass cover plate. Figure 22c shows a sealed column, with the inset providing a closer view of the channel cross section. A polydimethylsiloxane stationary phase (thickness of $\sim$1 μm) was employed and was deposited dynamically from a dilute pentane solution.

The detection unit (Figure 22d) included an integrated array of four chemiresistors, designed to produce a set of partially selective responses to vapors eluting from the separation column. The response pattern can then be combined with the retention time to identify the vapor, and the magnitude of the responses from the sensors can be used to quantify the vapor concentration. Each sensor consists of 20 pairs of interdigital Au/Cr electrodes (1.4 mm long, 15 μm wide, and spaced by 15 μm) on a Si substrate. Intersensor spacings are $\sim$1 mm. The chemiresistor array employs interfacial films of Au-thiolate monolayer-protected nanoclusters, whose resistances are shifted to different extents upon vapor sorption.[171,172]

There are many parameters in this complex system that influence its performance and have to be optimized with due regard to the target analytes and the analysis problem, such as gas flow velocity, flow rates, temperatures and temperature programs of GC column and preconcentrator, preconcentration time, and column and preconcentrator materials.

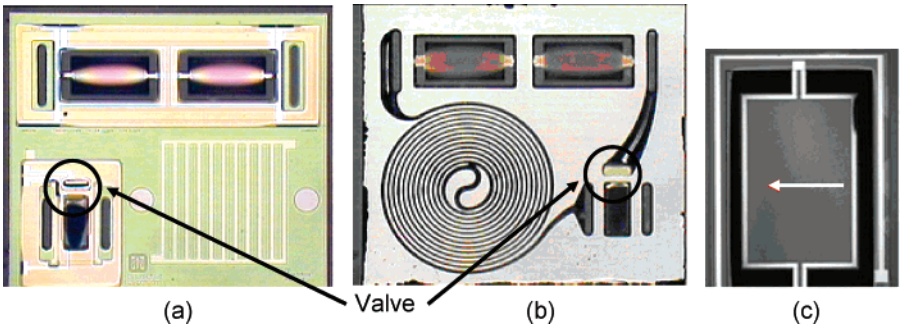

Figure 24. Optical photographs of a monolithic microanalysis system. (a) Front side surface micromachining is shown: dual pivotal-plate resonator sensors are evident as are multiple oblong through-wafer access ports, a preconcentrator in the lower left, and a gas chromatography resistive heater and circular coating ports in the lower right. (b) Reverse side deep etching: the spiral GC is on the lower left. (c) Close-up of the pivot-plate resonator, rotated 90° with respect to images (a) and (b). The direction of the magnetic field, set up by miniature magnets, is indicated by an arrow. Current lines follow the perimeter of the paddle and the two torsional suspension beams. Reprinted with permission from ref 158. Copyright 2006 IEEE.

For sample collection, 0.25 L of analyte-loaded air was drawn at 25 mL/min through the preconcentrator, where the vapors were trapped. The preconcentrator was then heated to 280 °C, and the desorbed vapor mixture was passed to the column and sensors at flow rates below 10 mL/min for separation and detection. A sample measurement is shown in Figure 23.[160] Figure 23a shows a 7-vapor chromatogram from one of the sensors (Au-6-phenoxyhexane-1-thiolate-coated sensor), illustrating that symmetric peak shapes and adequate separations can be achieved at 1.3 mL/min with the column temperature ramped from 25 to 80 °C at 1.4 °C/s. The separation required only 75 s. For this test, the entire desorbed sample volume was transferred to the separation column. A fraction of the sample flow can be diverted around the column and sensor array, since it was shown that sharper injection pulses are obtained at higher desorption flow rates (i.e., 0.3 mL/min) through the preconcentrator, and since it was also shown that the flow restriction imposed by the 3 m column length constrains the maximum flow rate through the column to values of <3 mL/min. The split ratio was adjusted by varying the length, and thereby the flow resistance, of the bypass. Figure 23b shows the chromatogram obtained with a 4:1 ratio: the preconcentrator flow rate (5.1 mL/min) was four times that passing through the column (1.3 mL/min). Retention times were increased slightly and all peaks became sharper and better separated than without a flow split (compare Figure 23a). Increasing the split ratio to 8:1 and reducing the column flow rate to 0.75 mL/min yielded the chromatogram shown in Figure 23c. The separation is improved substantially due to the narrower injection band and due to the operation of the column at a lower velocity. However, the time required for the separation increased by ~50%, and the magnitudes of all peaks are reduced because of the smaller fraction of the desorbed sample being passed through the column and because of the slight increase in dilution associated with the higher desorption flow rate.[160] The system is capable of separating, recognizing, and quantifying mixtures of moderate complexity (e.g., 11 vapors) in <1.5 min. The needed preconcentration time ranges from ~1 min (industrial work places, analyte concentration in the single ppm range) to 10 min or more for less-contaminated office or residential environments (ppb range).[160]

Development efforts in the field of microanalytical systems have taken another step forward in devising extremely compact monolithic systems with all components realized on the same silicon substrate.[158,173] There are advantages to hybrid systems, such as modular replacement of components, and the fact that the thermal isolation of the individual components is much easier to accomplish in hybrid systems, which is important, since the individual components often have different operation temperatures. However, the manifolds previously described often have cold transfer lines interconnecting the components. This can cause collection or condensation of analyte in the transfer lines, ultimately reducing sensitivity. Although the size of the manifold channels may be subminiature, there is still excess dead volume present. Moreover, the assembly of the hybrid system can add to the cost of the completed system, and physical isolation strategies and system timing can be used to mitigate thermal isolation issues for the monolithic system.[158] A monolithic "MicroChemLab" system on a 5 × 6 mm^2 size chip developed at the Sandia National Laboratories, Albuquerque, NM, is shown in Figure 24. The length of the spiral GC column is 8.1 cm in one design and, in another, 11.8 cm. The 8.1 cm long, 50 μm wide GC column is integrated with a preconcentrator and a novel magnetically actuated pivot-plate resonator sensor pair. The pivot-plate resonator is potentially more sensitive than the magnetically actuated flexural-plate-wave transducer used before[158] and is also actuated by making use of Lorentz forces. The pivot-plate resonator consists of a central paddle supported by two torsional beams. An alternating current passing through the transducer lines interacts via the Lorentz force with an orthogonal, in-plane magnetic field, causing the paddle to oscillate around the torsional beams (Figure 24c).[158]

The monolithic chip design also incorporates a surface-micromachined bypass valve, intended to switch the flow between the sampling and separation/detection portions of the overall analysis system. The valve consists of an electrostatically actuated silicon nitride flap situated over the bypass port. Machined glass lids, baseplates, and packages have been fabricated to coat and test the monolithic system, which is work in progress.[158]

6. Are More Sensors Better?

In the introduction to this chapter, we suggested that increasing the measurement-data dimensionality, either by adding more sensors or by extracting additional features, could offer substantial benefits with respect to the analytical capabilities of the instrument. The issue of whether or not "more sensors are better" is an ongoing debate in the chemical-sensor-array community.[174−177] Providing a general

answer to this question is difficult, if at all possible. On the one hand, the use of multiple sensors is central to the "electronic nose" paradigm; arrays of cross-selective sensors (i.e., first-order arrays) do provide more analytical capability and power than the individual sensors. Further, while it is evident that adding "orthogonal" sensors can improve the selectivity of the instrument, the use of redundant sensors can also be beneficial, e.g., in terms of increasing the fault-tolerance and sensitivity of the array. On the other hand, increasing the dimensionality of the feature space can have detrimental effects in terms of increased computational complexity, higher levels of noise, and an increased risk of overfitting (i.e., the modeling of noise in the training set), even if the additional dimensions are orthogonal. In the following subsections, we will provide a more detailed treatment of these issues.

6.1. Characteristics of High-Dimensional Vector Spaces

Humans have an uncanny ability to perceive patterns in the three-dimensional world in which we live. We can understand speech (a first-order signal) under much degraded acoustic conditions, recognize a familiar face (a second-order signal) at a large distance, or appreciate the gracefulness of a ballerina (a third-order signal) already upon a short glance. Unfortunately, our capabilities in the three-dimensional space do not scale up to higher dimensionality. To illustrate this point, we will highlight a few geometric and statistical characteristics of high-dimensional hyperspaces that defeat intuition.[178]

Consider a hypersphere of radius r, defined in d dimensions. It can be shown that the volume of the hypersphere is given by[179]

$$V_d(r) = \frac{2\pi^{d/2} r^d}{d\Gamma\left(\frac{d}{2}\right)} \quad (1)$$

where $\Gamma()$ is the gamma function, an extension of the factorial function to complex and noninteger numbers. Using elementary calculus, the fraction of this volume that is contained in an outermost shell of thickness, ϵ, can be computed as

$$f_d = \frac{V_d(r) - V_d(r-\epsilon)}{V_d(r)} = \frac{r^d - (r-\epsilon)^d}{r^d} = 1 - \left(1 - \frac{\epsilon}{r}\right)^d \quad (2)$$

It then follows that, as the dimensionality of the hypersphere increases, so does the fraction of the volume concentrated in the outermost shell. Likewise, it can be shown that the volume of a hypercube tends to be concentrated in the corners. Thus, high-dimensional spaces tend to be mostly empty, and the data tend to be concentrated in a low-dimensional manifold. The latter suggests that data can be projected onto a low-dimensional subspace without a significant loss of information. Unfortunately, finding an optimal projection becomes increasingly harder with more dimensions. According to the central limit theorem, any sum of independent and identically distributed random variables tends to be more normally distributed than the variables themselves, even if these are markedly non-Gaussian. Thus, as the dimensionality of the feature space increases, low-dimensional projections of the data have the tendency to become normally distributed, which may destroy any natural clustering of the data in a high-dimensional space.[178]

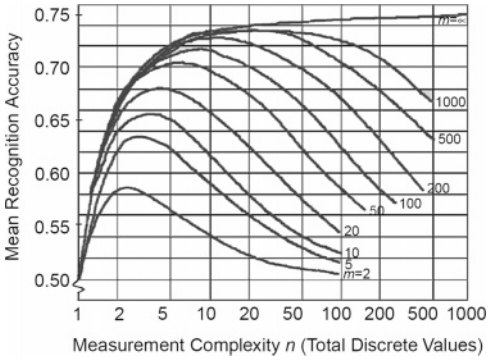

Figure 25. Performance of a statistical pattern classifier as a function of the feature-vector dimensionality, n, for a fixed dataset size, m. Reprinted with permission from ref 182. Copyright 1968 IEEE.

In addition, computation in higher-dimensional spaces increases the amount of data that is required to effectively train the models. It has been shown that the number of training samples should grow linearly with the feature space dimensionality for linear models,[180] in a quadratic fashion for Gaussian models, and exponentially for nonparametric models.[181] What this means is that, for a defined dataset size, there is an optimum number of dimensions, beyond which the performance degrades;[182] see Figure 25. Therefore, on the basis of statistical considerations, and assuming a given number of training samples, the smallest number of sensors that can provide the necessary chemical discrimination is better.

6.2. Orthogonality versus Independence

One of the potential advantages of higher-order sensor arrays, such as arrays based on different transducers, is their ability to produce "orthogonal" features.[88,183] In this context, two features are said to be orthogonal if they convey information about, e.g., different physicochemical properties of the target compounds. Thus, orthogonality is a geometric property defined in chemical space, where each dimension represents a unique molecular chemical or physical property. It is important to note, however, that sensor orthogonality is neither necessary nor sufficient to ensure higher analytical power of an array. In fact, the addition of an orthogonal sensor may even lower the performance of the array through the introduction of noise, if the information provided in the respective added feature is irrelevant to the discrimination and quantification of target compounds or, worse, if the feature is sensitive to the chemical background or to interferents. Consider, for instance, the problem of developing a new sensor array for CO, an example given by Stetter and Penrose.[177] One may be tempted to combine an optical infrared detector with a metal-oxide-covered conductometric device. Both sensors can be considered to be orthogonal, since the IR sensor measures molecular vibrations and the metal-oxide-based sensor relies on electronic effects. By adding a metal-oxide-based sensor, however, we may obtain little additional information. More importantly, since metal-oxides are very sensitive to a broad variety of gases, we may have rendered the array more vulnerable to interferences.

On the other hand, two sensors are said to be independent if the knowledge of the response of one sensor upon exposure to a target compound does not provide any information about

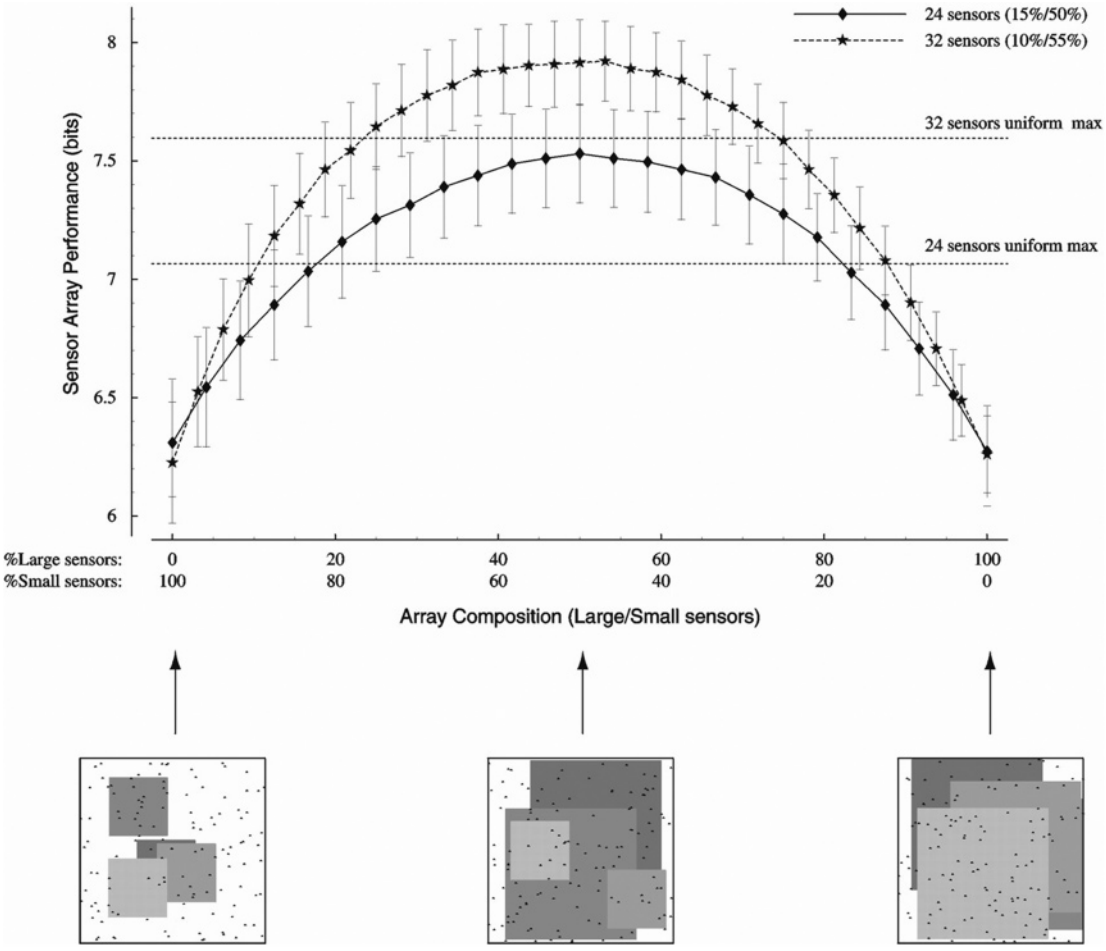

Figure 26. Array performance as a function of the relative proportion of broadly tuned (large) and narrowly tuned (small) sensors. The results show that the maximum performance is obtained when the array contains a mixture of "large" and "small" sensors. Dashed vertical lines indicate the performance of the array when all sensors have the same degree of selectivity. Reprinted with permission from ref 186. Copyright 2002 Oxford University Press.

the response of the other sensor.[183a] In other words, independence is a statistical property defined in the feature space, where each dimension represents a certain feature or sensor.[184] Thus, in contrast to orthogonality, sensor independence cannot be ensured unless the sensor array has been designed for an a priori known set of target analytes. In this context, more sensors are better, in the sense that increasing the number of sensors in the array also increases the odds that a subset of independent sensors can be found for a wider range of applications.

6.3. Cross-sensitivity and Diversity

The inherent cross-sensitivity of chemical sensors is commonly seen as both beneficial, to the extent that it broadens the detection range of the array, and detrimental, in that it makes the instrument vulnerable to interferences. Common sense seems to indicate that, if one were able to develop sensors that are specific to only one of the target compounds, the resulting array would be more accurate than a similar array of cross-sensitive sensors. Quite the contrary has been suggested by a number of theoretical results in computational neuroscience (see, e.g., Brown and Bäcker[185] and references therein) and machine olfaction.[175] According to these studies, arrays of broadly tuned sensors provide a more accurate representation of a stimulus than arrays of highly specific sensors, assuming that the stimulus is of high dimensionality (e.g., large number of target compounds). In fact, using computational models, Alkasab et al.[186] have estimated that an optimum configuration should include arrays in which each individual sensor responds to 25−35% of the target compounds. Several authors (see, e.g., refs 187 and 188) have also reported that the overall performance of large sensor arrays can be improved by allowing the individual sensors to have different degrees of selectivity by combining, e.g., broadly tuned and narrowly tuned sensors; see Figure 26. This theoretical result is particularly relevant in the case of higher-order devices, since different transduction principles and sensitive layers can be combined to produce sensor arrays of very distinct and diverse sensitivity and selectivity patterns. Experimental results on arrays combining selective and partially selective sensors are also consistent with the above theoretical predictions.[189] Therefore, from this perspective, one can argue that more sensors are better, provided that the respective selectivity profiles increase the diversity in the array.

6.4. Multiple Roles of Redundancy

Biological olfactory systems rely on a diverse and highly redundant population of sensory neurons to gather information about the stimulus; see ref 190 and references therein. Depending on the animal species, it has been estimated that 100−1000 different types of receptors are involved in the coding of chemical information at the olfactory epithelium. Each type of receptor is expressed on a large number of

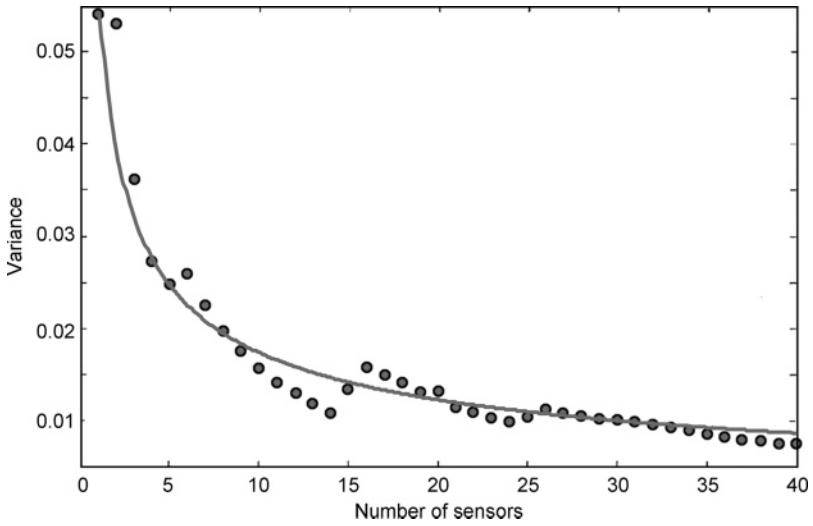

Figure 27. Effect of computing the average response of an array of homogeneous tin-oxide sensors: the variance of the array output decreases with the square root of the number of sensors. Reprinted with permission from ref 192. Copyright 2002 Wiley-VCH, Weinheim.

sensory neurons, with each neuron being specialized on one or a few receptor types. This massive degree of redundancy serves multiple purposes. First, it allows the system to cope with the massive turnover of sensory neurons, since the distribution of sensory neurons can be considered to be stationary over time with respect to the developmental stage of the individual neurons. Second, the integration of the response from multiple neurons can be used to average out uncorrelated noise, which effectively increases the sensitivity of the instrument. More specifically, theoretical estimates and experimental results show that signal integration improves the detection threshold by a factor of $\sqrt{n}$, where n is the number of identical (or identically responding) sensors in the array;[191] this result is illustrated in Figure 27 for an array of nominally identical tin-oxide sensors.[192] Third, by relying on a large population of sensors, the system becomes more robust and fault-tolerant. Thus, from this perspective, more sensors (of the same type) are better, provided that their noise characteristics are also independent.

7. Data Preprocessing

The term "data preprocessing" broadly refers to any transformation performed on the raw sensor data prior to building the main analysis model. The goal of data preprocessing is typically two-fold: (i) reduction of noise or removal of information that is known to be irrelevant to the analysis problem and model (e.g., interferences, drift) and (ii) numerical preconditioning of the data, such as scaling or normalization.[192] The selection of a suitable data-preprocessing approach can have a significant impact on the performance of the analysis model,[193] but, unfortunately, the data-preprocessing approach is highly dependent on the sensor technology (e.g., metal-oxide chemiresistors vs quartz crystal microbalance), the type of analysis (e.g., classification vs regression), the type of model (e.g., nearest-neighbors vs multiway), and the type of noise present in the data (e.g., baseline drift vs concentration effects). Thus, there is only a handful of general guidelines as to how to select the appropriate preprocessing technique (see, e.g., ref 194), and, in practice, a suitable technique must be selected empirically.[195−197]

Data preprocessing is particularly important in the case of higher-order sensor arrays, since these devices can employ a number of different transducer types and/or take advantage of the dynamical responses of the sensors. In the first case, a separate preprocessing technique may need to be applied to each type of transducer and then globally to the multivariate response of the array. In the latter case, it is important to ensure that the preprocessing technique does not destroy the higher-order structure of the data (e.g., trilinearity).[198]

Preprocessing techniques can be grouped into three categories: (1) baseline correction, (2) scaling, and (3) dynamic feature extraction. Baseline correction and scaling will be reviewed only briefly here, since they have been extensively covered in the literature.[192−196,199−201] Somewhat related to baseline correction is the issue of drift compensation. Due to the potentially large impact of drift on the analytical performance of the sensor array, computational methods to handle sensor drift will be treated separately in section 8. An emphasis will also be placed on dynamic feature extraction, since it constitutes one of the easiest ways to realize "higher-order" sensing; dynamic techniques will also be reviewed separately in section 9.

7.1. Baseline Correction

The objective of baseline correction techniques is to remove background noise from the raw sensor responses and to increase the contrast. Three types of baseline correction techniques are widely used: differential, relative, and fractional techniques.[193,202] Differential techniques subtract a baseline value from the sensor response and can be used to remove additive noise or interferences. Differential techniques are typically used for piezoelectric sensors,[203,204] where the response is a frequency or phase shift with respect to a reference analyte (and/or an uncoated reference sensor), and for MOSFET sensors,[205] where the response is a voltage shift in the I(V) curve. Relative techniques compute the ratio between the sensor response to the sample and the sensor baseline value and, therefore, can be used to reduce multiplicative noise. The relative technique is commonly used with metal-oxide devices, since their resistance upon exposure to a sample, R_S, is related to the baseline resistance, R_0, i.e., $R_S = R_0[C]^{-\beta}$.[206] Fractional techniques subtract the baseline value and then divide by the baseline value, which yields a per-unit response. It has been shown[202] that the use of fractional changes in conductance provides the best

Table 1. Dynamic Parameters That Can Be Extracted from Sensor Response Curves[72]

parameter	description
baseline	$(1/5)\cdot\sum_{T=\text{gasOn}-4s}^{\text{gasOn}}$ (sensor value)
final response, response	sensor value (averaged over 5 s) at gasOff−baseline
30/90 s on/off response	sensor value (averaged over 5 s) 30/90 s after gasOn/Off−baseline
maximum response	max (sensor value)−baseline
min/max derivative	min/max difference between two samples during measurement
on/off derivative	(sensor value 10 s after gasOn/Off−baseline)/10
plateau derivative	(response − 90 s on response)/30
on integral	$\sum_{T=\text{gasOn}}^{\text{gasOff}}$ (sensor value − baseline)
off integral	$\sum_{T=\text{gasOff}}^{\text{gasOff}+119s}$ (sensor value − baseline)
short on/off integral	$\sum_{T=\text{gasOn/Off}}^{\text{gasOn/Off}+9s}$ (sensor value − baseline)
response/on integral	response/on integral
*T*0−90%	time from gasOn for sensor value to reach baseline + 0.9 × response
*T*0−60%	or baseline + 0.6 × response
*T*100−10%	time from gasOff for sensor value to reach baseline + 0.1 × response
*T*100−40%	or baseline + 0.4 × response
polynomial on/off	$Y = A_3x^3 + A_2x^2 + A_1x + A_0$ On: Y = (sensor value − baseline) and x = time from gasOn to gasOff Off: Y = (response + baseline − sensor value), x = time from gasOff to gasOff + 240 s
1. exponential on/off	$Y = A(1 - \exp(-(x/T))$, where Y and x are defined like in the polynomial fit
2. exponential on/off	$Y = A_0 + A_1 \exp(-x/T_1) + A_2 \exp(-x/T_2)$, where Y and x are defined like in the polynomial fit
ARX on/off	$y(t) = a_1\cdot y(t-1) + a_2\cdot y(t-2) + b\cdot u(t-1)$ On: $y(t)$ = (sensor value − baseline), t = time from gasOn − 5 s to gasOff and $u(t)$ = 0 if test gas off and 1 if test gas on Off: $y(t)$ = (response + baseline − sensor value), t = time from gasOff − 5 s to gasOff + 240 s and $u(t)$ = 1 if test gas off and 0 if test gas on

Table 2. Summary of Baseline Correction and Scaling Techniques[a]

type	name	transform	application notes
baseline correction	differential	$x_i^{(k)} = x_i^{(k)} - x_i^{(ref)}$	removal of additive noise/drift
baseline correction	relative	$x_i^{(k)} = (x_i^{(k)}/x_i^{(ref)})$	removal of multiplicative noise
baseline correction	fractional	$x_i^{(k)} = (x_i^{(k)} - x_i^{(ref)})/x_i^{(ref)}$	has been shown to work well for metal-oxide chemoresistors
baseline correction	MSC	$x^{(k)} = (x^{(k)} - a^{(k)})/b^{(k)}$	removal of information correlated with a reference sample; $a^{(k}$, $b^{(k}$ are estimated for each sample
global scaling	feature norm	$x_i^{(k)} = (x_i^{(k)} - \min[x_i])/(\max[x_i] - \min[x_i])$	makes signal magnitudes comparable across sensors but can amplify noise and is sensitive to outliers
global scaling	autoscaling	$x_i^{(k)} = (x_i^{(k)} - \text{mean}[x_i])/\text{std}[x_i]$	makes signal magnitudes comparable across sensors but can amplify noise
global scaling	mean centering	$x_i^{(k)} = x_i^{(k)} - \text{mean}[x_i]$	removal of common-mode signal across samples
global scaling	whitening	$x = \Lambda^{-1/2}M^{\mathrm{T}}x$	yields uncorrelated, unit-variance features, but can also amplify noise
local scaling	vector norm	$x_i^{(k)} = (x_i^{(k)}/\sqrt{\sum_i (x_i^{(k)})^2})$	reduction of concentration dependence; useful for qualitative (discriminative) analyses
local scaling	SNV	$x_i^{(k)} = (x_i^{(k)} - \text{mean}[x^{(k}])/\text{std}[x^{(k}]$	reduces within-class scattering but makes the data "closed"
nonlinear transform	logarithm	$x_i^{(k)} = \log(x_i^{(k)})$	linearization and dynamic range compression
nonlinear transform	square-root	$x_i^{(k)} = \sqrt{x_i^{(k)}}$	linearization
nonlinear transform	Box−Cox	$x_i^{(k)} = \begin{cases} ((x_i^{(k)})^{\lambda} - 1)/\lambda & \lambda \neq 0 \\ \ln(\,{}_{\mathrm{i}}^{(k)}) & \lambda = 0 \end{cases}$	compensates for nonlinearities and compresses the dynamic range of the sensor
nonlinear transform	Horner−Hierold	$x_i^{(k)} = (x_i^{(k)}/x_i^{(\text{ref})})^{-1/\beta_i}$	linearization of metal-oxide chemoresistors; parameter β_i estimated from the data

[a] $x_i^{(k)}$ denotes the response of sensor i to sample k. $x_i^{(\text{ref})}$ denotes the response of sensor i to a reference sample. Notation: mean() and std() denote the sample mean and sample standard deviation.

pattern-recognition performance for (*n*-type) MOS chemoresistors. Fractional changes in resistance are also commonly employed with conducting-polymer chemoresistors.[207,208]

The above techniques operate on a sensor-by-sensor basis. Instead, baseline effects on the data set may be treated by means of multivariate techniques, such as multiplicative scatter correction (MSC).[209−211] Developed to remove light scattering and particle-size issues in near-infrared spectroscopy,[212] MSC has so far received little attention in the "electronic nose" or sensors community.[213] Given a feature vector $x^{(k)}$ and a reference sample $x^{(\text{ref})}$, MSC computes the regression model $x^{(k)} = a^{(k)} + b^{(k)}x^{(\text{ref})}$, and then uses the regression parameters (scalars $a^{(k)}$ and $b^{(k)}$) to rescale the feature vector by subtracting the intercept $a^{(k)}$ and dividing by the slope of the estimated regression $b^{(k)}$: $x^{(k)} = (x^{(k)} - a^{(k)})/b^{(k)}$. Thus, MSC can be used to correct for both multiplicative and additive effects. Table 2 summarizes the various forms of baseline correction techniques.

7.2. Scaling

The objective of scaling techniques is to either eliminate irrelevant information from the sensor data (e.g., concentra-

tion), or to precondition the data (e.g., decorrelating features). Scaling techniques can be grouped into global or local techniques, depending on whether they operate on a feature-by-feature basis or on a sample-by-sample basis.[194]

7.2.1. Global Techniques

Global techniques transform the data on a feature-by-feature basis across an entire database. The most common techniques are feature normalization and autoscaling. Feature normalization scales each feature to the range [0, 1] by subtracting the minimum value and then dividing by the overall measurement range of the sensor response, both computed across the entire database. Feature normalization makes full use of the input dynamic range but is very sensitive to outliers, since the range is determined by extreme values in the sensor data. In contrast, autoscaling normalizes each feature by subtracting the sample mean value and then dividing by the standard deviation, both computed across the entire database. Autoscaling cannot provide tight boundaries for the input range but is more robust to outliers than feature normalization. Moreover, robust statistics may be used to reduce the sensitivity to outliers.[214]

Multivariate techniques can also be used to globally scale the data. For instance, the whitening transform[180] may be used to produce uncorrelated and unit-variance features. The procedure consists of first projecting the data along the eigenvectors of the covariance matrix and then normalizing bythe corresponding eigenvalues, i.e., $x = \mathbf{\Lambda}^{-1/2}\mathbf{M}^{T}x$, where $\mathbf{M}$ contains the eigenvectors (arranged as columns) and $\mathbf{\Lambda}$ is a diagonal matrix with the corresponding eigenvalues. The whitening transform is closely related to principal-components analysis (PCA), with the key difference to PCA being that PCA only uses the eigenvectors corresponding to the largest eigenvalues (for dimensionality-reduction purposes). Note that the whitening transform is equivalent to autoscaling if the sensors/features are independent and zero-mean.

Global methods are typically used to ensure that sensor response amplitudes are comparable, preventing subsequent pattern-recognition procedures from being overwhelmed by sensors with arbitrarily large values. For instance, nearest-neighbor procedures[180,215,216] are extremely sensitive to feature weighting, and multilayer perceptrons, the most common type of feedforward neural networks, may saturate for excessively large input values. However, it must be noted that these techniques can amplify noise since all the sensors (including those which may not provide any useful information) are weighted equally.[217]

7.2.2. Local Techniques

Local techniques transform the data on a sample-by-sample basis across the feature vector. Local techniques include vector normalization and standard normal variate correction. In vector normalization, the response of each individual sensor is normalized (i.e., divided) by the L2 norm of the vector ($\|x\|_{L2} = \sqrt{\sum_i x_i^2}$). This forces the distribution of samples to be located on a hypersphere of unit radius. Vector normalization can be used to remove concentration effects, provided that all sensors in the array have the same concentration dependence, e.g., $x_i = k_i f([C])$. This is the case for surface and bulk acoustic wave sensors,[206] electrochemical cells and fluorescent indicators,[184] carbon-black sensors,[208] and metal-oxide sensors. Similar concentration-removal effects can be achieved by normalizing each sensor with the L1 norm ($\|x\|_{L1} = \sum_i |x_i|$) or with the response of a reference sensor. In the case of metal-oxide sensors, the concentration removal requires that the exponent β of the power-law dependence be the same for all sensors. However, an alternative normalization technique has been recently developed that allows this condition to be relaxed.[218] Vector normalization is beneficial for discrimination problems but should be avoided in concentration-estimation problems or whenever the vector norm is known to carry relevant information. For hybrid array data, vector normalization should be performed separately on groups of sensors with the same concentration dependence, such as sensors of the same type, possibly followed by a second normalization across the entire array.

The standard normal variate (SNV) transform[219] normalizes each sensor response by first subtracting the average across the array (for a given sample) and by then dividing through the standard deviation across the array (for a given sample). Thus, SNV can be thought of as an autoscaling of each feature vector. SNV is commonly used in near-infrared spectroscopy to effectively reduce in-class variance but has also been applied to chemical sensor transients.[198]

Care must be taken in employing local transforms, as they render the data set "closed," i.e., SNV forces the sum of the features to become zero, whereas vector normalization renders the sum-square equal to one. Closure can introduce spurious positive correlations between the sensors featuring the highest response levels and spurious negative correlations between sensors exhibiting the lowest response levels.[220] This issue is particularly relevant in the case of hybrid arrays, where each sensor type may have an intrinsically different range of signal magnitude. It is then advisable to first scale each sensor using a global technique, see, e.g., refs 221 and 222.

7.2.3. Nonlinear Transforms

Various transformations have been proposed to compensate for nonlinearities in the data, such as concentration dependencies, or saturation effects. They include logarithms, square-roots,[200] and the Box−Cox transform.[223] Of particular interest for metal-oxide sensors is a linearization transform proposed by Horner and Hierold,[224] which we describe here for illustration purposes. The method assumes a resistance-concentration dependence that can be described by

$$R_i = R_{0_i}\left(1 + \sum_{j=1}^{q}(A_{ij}[C_j])^{m_j}\right)^{-\beta_i} \quad (3)$$

where R_{0_i} is the sensor resistance in air, $[C_j]$ is the concentration of gas j, q is the number of gases, and A_{ij}, m_j, and β_i are model parameters. Suitable values for these parameters can be found by fitting the model to experimental data, $\{R_i,[C_j]\}$, by means of a nonlinear optimization technique (Levenberg−Marquardt). Once these parameters have been estimated, the following nonlinear transformation can be applied to linearize the sensor response with respect to the analyte concentration:

$$r_i = (R_i/R_{0_i})^{-1/\beta_i}; \quad [c_j] = [C_j]^{m_j} \quad (4)$$

8. Drift Compensation

The most serious limitation of current sensor arrays is the inherent drift of individual sensors, which results in a slow,

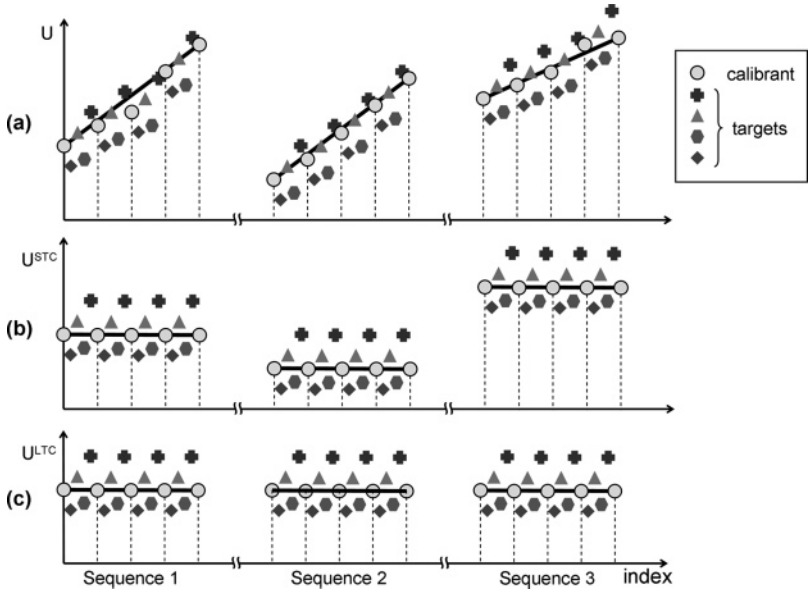

Figure 28. Illustration of the multiplicative signal correction method of Haugen et al.[229] Response of an individual sensor to the calibrant and target gases (a) before calibration, (b) after short-term correction (within sequence), and (c) after long-term correction (between sequences).

random temporal variation of the sensor response when exposed to the same analyte under identical conditions. As a result of drift, learned sensor response patterns may become obsolete over time, so continuous recalibration may be required. Following Holmberg and Artursson,[225] drift-like effects can be attributed to a number of sources. First, there are issues related to the sensor itself, such as aging (e.g., reorganization of the sensing layer) and poisoning (e.g., irreversible binding); only aging and poisoning are strictly considered as drift. These effects are very difficult to compensate for and have been the subject of many investigations, as will be detailed below. Second, drift-like effects can occur also in the measurement system due to, e.g., fluctuations in flow rate, temperature, pressure, or humidity content in the sensing chamber, or analyte condensation in the manifold. These types of artifacts can be most effectively addressed by measuring the variables that are known to fluctuate and by then compensating for the fluctuations in software. This includes, e.g., removing any variance due to fluctuating parameters from the sensor response. An effective compensation may pose a major challenge, when small environmental perturbations induce large changes in the sensor response. In addition, issues related to experimental procedures can give rise to effects that are often confounded with drift, such as memory effects (hysteresis, systematic errors due to fixed sampling sequences), short-term effects (system warm-up, thermal trends), or even the degradation of the samples themselves. These types of errors can be addressed with a proper experimental design, whereas the previously discussed two sources of drift will typically require some form of signal processing.

The modulation of the sensor operation temperature has been used to generate features that are significantly more stable than isothermal features. Along these lines, Roth et al.[226] alternated the temperature of a CO_2 gas sensor coated with an organic material and showed that the normalized slope of the sensor response remained much more stable over time in comparison to constant-temperature measurements. Aigner et al.[227] derived similar conclusions for Si-planar-pellistors.

A number of drift-compensation algorithms have been developed over the past decade, which can be grouped into univariate and multivariate techniques. These two types will be reviewed below.

8.1. Univariate Drift Compensation

Drift compensation may be performed for each sensor individually. At the simplest level, one may employ the baseline-correction techniques described in section 7.1; differential measurements can be used to remove additive (baseline) drift, whereas multiplicative (sensitivity) drift can be compensated for by conducting relative measurements using a reference gas (clean or purified air). Differential measurements can be made with respect to a calibration gas,[228] which must be chemically stable over time, and whose behavior should be highly correlated with the target analytes.[229,230] A practical calibration method that operates on a sensor-by-sensor basis has been developed by Haugen et al.,[229] in which drift compensation is performed on two time scales: (i) within a single measurement sequence and (ii) between measurement sequences. At each time scale, the method models temporal variations in a calibration gas by means of a multiplicative correction factor, which is then applied to the target samples. The process is illustrated in Figure 28. A multiplicative correction scheme has also been used by Sisk and Lewis.[230] More interestingly, these authors have shown that event-driven calibration provides superior performance with respect to periodic calibration. The events may be triggered when, e.g., unlabeled samples start to fall outside the decision boundaries of the classifiers, when outliers are detected, or after interruptions in the data collection. Needless to say, event-driven calibration is also most cost-effective, since it is only performed upon demand.

8.2. Multivariate Drift Compensation

Alternatively, one may correct for drift on the entire array data as a whole, rather than on a sensor-by-sensor basis. The advantage of this approach is that the procedure can exploit correlations between the sensors. The majority of these methods is based on adaptive modeling, system identification,

orthogonal signal correction, or blind signal deconvolution techniques, as will be detailed below.

Adaptive models are an interesting alternative for the problem of drift compensation. The basic idea behind these techniques is to model the distribution of training examples with a codebook (i.e., a collection of cluster centers) and then to adapt this codebook upon the presentation of the test data: an incoming (unknown) sample is assigned to the "closest-matching" class and is then used to adapt the class parameters. A variety of adaptive models have been used, which update one cluster center per class,[231] a single Kohonen self-organizing map (SOM)[232] for all the classes,[233−235] or a separate SOM per class.[236,237] A potential problem of these approaches is that they rely on correct classification; misclassification errors will eventually cause the model to lose track of the class patterns. In addition, all analytes need to be sampled frequently to prevent their patterns from drifting away too much.

System-identification techniques have also been used to model sensor dynamics and then predict drift effects. Holmberg et al.[231,238] have investigated a number of models (e.g., AR, ARMA, Box−Jenkins) to generate a prediction for the common-mode component of the drift for each sensor using the remaining sensors as inputs to the model,

$$\sum_{n=0}^{|A|} a_n \underbrace{x_s(k-n)}_{\text{sensor } s} = \sum_{\substack{i=1 \\ i\neq s}}^{|S|} \sum_{n=0}^{|B|} b_{in} \underbrace{x_i(k-n)}_{\substack{\text{all other} \\ \text{sensors}}} + \sum_{n=0}^{|C|} c_n \underbrace{e(k-n)}_{\text{white noise}} \qquad (5)$$

where $x_s(k)$ is the response of sensor s at time k and $x_i(k)$ is the response of all other sensors at time k. Model parameters $\{a_i, b_k, c_k\}$ can be learned off-line[231] or online by applying a recursive least-squares procedure.[238] For classification purposes, a separate dynamical model is built for each analyte class, and unknown analytes are assigned to the class, whose model displays the lowest prediction error. Nonlinear extensions of this approach, such as Volterra series or artificial neural networks, have been explored by Marco and coworkers.[239−241] Finally, Perera et al.[242] have developed a novelty-detection method based on recursive dynamic PCA[243,244] that can operate under drift conditions.

Approaches based on orthogonal signal correction[245] have been also successfully employed. As illustrated in Figure 29, the basic idea behind these methods is to subtract from the sensor-array response the components that account for as much of the variance as possible but which are uncorrelated with analyte information (mixture concentrations in multicomponent analysis or class labels in discrimination problems). Along these lines, Artursson et al.[246] have developed a drift-compensation method that first estimates the main direction of drift by computing the first principal component of the samples from a calibration gas. This direction is then removed from the multivariate sensor response by subtracting the corresponding bilinear component,

$$x_{\text{corrected}} = x - (x \cdot \mathbf{v}_{\text{cal}})\mathbf{v}_{\text{cal}}^{\text{T}} \qquad (6)$$

where $\mathbf{v}_{\text{cal}}$ is the first eigenvector of the calibration data, x_{cal}. A related procedure has been proposed by Gutierrez-Osuna.[247] Here, the experimenter first identifies a set of variables (y) whose variance can be attributed to drift or interferents. These variables can include, e.g., the response to a purging or reference gas, the date and time when the sample was collected, or measurements from temperature,

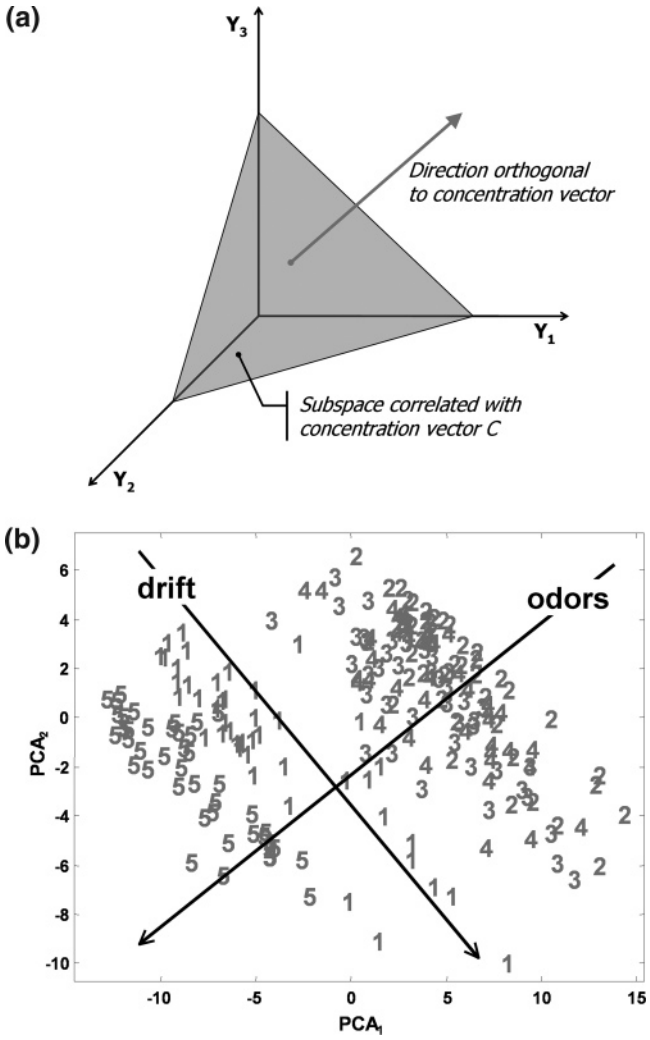

Figure 29. (a) Illustration of orthogonal signal correction; (b) principal-components analysis of the responses of an array of metal-oxide sensors to various food items. Notice that drift-related and class-related information are nearly orthogonal. Reprinted with permission from ref 217. Copyright 2002 IEEE.

pressure, and humidity sensors. Any variance in the measurement vector (x) that can be explained by y is then due to drift or interferences and should be removed. This can be done by means of regression/deflation methods as shown in eq 7. This technique is also closely related to "target rotation".[248]

$$x_{\text{corrected}} = x - Wy$$

$$\text{where } W = \text{argmin}|x - Wy|^2 \qquad (7)$$

Kermit and Tomic[249] have approached drift-compensation as a linear, blind-source-separation problem. In this approach, the sensor array response can be modeled as the weighted sum of a number of independent "sources", such as drift-related noise and discriminatory information. The authors use independent-component analysis (ICA),[250] an extension of principal-component analysis aimed at finding statistically independent projections of the data. As described in section 6.2, two variables x and y are said to be independent if their joint probability density function (PDF) $p(x,y)$ is equal to the product of their marginal PDFs: $p(x, y) = p(x)p(y)$, in other words, if knowledge of the value of one variable

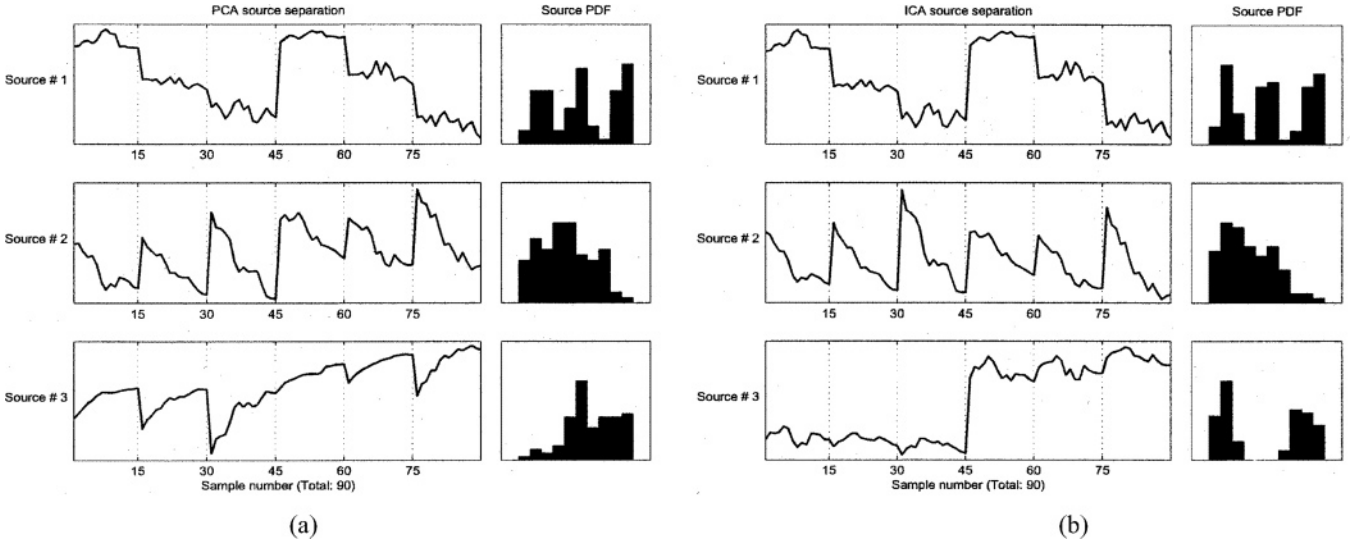

Figure 30. (a) Three principal components and (b) three independent components extracted from the response of a hybrid array to six different alcohols (headspace of 0.5% propanol, 1% propanol, 2% propanol, 0.5% butanol, 1% butanol, and 2% butanol in aqueous solution). Samples are sorted according to classes and time stamps within each class. The estimated probability density functions (PDFs) of each component are plotted at the right of each component. Note that most PCA and ICA projections have markedly non-Gaussian PDFs. Reprinted with permission from ref 249. Copyright 2003 IEEE.

does not provide any information about the value of the other variable. In contrast, two variables are said to be uncorrelated if the expected value (i.e., the average) of their product is equal to the product of their expected values: $E(xy) = E(x)E(y)$, where $E[\ ]$ is the expectation operator. Principal-component analysis finds uncorrelated projections, whereas independent-component analysis finds independent projections, which is a more restrictive criterion. To find the desired solution, ICA uses higher-order statistics (i.e., entropy), whereas PCA relies on second-order statistics (i.e., covariance). A clarification is in place at this point: "higher-order" statistics should not be confounded with "higher-order" sensing; the latter refers to the way in which the data are structured.

Experimental data in the study of Kermit and Tomic were obtained from a hybrid array with 10 MOSFET and 12 metal-oxide sensors, all of which were exposed to the dynamic headspace of 6 analyte solutions (0.5% propanol, 1% propanol, 2% propanol, 0.5% butanol, 1% butanol, and 2% butanol). Ninety measurements were made, 15 per solution, and processed off-line with fastICA.[250] The left panels of Figure 30 show the first three principal components, where samples have been ordered first by label (e.g., the first 15 samples are those from the first class) and then by time of presentation to the array. The right panel of Figure 30 shows the corresponding independent components. The first ICA captures information about the concentration of the analytes (notice the six distinct steps, which correspond to concentrations of 0.5%, 1%, 2%, 0.5%, 1%, and 2%), whereas the second ICA source captures information about the drift (notice the trend for the 15 measurements from each analyte), and the third ICA source captures information about the identity of the analytes (i.e., low for the first 45 samples (propanol) and high for the last 45 samples (butanol)). Thus, ICA is able to separate the three sources of information in the sensor response: analyte identity, analyte concentration, and drift effects. In contrast, PCA is only able to separate concentration information (first principal component), but analyte identity and drift are mixed together in the second and third principal components. It is important to note, however, that the ICA model proposed here computes a solution off-line, i.e., after all the data have been collected. The question remains, though, whether or not these results will hold, when the ICA demixing matrix (equivalent to the eigenvectors in PCA) is tested on data that have not been included in the training set.

9. Feature Extraction from Sensor Dynamics

As described in sections 2.1 and 2.2, one may achieve "higher-order" sensing by exploiting the dynamic properties of the sensors for analytical purposes. In this review, we will concentrate on two strategies that have been extensively used in the literature: the analysis of the transient response of the sensors to sudden changes in the sample concentration (or temperature) and the modulation of the operating temperature of metal-oxide chemoresistors.

9.1. Transient Analysis

When performing data analysis of chemical sensor arrays, it is, in most cases, convention to assume that the information of interest is contained in the quasi-steady-state (or final) response of each sensor. While this approach yields measurements that are simple to conduct and evaluate, it ignores useful information that may be contained in the transient response of the sensor (see, e.g., Table 1). The transient response is the result of dynamic processes that take place when the sensors interact with the target sample. These dynamic processes are unique for each sensor−analyte pair and, therefore, are potentially very useful for analytical purposes. They are typically triggered by modulating an internal parameter of the sensor, such as the operating temperature, or an external one, such as the gas-phase composition of the sample.[251]

The most straightforward but not necessarily the most robust approach consists of analyzing the evolution of the sensor response upon dosing the sample. One of the earliest accounts of this approach is the work of Müller and Lange,[252] who showed that a single cross-selective sensor may be used to discriminate a number of target compounds at different

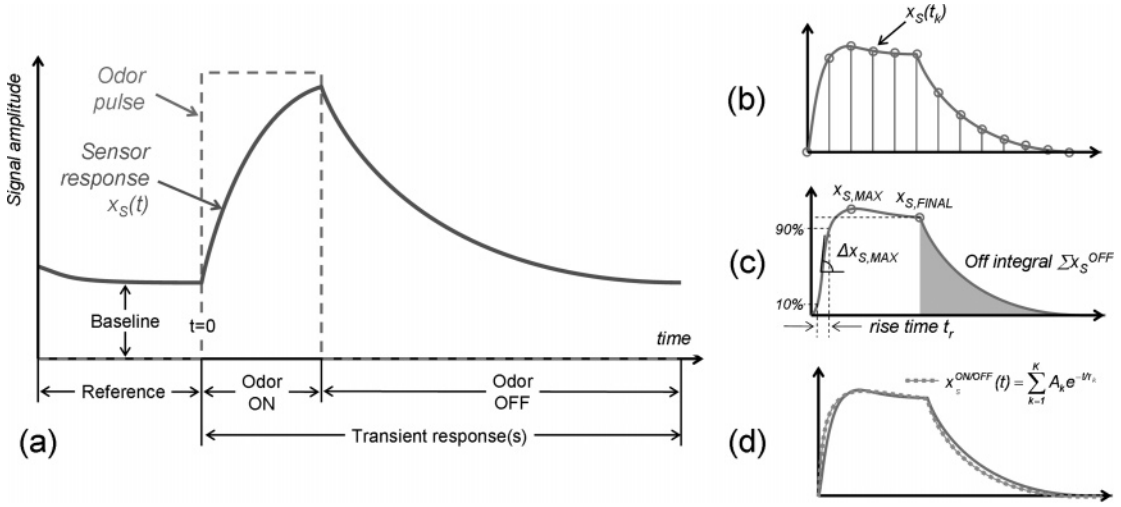

Figure 31. Gas sensor transient response to a short odor pulse (a). Transient analysis approaches: (b) oversampling, (c) parameter extraction, and (d) model fitting. Reprinted with permission from ref 194. Copyright 2002 Wiley-VCH, Weinheim.

concentrations (something that cannot be achieved using only the steady-state response). In their landmark study, the authors extracted two parameters from the transient response of a zeolite-covered metal-oxide sensor: the initial slope (S_1), which was shown to be proportional to the concentration of the gas, and the steady-state response (S_2), which was proportional to the square root of the concentration. As a result, the authors showed that the variable S_1/S_2^2 could be used to discriminate different simple gases regardless of their concentrations. Though this concentration-independent parameter may be different for other sensors (see, e.g., Vilanova et al.[253] for a different case), the study of Müller and Lange is important because it illustrates that more than one parameter may be extracted from the sensor response.

While the transient response will depend on the odor delivery system (see, e.g., the discussion in sections 2.2 and 4.1, as well as in Chapter 6 in ref 206), transient parameters have, in some cases, been shown to be more repeatable than static descriptors; see ref 254. In addition, transient analysis can reduce the data acquisition and calibration time.[255] If the initial sensor transients contain sufficient discriminatory information, one may avoid the lengthy acquisition time required to reach steady state. As a consequence, the sensors also require less time to recover to their baseline, a process that can be particularly slow when the target analytes are present at high concentrations. By reducing the duration of the analyte pulse, and by thus minimizing irreversible binding, the lifetime of the sensors can also be increased. Furthermore, in the case of dynamic headspace analysis, a steady-state response may not even be attainable, since the volatiles in the headspace may be depleted faster than they can be released from the sample. In these cases, the transient response to a short concentration pulse, as illustrated in Figure 31a, may provide sufficient information.[256]

The remainder of this section will provide an in-depth review of different computational methods that have been proposed to extract information from the transient responses of gas sensors. These methods can be grouped into three broad categories: (i) oversampling, (ii) parameter extraction, and (iii) model-based methods, as illustrated in parts b−d of Figure 31. Outputs from these methods can then be treated using conventional pattern classification, regression, and clustering techniques.[217] Alternatively, the entire transient response may be processed with suitable classification or regression models; the reader is referred to section 10 for a discussion of these methods.

9.1.1. Oversampling Procedures

The most straightforward approach to capture transient information is to oversample the sensor transient at different time intervals during the odor exposure and/or odor recovery phase, as illustrated in Figure 31b. The term "oversampling" is used here to emphasize that the sensor is sampled more frequently than at steady state; the opposite term "decimation" is sometimes used in the literature to emphasize that the sensor transient is first measured with a very fine time scale, and then a subset of those measurements is used as a feature vector (i.e., the finely sampled transient is said to have been decimated). Leaving aside terminology, when using oversampling/decimation techniques the dynamic information is represented implicitly, in the correlation of these measurement values, rather than explicitly, as is the case for the other two approaches. Nanto et al.[257] characterized the transient response of thickness-shear-mode resonators by means of nine parameters, which correspond to the sensor response values at defined times {t = 1, 2, 3, ..., 8, 14 min}, normalized with respect to the maximum sensor response during the transient. The authors show that a multilayer perceptron trained on these parameters was able to discriminate among different types of wines and liquors using a single sensor. Saunders et al.[258] used the transient response of thickness-shear-mode resonators during the odor exposure and recovery times. The authors extracted 50 measurements from these transients and normalized them with respect to the baseline frequency and the maximum response of the sensor during the transient, and used then as input features into a bank of multilayer perceptrons (one per sensor). The normalized transient responses (termed "kinetic signatures" in their article) were shown to be very consistent for each sensor across repeated trials, despite a drift in the baseline and in the maximum response parameters. Hongmei et al.[259] employed a similar kinetic-signature procedure to simultaneously determine the concentration of sulfur dioxide and relative humidity using a single piezoelectric quartz thickness-shear-mode resonator. White et al.[260] used an array of fiber-optic sensors to identify single analytes, binary mixtures, and the relative component concentrations. Analytes were delivered to the distal end of the fibers using a

short 2 s pulse, and the transient response was resampled to yield 10 measurement values, each representing the average sensor response of 6 consecutive time points. Their results show that multilayer perceptrons trained on the oversampled transient significantly outperform those trained on only the integral response of each sensor transient. Kermani et al.[261] proposed a time-windowing technique to extract transient information. Their method relies on four overlapping bell-shaped kernel functions, which are used to compute a weighted integral response of the sensor at different times during the sensor transient. Using an array of 15 metal-oxide sensors, their method was shown to significantly outperform the steady-state and the transient integral on a number of odor databases.[196] A family of five uniform time-windows was used by Brahim-Belhouari[262] to extract information from the transients of an array of eight SnO_2 microhotplates. However, while the time-windowed features outperformed steady-state features, the authors showed that similar performance could be obtained by combining steady-state signals with the slope of each transient, measured during the first minute of the sensor exposure.

9.1.2. Ad hoc Transient Parameters

Alternatively, a wide range of parameters may be extracted from the transient response of a gas sensor, such as rise times, derivatives and integrals, computed at different time points during the exposure and recovery phases, as shown in Figure 31c. With little computational expense, these methods can provide a more compact representation of the information contained in the sensor transients. As discussed earlier, a combination of the initial slope of the transient and the steady-state response was used by Müller and Lange[252] to discriminate multiple analytes at different concentrations. More recently, Llobet et al.[254] characterized the transient response of metal-oxide sensors by means of the conductance rise time, measured from 20% to 60% of the total conductance change ($G(0) - G(\infty)$). An important result of this study is that the rise time appears to be significantly more repeatable than the steady-state response. Moreover, an analysis of variance also showed that the response time was independent of the analyte concentration (toluene and *o*-xylene in the range 25−100 ppm) and only depended on the vapor/sensor pair. Roussel et al.[263] evaluated a large number of ad hoc features for the purposes of discriminating off-odors in wines with an array of five tin-oxide sensors. Different features were computed from the transient response and their first- and second-order derivatives, including the response values at different time intervals and the response maxima/minima, yielding a total of 29 features per sensor. Features were evaluated with respect to three different criteria: repeatability across trials (within-class variance), discrimination results (ratio of between-class to within-class variance), and correlation with other features. Their results show that (1) the best features include the maximum sensor response values, the maximum slope during the exposure transient, and the minimum slope during recovery, and that (2) the most suitable features are the same for all five sensors. Paulsson et al.[264] performed a feature-selection study for various preprocessing and transient-analysis techniques on experimental data from a real-life application: the evaluation of breath alcohol contents using a hybrid array of MOSFETs, chemoresistors, and an infrared sensor. The sensor features included the final response value, the maximum response values, the response integral, and the maximum response slope. However, their results showed no systematic advantage for using any of these feature types.

Employing concepts from dynamic systems, Martinelli et al.[265] proposed to extract transient information from the phase plot of each sensor. In their article, the state variables were the sensor response and its derivative. A single transient feature was extracted from each sensor: the area circumscribed by the phase plot of each sensor during the adsorption and desorption processes. The method was validated on an experimental database containing the transient response of thickness-shear-mode resonators when exposed to the headspace of apples with different degrees of internal defects. The results showed that phase-space transient features outperform steady-state features in terms of both uncorrelatedness and discrimination capabilities. In a subsequent study, Martinelli et al.[266] proposed to extract additional information from the phase space, arguing that the evaluation of the area of the phase plot does not take into account information that may be present in the shape of the trajectory. For this purpose, they computed a number of higher-order geometric moments[267] from the phase plot of the sensor transient. In this study, the phase space was defined by the sensor response and a time-delayed version, i.e., $[s(t), s(t - \tau)]$. The use of such "dynamic moments" was shown to yield better results for two experimental databases in comparison to only using steady-state information. However, the authors acknowledged that the optimum time delay (τ) is application-specific and, more importantly, that the dynamic moments tend to be rather sensitive to small changes in the sensor dynamics. Similar results and conclusions for dynamic moments have been reported on by Vergara et al.,[268] using metal oxide sensors to detect the rancidity of crisps (potato chips). In a related study, Pardo and Sverbeglieri[269] compared five different features: the steady-state response, the phase-space area,[266] and the transient integral, with the latter two computed for both the exposure and the recovery process. While their results are not unequivocal as to which type of feature is best, and while the evaluation was performed on a small data set (coffee ripening), the authors suggest that the phase-space area during the recovery process outperforms steady-state and transient integral information and that features calculated during the recovery interval (either phase-space area or integral) consistently provide better performance than those calculated for the exposure interval.

9.1.3. Model-Based Parameters

Transient information can also be captured by fitting an analytical model to the experimental transient, and then using the resulting parameters as features. Various types of models have been used for this purpose, such as autoregressive and polynomial methods, but multiexponential models are most common due to the exponential nature of the transient response, as shown in Figure 32. Transients are generally modeled by a sum of exponential functions of the following form:

$$f(t) = \sum_{i=1}^{M} G_i \, e^{-t/\tau_i} \tag{8}$$

Although conceptually easy, the task of modeling a curve with a set of exponential functions with real exponents is ill-conditioned. Unlike the familiar sinusoidal functions used in Fourier analysis, exponential functions do not provide an orthogonal expansion. Therefore, if one tries to determine

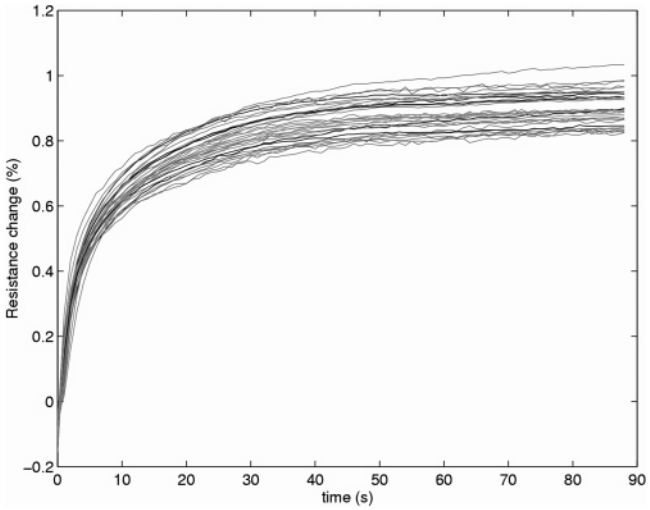

Figure 32. Transient responses of an array of conducting-polymer sensors. Reprinted with permission from ref 283. Copyright 1999 Elsevier.

the coefficients $\{G_i, \tau_i, i = 1, ..., M\}$ from finite-time and finite-precision samples of the transient, the distribution function of time constants will not be unique. An additional problem is the determination of M, the number of exponential components that should be used for the fit. This issue has been known for over 40 years, when Lanczos[270] demonstrated that three-exponential curves with similar time constants could be fitted accurately with two-exponential models with significantly different amplitudes and time constants.

The task of performing a multiexponential fit according to eq 8 is of importance in a variety of disciplines in science, such as gas relaxation kinetics, fluorescence, radioactivity, and nuclear magnetic resonance.[271] A number of methods has been developed, which can be grouped into three classes:[272]

(a) Stepwise or exhaustive methods, which extract the different exponential components in a sequential manner, as in the case of the "graphical" peeling-off.[273] These methods can be considered as nonglobal, because each component is extracted independently of the rest.

(b) Global approximation or least-squares methods, which approximate the experimental transient using a defined number of exponential components by minimizing a figure of merit of the fit. These methods are not aimed at component detection.

(c) Global detection or integral transforms methods. These methods exhibit similarities to (a) and (b): like (a), they are true component detectors, and like (b), they are global, because all model parameters are extracted simultaneously. Representative examples of these methods include the Gardner transform,[274] multiexponential transient spectroscopy,[271,275] and the Pade-Laplace/Pade-Z transform.[276]

In the context of modeling chemical-sensor transients, the vast majority of multiexponential approaches rely on global approximation, arguably due to the broader availability of optimization tools. One of the earliest reports on multiexponential modeling is by Vaihinger et al.,[69] who showed that two or more exponentials were required to provide an accurate fit to experimental data from amperometric sensors. Their results suggest that the extracted time-constants are gas-specific but concentration-independent, whereas the corresponding amplitudes are concentration-dependent. Vilanova et al.[253] used a diffusion-reaction model developed by Gardner[73] to fit transients of metal-oxide sensors exposed to individual gases. Their method provides a single time constant, which is also shown to be gas-specific and concentration-independent. In ref 277, a general diffusion-reaction model is applied to gas mixtures in the low-to-medium concentration range, where interactions between gas species can be ignored. This new model is shown to provide a good fit to the transient response of binary mixtures and yields time constants (one per gas in the mixture) that are also concentration-independent. Eklöv et al.[72] performed curve-fitting to transients of Pt-MOSFET sensors with one-exponential and two-exponential models (see Table 1). While the two-exponential model provided a better overall fit to the experimental transient, the model parameters were shown to be unstable. In contrast, parameters from the single-exponential model had rather high signal-to-noise ratios, comparable to those of the "simple" parameters mentioned already in section 2.2. Galdikas et al.[278] used an array of ten metal-oxide sensors to monitor the freshness of poultry. Samples of poultry meat were stored in a room at 17 °C and 45% RH (relative humidity) and monitored continuously with the sensor array. The authors analyzed the steady-state response of the sensors, as well as the time constants of a biexponential fit to the sensor transients. The steady-state response did not show any significant changes until after 16 h, whereas the smallest of the two time constants started to show significant changes after 2−3 h, which could be used to provide an early detection of food spoilage. Nakamoto et al.[256] used two-exponential models to fit the recovery phase of thickness-shear-mode resonators upon short pulses of various odorants. Parameters of the exponential component with the largest contribution to the response of each sensor were then selected as features. In comparison to the maximum response values of the sensors upon a concentration step, the transient parameters were shown to have better discrimination properties. Di Nucci et al.[279] used one-exponential models to approximate the exposure and recovery transients of thickness-shear-mode resonators to various odorants. Their exponential parameters were shown to provide more discriminatory information than the steady-state response of the sensors, a result that is consistent with those reported in ref 72. Baumbach et al.[280] used a biexponential model to extract information from the transient response of semiconductor microsensors upon steps in their operating temperature. One exponential component was used to explain temperature effects, which were relatively fast owing to the low thermal mass of their microsensors. This term had a fixed (i.e., gas-independent) time constant. The second exponential component was used to explain the slower effects, which were due to the interaction between the gases and the sensing layer. This term had a gas-dependent time constant. The authors showed that a simple decision tree could be used to discriminate CO, H_2, and their mixture using the parameters of the biexponential model.

Global detection techniques have only in a few cases been used to build multiexponential models for sensor transients. Nakamura et al.[281] proposed a system-identification method to estimate the parameters of the exponential components: an autoregressive (AR) model was fitted to the sensor transient,

$$x(k) + \sum_{i=1}^{L} a_i x(k-i) = e(i) \qquad (9)$$

where $x(k)$ is the sensor response at time $t = kT$, L is the

order of the model, and $e(i)$ is the residual error of the model. While AR coefficients $\{a_i\}_{i=1}^{L}$ could be used as features, these parameters (also known as linear predictive coefficients in speech processing) have poor interpolation properties. Instead, by computing the real roots of the characteristic equation, AR coefficients were converted into time constants and amplitudes of a multiexponential model. The results show that, in the case of single gases, 2−3 real roots (exponential components) could be found using the AR model, whereas 3−4 real roots could be found for gas mixtures. However, only one of these exponential components appeared to be stable from run to run (for both single gases and mixtures), which, again, is a hint to the ill-conditioned nature of multiexponential models. Artursson et al.[282] also used multiexponential models to extract information from an electronic tongue based on pulse voltammetry. Their model consisted of two exponential components, which were assumed to represent the two types of currents present during the measurement: Faradaic and capacitive currents. Model parameters were found in a linear-least-squares fashion through a reparametrization of the biexponential model into a homogeneous differential equation. The resulting time constants were then converted into the coefficients of the corresponding characteristic equation; this step ensured that the final features were invariant to the optimization algorithm. These final features were shown to provide better class separability than the original data, while also filtering out experimental noise and providing near-lossless compression.

Rather than finding the discrete coefficients of the multiexponential model in eq 8, one may instead attempt to recover the spectrum of time constants, $G(\tau)$:

$$f(t) = \int_0^\infty G(\tau)\, \mathrm{e}^{-t/\tau}\, \mathrm{d}\tau \tag{10}$$

As pointed out by Samitier et al.,[271] spectral methods have several advantages. First, the number of exponential terms does not need to be known a priori: the individual exponential components will be detected as peaks in the spectrum. Second, spectral methods are global methods, since all the components are obtained simultaneously in the spectrum. Third, the width of the peaks can be used to infer the resolution power of the spectral method, e.g., wider peaks suggest that two or more exponential components with similar time constants have not been resolved. Multiexponential transient spectroscopy (METS) is one such spectral method, which has been shown to be suitable for modeling gas sensor transients.[271,275] METS recovers a spectrum of time constants through a multiple differentiation of the experimental transient on a logarithmic scale; higher spectral resolution can be achieved at higher orders of differentiation at the expense of amplifying experimental noise. Samitier et al.[271] applied METS to the transient response of electrochemical fuel cells; their results showed that the amplitude of the spectral peak was proportional to the concentration of the gases (ethanol, methanol, and 2-propanol in their study), whereas the location of the peak, i.e., the time constant, was gas-specific. The Gardner transform[274] can also be used to recover a pseudo-spectrum $g(\tau)$, in which the amplitude and time constants are coupled: $g(\tau) = G(\tau)\tau$; this condition biases the Gardner transform toward exponential curves for which the product of the amplitude and the time constant of the components are on the same order of magnitude, see, e.g., ref 283. Alternatively, one may employ a fine-grained set of time constants, $\{\tau_i\}$, and solve eq 8 for the amplitudes by using least-squares:

$$\{G_i\} = \arg\min_{G_i}\left[\sum_{k=0}^{N-1}\left(f(k) - \sum_{i=1}^{M} G_i\, \mathrm{e}^{-kT/\tau_i}\right)^2\right] \text{ with fixed } \{\tau_i\}_{i=1}^{M} \tag{11}$$

The resulting distribution of amplitudes $\{G_i\}$ can be treated as a spectral representation of the transient. This approach, also known as the exponential series,[284,285] has the advantage that the minimization problem in eq 11 is linear in the amplitudes, so it can be solved efficiently. In practice, regularization techniques need to be used to ensure a smooth distribution of amplitudes, e.g., by adding an identity matrix to the data covariance matrix that results from solving eq 11 through least-squares.[286]

An alternative approach to model sensor transients has been recently proposed by Carmel et al.[287] Their model is derived from a simple physical description of the measurement system,

$$f_i(t) = \alpha_i \int_0^\infty h_i(u) k(t - t_i - u)\, \mathrm{d}u \tag{12}$$

where α_i is a sensor-specific constant, t_i is the time it takes a gas molecule to travel from the gas inlet to the surface of the ith sensor, $h_i(u)$ represents the probability that a gas molecule absorbed in the ith sensor at time t is still present at time $t + u$, and $k(t)$ is the shape of the injected stimulus (e.g., a step or a pulse in concentration). In ref 287, the Lorentzian decay function $h(t) = \tau_i^2/(t^2 + \tau_i^2)$ was found to provide a good fit to the exposure and recovery transients of both thickness-shear-mode resonators and metal-oxide sensors. Assuming a pulse function of duration T for the injected stimulus, eq 12 can be transformed into the following:

$$f_i(t) = \begin{cases} 0 & t < t_i \\ \beta_i \tau_i \tan^{-1}\left(\dfrac{t - t_i}{\tau_i}\right) & > t_i \le t \le t_i + T \\ \beta_i \tau_i \left[\tan^{-1}\left(\dfrac{t - t_i}{\tau_i}\right) - \tan^{-1}\left(\dfrac{t - t_i - T}{\tau_i}\right)\right] & t > t_i + T \end{cases} \tag{13}$$

From this equation, the model parameters $\{\beta_i, T, t_i, \tau_i\}$ that best fit the experimental transient can be found through a simplex optimization procedure.[288] Doing this for every sensor−analyte pair yields a 4-dimensional feature vector that captures the shape of both the exposure and the recovery transient. In ref 287, the model was validated on experimental data of a hybrid sensor array exposed to 30 different odorants. The results showed that the Lorentzian model parameters $\{\beta_i, T, t_i, \tau_i\}$ provide significantly better recognition performance than standard transient features. Carmel et al.[289] have also shown that the Lorentzian parameters are robust with respect to distortions in the sensor transients, a feat yet to be matched by multiexponential models. The Lorentzian model has also been generalized for the use with sensor transients containing multiple peaks.[290]

9.1.4. Comparative Studies

Eklöv et al.[72] provided a systematic investigation of transient parameters, including simple features such as pulse

heights, integrals, and derivatives at various times during the exposure and desorption phases, and model-based parameters obtained by fitting the experimental transient by means of three types of analytical models (see also Table 1): multiexponential, autoregressive (ARX), and polynomial. The data set consisted of the response of Pt-MOSFET sensors exposed to mixtures of hydrogen and ethanol. Several conclusions can be derived from this study. First, most of the simple parameters have relatively high signal-to-noise ratios, including those from one-exponential models. Second, time-critical parameters such as derivatives, time constants, short integrals, and ARX models tend to be very much influenced by the exact timing of the gas delivery, which renders them unsuitable for pattern-recognition purposes. Third, the selection of model-based parameters based on their fitting performance can be misleading; ARX and two-exponential models provide the bests fits but also have very low signal-to-noise ratios. The main conclusion of the study is that a combination of simple parameters (final response, windowed response, derivatives, and integrals) can provide a performance comparable to parameters obtained through computationally intensive fitting procedures. In a follow-up study, Eklöv et al.[291] performed a feature subset selection on the same database to identify the most relevant parameters. Features were selected using a sequential forward procedure (see section 11.2), where the selection criterion was the root-mean-square reconstruction error from a multilinear regression model. Their results indicated that discriminatory information is broadly distributed in the exposure and desorption transients, with 7 of the top 10 features being "simple" transient parameters.

Delpha et al.[292] compared the performance of parameters of a two-exponential model to the dynamic slope of the transient on a database consisting of six Taguchi sensors. The array was exposed to humid air at different relative humidity levels, to dry Forane 134a (a refrigerant gas), and to humid Forane 134a (different relative humidity levels). The dynamic slope was computed using the sensor response between 1 and 5 min after introduction of the sample, whereas the biexponential parameters were computed from the entire transient, once the sensors had reached steady state in a 60 min long exposure. The prediction performance of the biexponential parameters was 60% on the test data but increased to 100% when combined with the dynamic slope. Although no performance results were provided for the dynamic slope alone, the authors concluded that the biexponential and dynamic slope parameters provide complementary information.

Distante et al.[293] compared several transformation and feature extraction techniques using experimental data from an array of metal-oxide sensors exposed to concentration pulses of acetone, hexanal, and pentanone, each in humid and dry air. In this study, the authors advocate the use of a discrete-wavelet-transform (DWT) technique to extract transient information. Unlike the Fourier transform, which is only localized in frequency only, wavelets are localized in space and frequency, which renders them more suitable for the analysis of transient signals since they capture both spectral and temporal information. DWT coefficients were compared to those of a fast Fourier transform (FFT) as well as with feature vectors containing the integral and derivative in several locations of the transient. Their results show that the DWT provides the best performance, with integral features being a very close second. Derivative and FFT features appear to be only marginally worse than the previous two techniques.

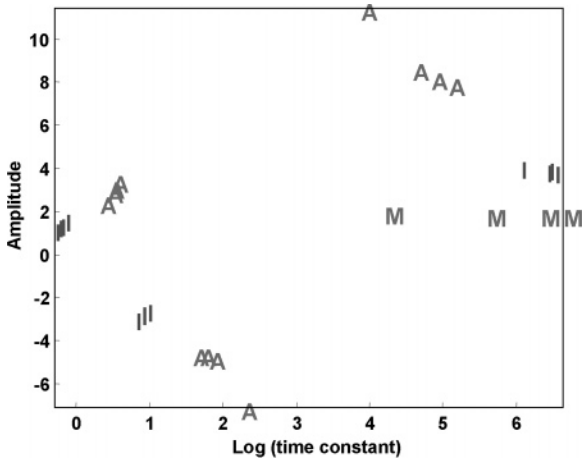

Figure 33. Time constants and signal amplitudes extracted from a 5−6V thermal transient of a TGS2620 sensor by the Pade-Z method: A, acetone (10^{-4} volume %); I, isopropyl alcohol (10^{-1} volume %); M, ammonia (1 volume %). Four samples of each analyte were extracted. Reprinted with permission from ref 286. Copyright 2003 Elsevier.

Gutierrez-Osuna et al.[286] compared the performance of METS,[275] the Pade-Z transform,[276] transient oversampling,[196] the exponential series in eq 11, and steady-state isothermal responses. All these methods were evaluated using a data set of Taguchi sensors exposed to various concentrations of acetone, isopropyl alcohol, and ammonia under a stepwise change in temperature. As shown in Figure 33, the Pade-Z was able to recover several stable multiexponential models for the three analytes, though with different numbers of exponentials. Since most pattern-recognition techniques assume fixed-length feature vectors—but see rational kernels[294] for an exception—the Pade-Z models were transformed into the coefficients of a fixed-length Taylor series expansion. Experimental results show that the exponential series method provides the best performance, whereas METS, Pade-Z, and transient oversampling show comparable performance, which is still better than that of using the steady-state response.

Shafiqul Islam et al.[295] compared a number of "simple" parameters, such as levels, slopes, and integrals at different times, to the coefficients of a third-order polynomial fit of the sensor transient. The experimental data set consisted of responses of an array of thickness-shear-mode resonators to various solvent exposures. While the simple parameters provided better separability than the polynomial coefficients, a combination of these two types of features appeared to improve the overall performance of the array. Altogether, these studies indicate that models that provide the best curve-fitting results do not necessarily contain the most analytical information. Simple parameters should be used first, since they tend to have higher signal-to-noise ratios, though complex parameters can sometimes provide complementary information.

9.2. Temperature-Modulation Analysis

It has long been known that the selectivity of metal-oxide sensors is greatly influenced by the operating temperature of the device, since the reaction rates of different volatile compounds and the stability of surface-adsorbed oxygen species are a function of the temperature.[296] As a result,

modulation of the operating temperature can give rise to gas-specific temporal signatures, which provide a wealth of discriminatory and quantitative information. One of the earliest reports on the use of temperature modulation is a 1975 patent by Le Vine, in which a sensor was operated at two temperatures: a low temperature, at which the sensor was preferentially selective to CO, and a higher temperature, at which the sensor was less selective, and which was used to purge the sensor of CO.[297] However, it is the modeling work of Clifford and Tuma[65] and the algorithms of Sears et al.[298] that are often credited for bringing the concept of temperature modulation to the attention of the sensors community. An excellent account of early work on temperature modulation in the 1980s and 1990s was written by Lee and Reedy.[22] Hence, we will focus our review on later work (1998−2007), with an emphasis on computational methods for extracting information from temperature-modulated signals.

Temperature-modulation approaches for MOS sensors can be broadly classified into two categories: (i) thermal transients and (ii) temperature modulation. In thermal transients, the sensor is driven by a step or pulse waveform in the heater voltage, and the discriminatory information is contained in the thermochemical transient induced by the fast change in temperature. Thermal transients have the advantage that one does not need to wait for the sensor to stabilize following power-up, which allows for an immediate evaluation of the signal. In addition, by intermittently powering down the sensor, a significant reduction in power consumption can be achieved. Data analysis for thermal transients resembles that of concentration transients, so that the methods described in section 9 will be generally applicable here as well (see, e.g., ref 286 for an example of multiexponential methods for thermal transients).

For temperature modulation, however, the sensor is subjected to a continuous, sometimes periodic, heater voltage variation. To help resolve the various peaks in sensitivity that may occur during such a cycle, a slowly varying sine wave is often used.[299] If the heater waveform is slow enough to allow the sensor to settle at the respective temperatures, the behavior of the sensor at each temperature may be treated as a "pseudo-sensor" by virtue of the relationship between operating temperature and sensor selectivity. It is broadly accepted that temperature cycling is the most promising approach to temperature modulation[22] and will, therefore, be the focus of this section.

Information from the temperature-modulation response can be captured in a variety of ways, but there are three general approaches that parallel those of transient analysis. First, the sensor response can be oversampled at a number of points during the modulation pattern to form a feature vector.[300,301] Second, a number of "simple" features can be extracted from the response, such as maxima/minima, and their corresponding occurrence times.[301−303] Finally, transform methods such as the fast Fourier transform (FFT) or the discrete wavelet transform (DWT) may be used to convert the temporal response into the frequency or time-frequency domain, respectively. Most of the early work on transient analysis relied on the FFT; see, e.g., refs 19 and 304−308. Recent work, however, indicates that the DWT is a much better choice for processing temperature-modulated patterns, which are markedly nonlinear and nonstationary. The interested reader is referred to ref 309 for a brief introduction to wavelet analysis or to ref 310 for a more thorough presentation.

Corcoran et al.[301] performed a systematic comparison of temperature-modulation parameters. An array of eight Taguchi sensors was exposed to the headspace of three types of loose-leaf teas while modulating the operating temperature with a triangular waveform (period = 240 s, temperature range = 250−500 °C). Three types of features were extracted from the sensor conductance measurements: single temperature measurements (STM), dynamic parameters (dynamic parameter method, DPM), and total signature differences (TSDs). In the STM, a single measurement was extracted from the temperature-modulated response, yielding an 8-dimensional feature vector; the results of this method served as a benchmark. In the DPM, eight different "simple" measurements were obtained, including the derivative maxima/minima and their occurrence times, resulting in a 64-dimensional feature vector. In the TSD method, the temperature-modulated response was oversampled at 26 different times, yielding a 208-dimensional vector. In addition, a genetic algorithm (GA) was used to select a feature subset from the DPM feature vector using a measure of between-to-within-class scatter as a figure of merit.[217] Validation on unseen test data using multilayer perceptrons showed that, despite its relatively high dimensionality, the TSD method provided the best overall performance. DPM features ranked second, whereas STM features performed worst, as expected. Feature subsets from the GA procedure ranked (on average) between STM and DPM features. These results suggest that there was more information in the temperature-modulated response than could be captured by using the simple DPM features. Gutierrez-Osuna et al.[300] have investigated the effect of the modulation frequency on the information content and the stability of the sensor patterns. Two metal oxide sensors were exposed to four analytes at dilution levels close to their isothermal detection threshold. The sensors were heated using sinusoidal heater voltage variations of different frequencies (125 mHz, 250 mHz, 500 mHz, 1 Hz, 2 Hz, and 4 Hz) and then exposed to the four analytes during 10 consecutive days. The authors showed that the classification performance decreased monotonically with increasing frequency, since the sensors approached isothermal behavior. Normalization of the raw temperature-modulated response patterns in the [0, 1] range was shown to minimize drift effects at low modulation frequencies, where sufficient discriminatory information is preserved in the shape of the response, but not at high frequencies, at which information tends to be contained in the dc response of the sensor.

Building upon extensive prior work,[311−315] Nakata et al.[316] analyzed the nonlinear properties of a TGS sensor exposed to various target gases under sinusoidal temperature variation. The purpose of this study was to investigate the effect of the sinusoidal dc offset (T0) and the modulation frequency on the sensor response. The effect of T0 is shown in Figure 34, which indicates that the optimum temperature range is dependent on the gas species to be detected. FFT analysis showed that the concentrations and the kinetics of the different gas species were reflected in the higher-order harmonics of the signals.[317] Thus, the authors argue that the nonlinear characteristics of chemical sensors should not be viewed as a drawback but rather as a property to be exploited for discrimination purposes. In a subsequent study, Nakata and Ojima[318] showed that these higher-order harmonics could be used to estimate the concentration of a target analyte, even in the presence of water vapor. More recently, Nakata et al.[319,320] have proposed a method to increase the discrimina-

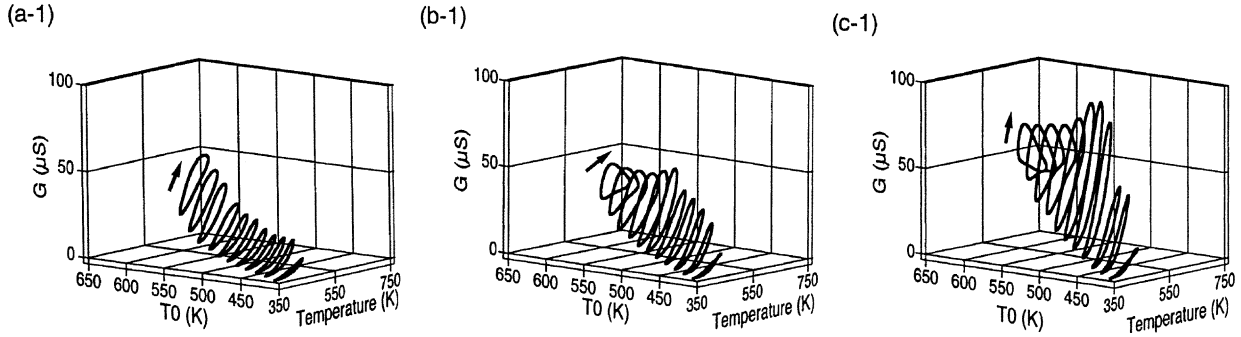

Figure 34. Dynamic response of a semiconductor sensor to (a) methane, (b) ethane, and (c) propane in different temperature ranges with a modulation frequency of $f = 0.04$ Hz. Reprinted with permission from ref 316. Copyright 1998 Elsevier.

tion capabilities of the nonlinear sensor responses by applying a second-harmonic perturbation to the temperature-modulation program. For a given heater voltage modulation, $v_1(t) = v_{a0} + v_{a1} \cos 2\pi f_0 t$, the authors showed that superimposing a second heater voltage function of the form $v_2(t) = v_{a1}/2 \cos(4\pi f_0 t + \theta_2)$ can have a unique effect on the nonlinear sensor response to each target analyte. Thus, by properly selecting the phase shift θ_2 of the second-harmonic heater voltage modulation $v_2(t)$, the sensor response can be optimized for different analytes.

Other authors have also investigated temperature-modulation procedures in recent years. Fort et al.[18] have compared the performance of chemical transients, temperature transients, and temperature modulation. In this study, an array of eight metal-oxide sensors was exposed to the headspace of water solutions containing basic constituents of wine. Principal-components analysis suggests that the chemical transients can only be used to detect the presence of esters. In contrast, a PCA of the first, third, and fourth harmonics of the temperature-modulated response shows a clear discrimination of the different solutions. These results suggest that temperature modulation provides maximum discriminatory power.[321] Schütze et al.[303] used a single semiconductor gas sensor to discriminate six model substances (benzene, diethyl ether, isopentane, methyl butyl ether, methyl alcohol, and propylene oxide). The sensor was operated using two different temperature programs (each consisting of several steps in temperature during a period of 20 s). Then, a number of "simple" features was extracted, such as signal levels at different temperatures and response slopes after a temperature change. The resulting feature vector was processed in a hierarchical fashion, so that different types of features were used to discriminate subgroups of target gases. Most interestingly, the authors showed that a division of the temperature-modulated conductance-value pattern by its average value almost entirely eliminated the effects of relative humidity in the sample and also improved the repeatability of the responses over a period of several months. Huang et al.[322] investigated the effects of temperature modulation, frequency, and waveform on the response patterns of thick-film tin-oxide sensors exposed to various gases (butanone, acetone, ethanol, methanol, formaldehyde, and cyclohexanone). The authors compared the sensor responses to temperature pulse trains in five different temperature ranges (25−100, 100−150, 150−200, 200−250, and 250−300 °C). In the low-temperature ranges, the sensor response were shown to be monotonic (first-order response) and did not carry much information, since most reactions occur at the surface level. At high temperatures, response patterns became complex and characteristic of the target gases, as they increasingly involved bulk reactions. The authors also compared several temperature-modulation waveforms, including rectangular, triangular, sawtooth, sinusoidal, and trapezoidal shapes. Each waveform gave rise to a unique sensor-response pattern, which the authors ascribed to characteristic changes in the actual surface temperatures of the sensor.

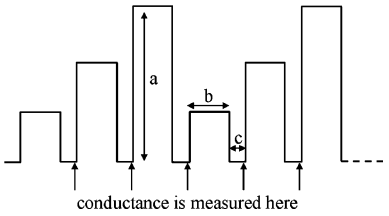

Figure 35. Temperature-programmed sensing: (a) temperature pulse amplitude (20−450 °C), (b) pulse duration (10−300 ms), and (c) delay (5 ms). Notice that the conductance is measured immediately after the sensor returns to room temperature. Reprinted with permission from ref 21. Copyright 1998 Elsevier.

For well over a decade, Semancik and co-workers at the National Institute of Standards and Technology have used temperature programming for microhotplate-based gas sensors.[21,51,323−328] While a review of this technology will be available in an article by Benkstein and Semancik in this issue,[42] it is noteworthy that this research group uses a unique approach to measuring the conductivity of the sensors. As illustrated in Figure 35, conductance is always measured at room temperature, so that thermally controlled chemical effects can be separated from temperature-dependent changes in the sensing material; this is possible because of the very low thermal time constant of the microhotplates, which has been estimated to be on the order of a few milliseconds.

A great deal of work on temperature modulation has been performed by Llobet and co-workers during the past few years[268,329−334] (see also section 11.3). In ref 335, the authors compared the DWT and the FFT for the purpose of extracting information from the response of a tin-oxide microhotplate sensor exposed to mixtures of CO and NO_2. The temperature of the sensor was modulated between 243 and 405 °C by means of a 50 mHz sinusoidal waveform. Four temperature-modulation cycles were used to compute the FFT, from which the amplitudes of the first six harmonics were used as features. In contrast, a single temperature-modulation cycle was used to compute the DWT. Experimental results show that the DWT leads to improved separability as compared to the FFT. In addition, the DWT coefficients can be obtained from a single modulation cycle, whereas the FFT require a larger number of cycles to accurately estimate the spectral content of the signal (a more in-depth analysis of these results may also be found in ref 330). Later studies have also suggested (through simulation) that DWT features are more

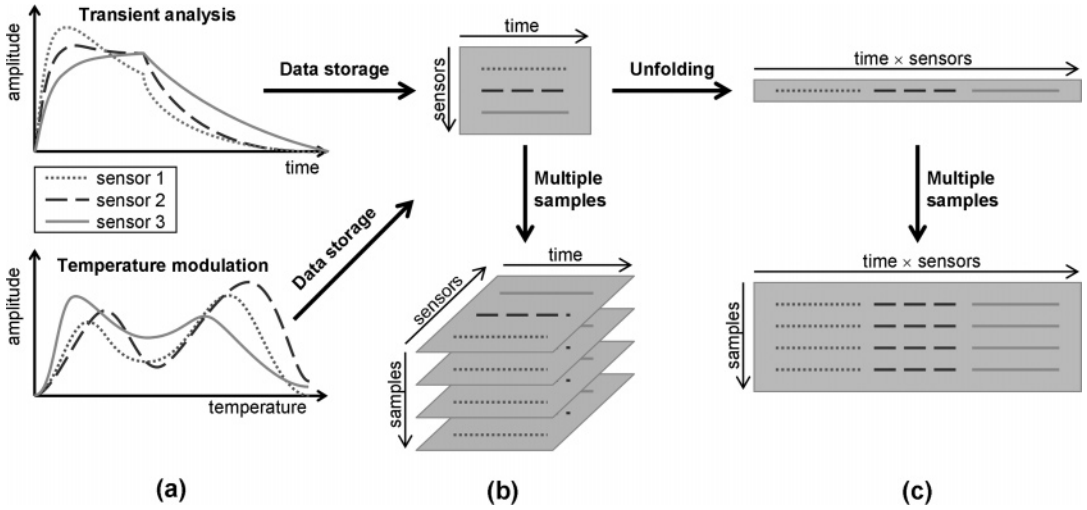

Figure 36. (a) Transient or temperature-modulated response of a sensor array naturally leads to (b) a 2D matrix per sample, and a 3D matrix for all the samples in the dataset. (c) Unfolding the data leads to the traditional 2D data structure, where each row represents a sample and each column represents a feature.

robust than FFT features to additive noise and additive drift.[334] Ding et al.[336] have also compared the DWT and FFT for the purpose of extracting information from temperature-modulated signals. Two commercial metal-oxide sensors were exposed to CO, H_2, and CH_4 at concentrations ranging from 50 to 1000 ppm under a 20 mHz sinusoidal temperature-modulation signal. Sensor signals were first normalized to the [0, 1] range and then processed with the DWT and FFT. The results showed that the DWT features are gas-dependent and fairly stable across various concentrations; more importantly, these features were shown to be repeatable across sensor responses recorded 4 months apart. In contrast, FFT harmonics were shown to be noisier and had a more pronounced concentration dependence.

10. Multivariate Calibration

Once dynamic features have been applied using the techniques reviewed in section 9, the experimenter will usually build a calibration model to obtain the dependent variables, such as class labels or concentrations, from those features. A number of pattern-recognition techniques are available at this point, which include various statistical methods (nearest-neighbor or quadratic classifiers), multilinear regression methods (partial least-squares (PLS) or principal-components regression), and neural networks (multilayer perceptrons, radial basis functions, or support vector machines), to mention but a few. These models have been extensively reviewed in a number of recent articles and book chapters.[195,199,217,337,338] For this reason, we will focus our attention on calibration techniques that are particularly well-suited to handle the raw time-dependent response of the sensor, without the need of a preceding feature-extraction stage.

10.1. Multiway Analysis

The transient (or temperature-modulated) response of a chemosensor array is naturally represented as a two-dimensional matrix, where each row corresponds to the response of a sensor over time (or operating temperature), and each column represents the response of the array at a particular time or temperature. When the time-dependent response of the array is recorded for multiple samples, then the data set is naturally represented as a 3D matrix, a tensor, as shown in Figure 36b. While it is possible to unfold this data set into a 2D structure, where each row represents a sample and each column represents a variable (see Figure 36c), this "unfolding" adds extra degrees of freedom to the model, because it treats the response of each sensor at a given time, $[x_1(t), x_2(t), ..., x_N(t)]^T$, as an independent variable, where in reality these measurement data were collected at the same time or at the same temperature. Preserving the multiway structure of the data in Figure 36b can lead to a more parsimonious, i.e., simpler, solution, which is likely to be more robust and easier to interpret. It may also provide the "second-order" advantage discussed in section 1 so that target analytes can be quantified even in the presence of unknown interferents.[339,340] Despite these potential advantages, however, multiway methods have only recently received attention in the "electronic nose" literature.[197,198]

A number of decomposition methods have been developed to analyze multiway data, with the most common being parallel factor analysis (PARAFAC),[341,342] Tucker3,[343] and unfold-PCA. As illustrated in Figure 37b, PARAFAC decomposes a 3-way data matrix **X** (a tensor) in a trilinear fashion,

$$x_{ijk} = \sum_{f=1}^{F} a_{if} b_{jf} c_{kf} + e_{ijk} \qquad (14)$$

where F is the number of factors in the decomposition. Figure 37b shows the case for $F = 2$. The solution to this decomposition, i.e., the loading matrices **A**, **B**, and **C**, is commonly found by a method known as alternating least-squares (ALS), which works as follows: first, two of the loading matrices (say **B** and **C**) are initially set to a good starting value,[339] and the third matrix (**A**, in this case) is estimated by least-squares regression from **X**, **B**, and **C**. This process is subsequently repeated for matrix **B** and then **C**, and the cycle (reestimate **A**, then **B**, then **C**) is repeated until convergence occurs. It can be shown[339] that ALS will improve the solution with every iteration. The algorithm can be computationally intensive, but several acceleration strategies have been devised.[339] More importantly, PARAFAC is also known to produce a unique solution under certain rank constraints (e.g., the sum of linearly independent columns in matrices **A**, **B**, and **C** must be larger than or equal to $F +$

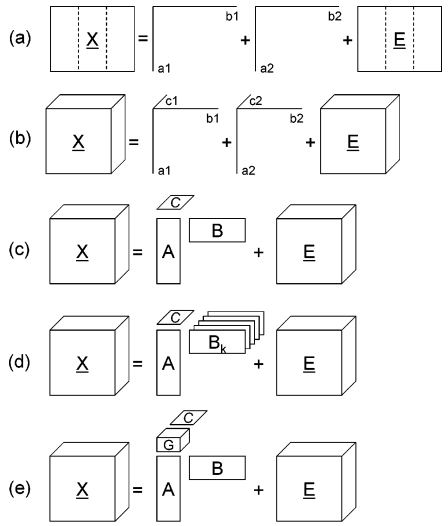

Figure 37. (a) Bilinear decomposition with unfold-PCA. The three-way data matrix is first unfolded into a two-way matrix (see Figure 36 for an example) and then modeled as a sum of terms, with each term being the outer product of two vectors. The term *E* is the residual error. (b) Trilinear decomposition with PARAFAC. In this case, the three-way data matrix is modeled with three factors, one per dimension. The term *E* is also a residual error. (c) PARAFAC illustrated in compact form. (d) PARAFAC2 is an extension of PARAFAC, which allows each sensor, *k*, to have its own time loadings, $\mathbf{B}_k$. (e) Tucker 3 is an extension of PARAFAC, which introduces a core matrix **G** to allow different interactions among loadings. Adapted from ref 347.

2). Unlike PCA, where the loadings (eigenvectors) and scores (principal components) can be rotated without increasing the reconstruction error, there is only one rotation of the PARAFAC loadings that provides a minimum error: using PCA, one can replace the top eigenvectors with linearly independent combinations of these (which constitutes a rotation) and will still capture the same percentage of the total variance in the data. Unlike two-way data, however, centering and scaling (see section 7) must be done carefully to preserve the trilinearity of the data. The reader is referred to Gurden et al.[344] for a discussion of preprocessing strategies for multiway data.

Tucker3 (named after Ledyard R. Tucker, who proposed the model in 1966[345]) provides a more flexible decomposition of the data matrix **X**, where the main difference with PARAFAC is the addition of a "core" matrix **G**, which defines how the individual loadings in the different modes (**A**, **B**, and **C**) interact:

$$x_{ijk} = \sum_{d=1}^{D}\sum_{e=1}^{E}\sum_{f=1}^{F} a_{id} b_{je} c_{kf} g_{def} + e_{ijk} \qquad (15)$$

Finally, unfold-PCA first converts the tensor **X** into a 2D matrix (see parts b and c of Figure 36) and then performs a bilinear decomposition:

$$x_{ij} = \sum_{f=1}^{F} a_{if} b_{jf} + e_{ij} \qquad (16)$$

The decompositions performed by each of the three methods are graphically summarized in Figure 37 (parts a−c and e). It can be shown[346] that PARAFAC is a "constrained" version of Tucker3, which, in turn, is a constrained version of unfold-PCA. Here, "constrained" means that there are fewer degrees of freedom to fit the data. An example by Bro[339] will help one to understand this hierarchy of models. Consider an experiment in which 10 samples have been collected from 20 sensors, with each sample measurement extending over 100 s. These data can be represented by a $10 \times 100 \times 20$ matrix. Assume that we seek to decompose these data into five factors. For unfold-PCA, this will produce a model with 10 500 parameters (!), whereas Tucker3 will require 775 parameters and PARAFAC will require only 650 parameters. Clearly, unfold-PCA will provide the best fit to the data in terms of mean-square-error (in fact, PCA does provide optimal reconstruction in the mean-square sense[180]), whereas Tucker3 and PARAFAC will produce larger errors. But, as has been pointed out in section 9.1, curve-fitting accuracy does not necessarily lead to good analytical performance. If PARAFAC returns results that are reasonable, then it is very likely that the extra degrees of freedom in Tucker3 and unfold-PCA will be used to model noise in the data.[339] Thus, all things being equal in terms of curve-fit (and sometimes things not being equal), the simpler model should always be preferred.

In the context of chemical sensor arrays, however, PARAFAC may be too restrictive, since it is unable to model shifted profiles or different shapes; this may occur, for instance, if the sensors are placed at different locations along the manifold or have intrinsically different dynamics. In these cases, the additional flexibility of Tucker3 may be helpful.[347] However, this comes at a price: unlike PARAFAC, Tucker3 is sensitive to rotational ambiguities, i.e., a unique solution does not exist. Alternatively, an extension of PARAFAC known as PARAFAC2[348] may be used in some cases. As illustrated in Figure 37c, PARAFAC2 allows each sensor to have a unique set of time loadings so that PARAFAC2 can deal with non-trilinear data (as Tucker3 does), while a unique solution is ensured—provided that some constraints on the $\mathbf{B}_k$ matrices are met.[197]

Shaffer et al.[349−351] provided one of the first studies of multiway analysis methods for sensor-based instruments. In this work, the authors developed a second-order instrument that consisted of an array of five surface-acoustic-wave sensors and a preconcentrator unit. Samples of four nerve agents (ethyl *N*,*N*-dimethylphosphoramidocyanidate, GA; *O*-ethyl-*S*-(2 isopropylaminoethyl)methyl phosphonothiolate, VX; pinacolylmethylphosphofluoridate, GD; isopropylmethylphosphonofluoridate, GB) and one nontoxic simulant (dimethylmethylphosphonate, DMMP) were absorbed in a preconcentrator unit in the presence of several interferents (water, bleach, ammonia, sulfur dioxide, isopropanol, dichloroethane, diesel exhaust, and jet fuel) and then subsequently rapidly desorbed by heating the sorbent column, a process that additionally provided some chromatographic separation of the mixture components. The response of the instrument to a mixture of water, gasoline, and one nerve agent (GA) is shown in Figure 38a. To analyze these responses, the authors compared three types of score plots: (1) PCA performed on the peak signal amplitude of each sensor response, (2) PCA of the peak signal amplitude and the peak location, and (3) unfold-PCA on the entire sensor transient. As shown in Figure 38 (parts b−d), combining peak amplitude and peak location provides better discrimination performance than using peak amplitudes alone; unfold-PCA further decreases the spread of the nerve agent VX and the dimethylmethylphosphonate DMMP clusters, but it also seems to impair the discrimination of the GA samples. A

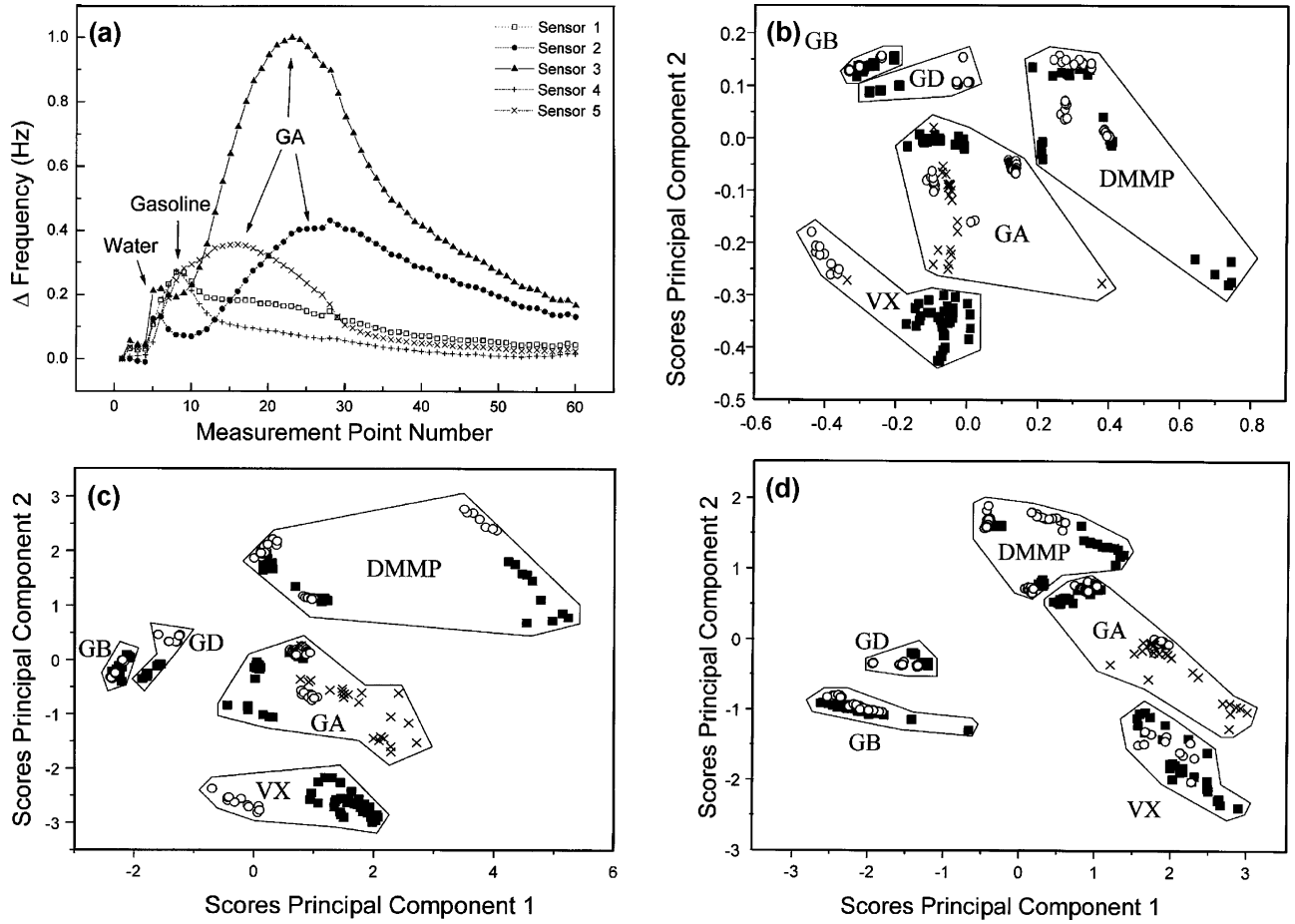

Figure 38. (a) Response of an array of SAW sensors to the thermal desorption of a preconcentrated ternary mixture of one nerve agent (GA) and two interferents (water and gasoline). Score plots of (b) PCA of the peak amplitudes, (c) PCA of the peak amplitudes and their locations, and (d) unfold-PCA on the entire sensor transient. Training and test data are depicted as solid squares and open circles, respectively, whereas mixtures of GA with interferents are depicted as crosses. GA, ethyl-*N*,*N*-dimethylphosphoramidocyanidate; VX, *O*-ethyl-*S*-(2-isopropylaminoethyl)methylphosphonothiolate; DMMP, dimethylmethylphosphonate; GD, pinacolylmethylphosphofluoridate; GB, isopropylmethylphosphonofluoridate. Reprinted with permission from ref 351. Copyright 1998 Wiley, New York.

visual comparison of PCA scatter plots, however, can be misleading; a more objective measure of performance is the predictive accuracy on test data. To this end, the authors compared the performance of two classifiers (nearest-neighbors and linear discriminants) on three feature vectors: (1) the peak amplitudes, (2) the peak amplitudes and their locations, and (3) the entire sensor transient. Using the entire sensor transient provided the highest performance (96−100% correct classification), closely followed by peak amplitudes and locations (94−98%), and then peak amplitudes (81−83%). A second comparison of four models was performed: unfold-PCA, multiway-PCA (PARAFAC), unfold-PLS, and multiway-PLS. This comparison, however, failed to show any advantage of PARAFAC and multiway-PLS over their unfolded counterparts. Interestingly, the location of the peaks in Figure 38a is sensor-dependent, and the authors report a shift of those peak locations with increasing analyte concentration; both results suggest that the PARAFAC model may have been too restrictive for these data. Furthermore, none of these four models performed better than a direct classification using the raw data. It is quite possible, though, that the lack of improvement may have been a result of ceiling effects, since the raw data could already be classified with 96−100% success.

Skov and Bro[197] analyzed the transient response of an array of 12 metal-oxide sensors exposed to three kinds of licorice (good, bad, and fabricated bad). The authors applied various types of baseline compression and scaling, and compared the performance of three decomposition methods: PCA on the steady-state signals of the sensors, PARAFAC, and PARAFAC2. For each of the PARAFAC models, a two-factor decomposition was performed. Figure 39a shows the loadings of the PARAFAC decomposition, whereas parts b and c of Figure 39 shows the loadings of PARAFAC2 (two loadings per sensor). While the loadings of PARAFAC are easier to interpret, those of PARAFAC2 indicate that the starting time of the transient responses of some sensors may be shifted, which renders the PARAFAC model too inflexible (interestingly, the "electronic nose" used in this study contained two sensor chambers, which might explain why some sensor transients appear to be shifted in time). This interpretation can be confirmed by analyzing the scores in parts d and e of Figure 39, which show that PARAFAC2 provides much better separability of the three types of licorice. Figure 39f shows the scores when only the steady-state signal of each sensor is used as a feature. While PARAFAC2 seems to return more compact clusters, it also appears that the steady-state signals already contain sufficient information to solve the discrimination problem.

Padilla et al.[198] have also used PARAFAC to analyze the transient responses of gas sensors. In this study, an array of 13 metal-oxide sensors was exposed to the headspace of

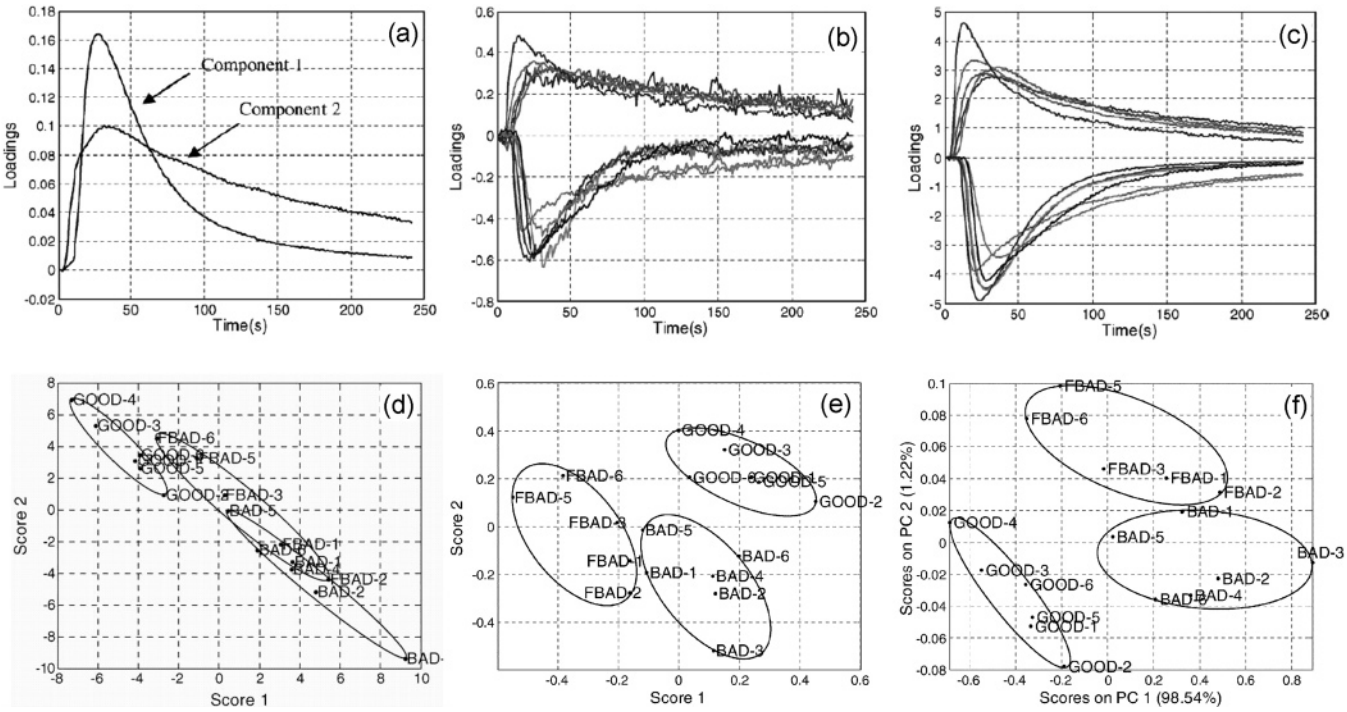

Figure 39. (a) Loadings 1 and 2 of a two-factor PARAFAC decomposition. These loadings define matrix **B** in Figure 37c. (b) Loading 1 (one per sensor, as illustrated in Figure 37d) in a two-factor PARAFAC2 decomposition. (c) Loading 2 of the same two-factor PARAFAC2 decomposition. Loadings 1 and 2 in (b and c) represent the matrix $\mathbf{B}_k$ in Figure 37d. Scores of the samples with (d) PARAFAC, (e) PARAFAC2, and (f) PCA; the PCA decomposition used only the maximum response of each sensor. Separability in (d) is rather poor, which indicates that the PARAFAC model is too restrictive to explain the data. In contrast, PARAFAC2 provides significantly better separability. Note that PARAFAC2 is only marginally better than PCA; this result suggests that the peak response of the sensors already contains most of the discriminatory information. Reprinted with permission from ref 197. Copyright 2005 Elsevier.

potato chips with different amounts of flavor agents. To check for trilinearity, the 3-dimensional data set (samples × sensors × time) was unfolded onto each one of the three dimensions, and the number of factors was computed for each unfolded matrix by means of singular value decomposition. Each of the three matrices appeared to have the same number of factors, which suggested that the data were trilinear.[347] The dataset was preprocessed by means of differential baseline correction and standard normal variate normalization methods (see section 7); these techniques were found to preserve the trilinearity of the data, an important safety check before applying PARAFAC. Using a core-consistency diagnosis proposed by Bro and Kiers,[352] the authors determined that the dataset was best described using a three-factor model. The corresponding scores (matrix **A** in Figure 37c) were then used to predict the concentration of the flavor additives by means of an inverse-least-squares regression model. A correlation coefficient of 0.902 between true concentrations and predictions on calibration data was found using the PARAFAC-ILS model; predictions on a test data set were comparably accurate.

10.2. Dynamical Models

Dynamical models may also be used to process information directly from the sensor transient, i.e., without the use of a feature extraction stage. Various types of recurrent neural networks, as well as hidden Markov models, have been used for this purpose, as will be reviewed in this section.

Pardo et al.[241] investigated various approaches to model the nonlinear inverse dynamics of a gas sensor array. The overarching goal of this study was to build a model that could predict the inputs (concentration pulses) to a gas sensor system from the sensor responses, in particular for rapid variations of the input concentrations. This inverse problem is known to be ill-posed because of the collinearity across sensors, nonlinearities in the steady-state and the response dynamics of the sensors, and long-term drift, and the fact that the sensors and the flow manifold act as low-pass filters. An array of four thickness-shear-mode resonators with GC stationary-phase coatings was exposed to mixtures of toluene and octane, which were delivered as odor pulses of Gaussian-distributed concentrations. It has to be noted here again that, due to the very short response time of polymer-coated thickness-shear-mode resonators, there is the risk of recording the dynamic gas manifold characteristics rather than those of the sensors. Several models were explored, which included static models, linear autoregressive models, Elman networks, Wiener series expansions, radial-basis function (RBF) networks, and multilayer perceptrons (MLP). In the static models, the concentration inputs were predicted directly from the sensor outputs on a sample-by-sample basis, whereas in the linear autoregressive models, concentration inputs were predicted from a short history of the sensor outputs. Elman networks[353] are recurrent neural networks whose hidden units have feedback connections, which serve as a short-term memory to enable the model to "remember" preceding inputs. Wiener series expansions are a parametric model with finite memory that approximates a nonlinear system by a series of functionals, with the advantage of this model being that the parameters can be estimated through least-squares methods.[239,240] Finally, radial-basis-function networks and multilayer perceptrons are feedforward neural networks, which act as nonlinear regression models;[216] short-term memory in these models was implemented by means of tapped-delay inputs. Results of this study are summarized

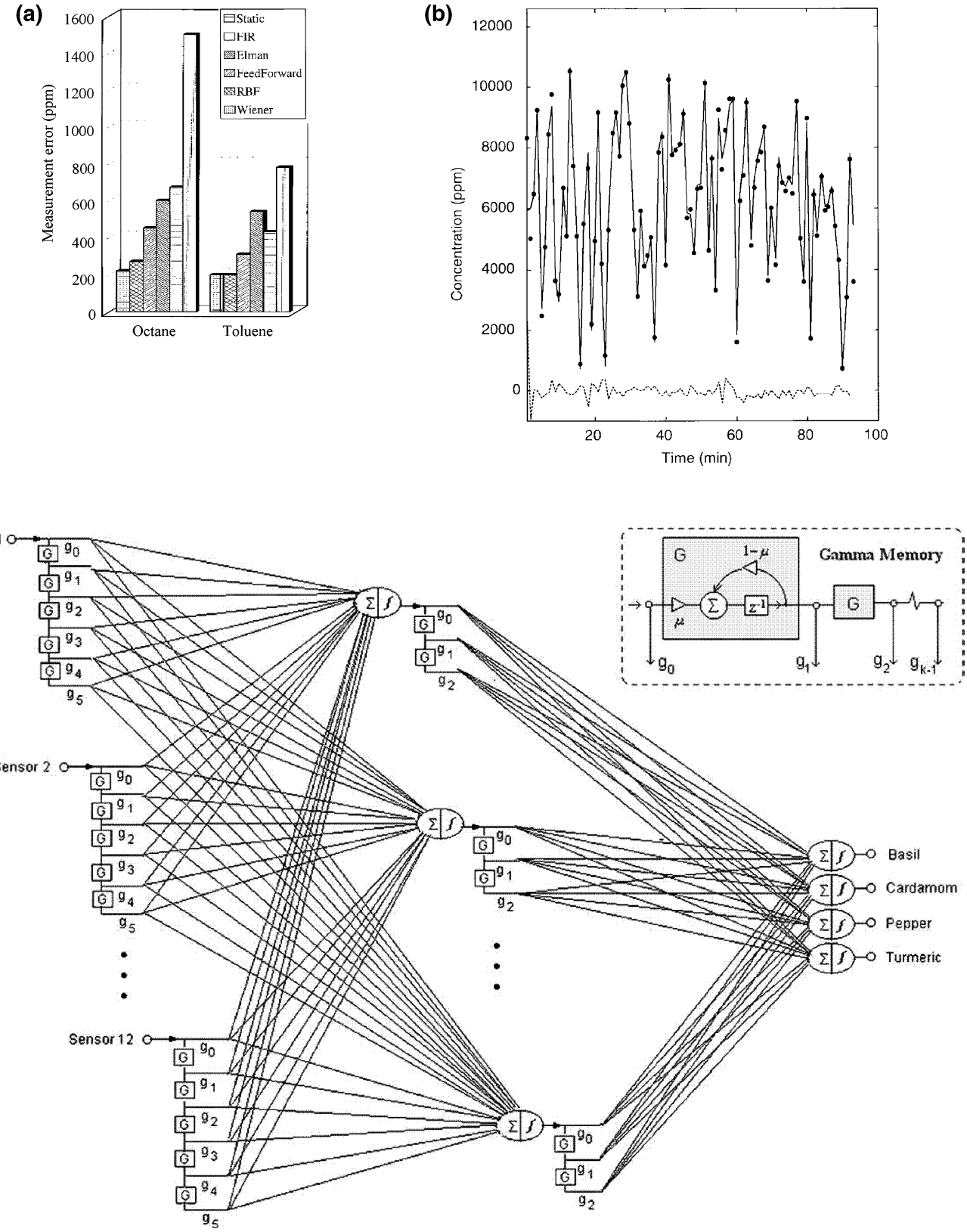

Figure 40. (a) Average prediction capability of various inverse dynamical models. (b) True concentration of toluene (dotted line) vs predictions of the Wiener series expansions (solid line); residual errors are shown as dashed lines. Reprinted with permission from ref 241. Copyright 1998 IEEE. (c) Structure of the time-delay neural network as used in the study of Zhang et al.[357] Reprinted with permission from ref 357. Copyright 2003 Elsevier.

in parts a and b of Figure 40. The best results were obtained by the Wiener series, closely followed by the RBF network. Surprisingly, the Elman network did not perform better than the simple linear model. As expected, the static model showed the poorest performance, since it does not account for the dynamics of the system.

Roppel et al.[354] used an Elman network to classify analytes using the transient responses of an array of 15 metal-oxide

sensors. Sensor transients were converted into a binary pattern by means of an adaptive-threshold method and then passed on to an Elman network. A network with 15 input units (one per sensor), 15 hidden units, and 9 outputs (one per analyte class) was trained on a set of 27 samples (3 samples of each analyte). For validation purposes, the 27 training samples were presented in a different (random) order. Since the network is time-dependent, this validation procedure can give some indication of the degree to which the network is able to generalize. However, no results were reported on the generalization performance of the network with respect to previously unseen transient signals. More recently, Tan and Wilson[355] have used hidden Markov models (HMMs)[356] for outlier detection. HMMs are the "gold standard" in automatic speech-processing applications because of their ability to model nonstationary time series. The goal of the study by Tan and Wilson was to determine whether or not HMMs could be used to discriminate "normal" transient responses of a sensor from "unhealthy" ones. Training data consisted of the transient responses of 10 polymer-coated sensors to a concentration step of 5 different analytes. Ten HMMs (1 per sensor) were trained on multiple transient responses to each of the 5 analytes. For validation purposes, each HMM was then tested on transient responses of a different sensor to each of the analytes. HMMs were shown to be able to distinguish "normal" responses (transients of the specific training sensor) from "unhealthy" ones (transients of any other sensor).

Zhang et al.[357] used a time-delay neural network (TDNN) to classify four different types of spices using the transient responses of an array of 12 conductive-polymer sensors. As shown in Figure 40c, a TDNN is a feed-forward network that has local memory in the form of a tapped-delay line (a first-in-first-out buffer that stores previous values, a very simple form of (short-term) memory) at the inputs and the hidden units. In this study, the tapped delay was replaced by a gamma memory,[358] which can be thought of as a cascade of low-pass filters (see insert in Figure 40c). The TDNN was compared to a conventional MLP and a linear-discriminant-function (LDF) method, both trained on the steady-state responses of each sensor. The TDNN was able to correctly classify 100% of the samples in a separate test set, whereas the MLP and LDF provided 63% and 59% correct classification. While these results cannot be extrapolated to other data sets, the large improvement in the classification rate suggests that the TDNN-gamma model is well-suited to exploit differences in the transient responses of gas sensors.

11. Array Optimization

As described in the previous sections, a wide variety of sensors and feature extraction methods are available to the experimenter when approaching a new sensing problem. Which of the sensors or features should be selected? How should the experimenter proceed to find the "optimal" combination? Both of these questions are intimately related and have been extensively covered in the literature under the notion of "array optimization" and "feature subset selection".

11.1. Sensor Selection

A number of theoretical studies have addressed the issue of array optimization with nonspecific sensors. One of the earliest investigations was performed by Zaromb and Stetter over 20 years ago.[359] The authors assumed an array of S sensors, each capable of operating in M distinct modes, to develop a theoretical estimate of the minimum number of parameters P ($=S$ sensors $\times$ M modes) that would be required to discriminate mixtures of up to A analytes from a pool of n different analytes. Assuming the sensors to be noiseless and binary (i.e., response/no response), this estimate was shown to be

$$2^P - 1 \geq \sum_{i=1}^{A} \frac{n!}{(n-i)!i!} \tag{17}$$

A rule of thumb is proposed in this study, according to which sensors and operating modes should be selected so that each of the P parameters does not respond to more than P/A individual compounds. While the assumption of noiseless and binary sensor responses is clearly simplistic, the rule of thumb is qualitatively similar to the simulation results of Alkasab et al.,[186] which have been discussed in section 6.3. Niebling and Müller[360] proposed an "inverse" feature space to design sensor arrays. In this inverse feature space, each of the n analytes is represented as a separate dimension, and each of the s sensors is represented as a point in this n-dimensional space. The authors show that this visual representation enables the experimenter to detect potential discrimination problems and to design new sensors to address these problems. Gardner and Bartlett[37] proposed a computational model for cross-selective sensors that also considers the effects of noise and errors. An upper limit of the number of analytes that can be discriminated by a given array was estimated by the ratio between the total volume of the sensor space and the volume made up by the sensor errors. A measure of performance was proposed, which was essentially equivalent to the classical Fisher's ratio (i.e., the ratio of between-class distance to within-class variance). More recently, Pearce and Sanchez-Montanes[175] have improved the model of Gardner and Bartlett by incorporating the concept of hypervolume of accessible sensor space (V_S), which is defined as the volume in sensor space that contains the sensor-array response to a set of analytes. As shown in Figure 41a for a three-odor, two-sensor problem, collinearity limits the number of possible sensor responses. Therefore, the maximum number of analyte mixtures that can be discriminated by the array is limited by the ratio between V_S and V_N, the hypervolume defined by the accuracy of the sensor array response, as illustrated in Figure 41b.

Assuming that errors/noise do not exhibit any correlation with the analyte stimulus, the authors show that the geometric interpretation in Figure 41 can be expressed by means of the Fisher information matrix (FIM), defined as

$$J_{ij}(\vec{c}) = \int p(\vec{x}|\vec{c}) \left(\frac{\partial}{\partial c_i} \ln p(\vec{x}|\vec{c}) \right) \left(\frac{\partial}{\partial c_j} \ln p(\vec{x}|\vec{c}) \right) d\vec{x} \tag{18}$$

where $\vec{c}$ is a vector containing the concentration of the analytes, $\vec{x}$ is the response of the sensor array to the stimulus $\vec{c}$, and $p(\vec{x}|\vec{c})$ is the conditional probability of observing the sensor response $\vec{x}$ upon a given stimulus $\vec{c}$. The FIM is important because it provides a lower bound (i.e., best-case case) on the accuracy with which the stimulus, $\vec{c}$, can be predicted from the sensor response, $\vec{x}$. This lower limit has been determined as

$$\mathrm{var}(\vec{c}'|\vec{c}) \geq \sum_{i=1}^{S} (J^{-1}(\vec{c}))_{ii} \tag{19}$$

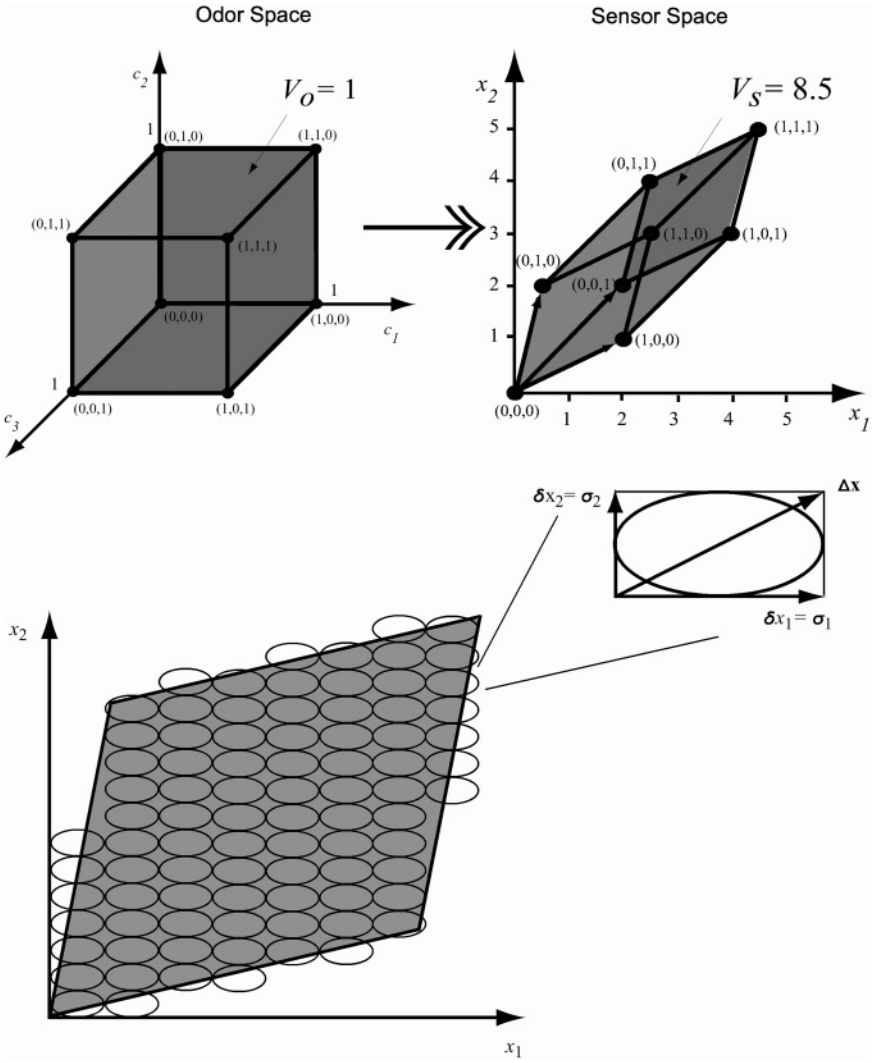

Figure 41. (a) Visualization of a three-odor-to-two-sensor transformation. (b) The maximum number of feature vectors that can be discriminated is the ratio between the hypervolume of the accessible sensor space (V_S) and the accuracy of the sensor array response. Reprinted with permission from ref 175. Copyright 2003 Wiley-VCH, Weinheim.

where $\vec{c}'$ is the prediction of $\vec{c}$ from $\vec{x}$ through a calibration model. To use these theoretical constructs in practice, one would (1) assume a parametric density $p(\vec{x}|\vec{c})$ for each individual sensor, (2) estimate the parameters from experimental data (i.e., by measuring the sensor array responses to a number of analyte mixtures), (3) compute the FIM using eq 18, and (4) compute the expected accuracy of the array from eq 19. This accuracy estimate would then be used as a "figure of merit" to select an optimal array configuration from a pool of cross-selective sensors. Once this "optimal" array has been found, further improvements can be obtained by replicating the array a number of times; see Di Natale et al.[361] and Wilson[362] for an authoritative discussion of redundancy in sensor arrays.

11.2. Feature Selection

In most cases, however, array optimization is approached empirically by defining alternative figures of merit that can be computed more conveniently. This approach is typically referred to as *feature subset selection* in the pattern-recognition and machine-learning literature. A number of empirical figures of merit can be used for this purpose, which can be grouped into two categories: filters and wrappers.[363] A filter is a measure of the information content provided by a given combination of features, where "information" can be associated with variance (e.g., assessed through the PCA eigenvalues), interclass discrimination (Fisher discrimination, e.g., measured with the LDA eigenvalues), or correlation (e.g., between the feature vectors and the dependent variables), to name but a few. The advantage of this method is that the "figure of merit" is independent of the type of calibration model used to process these features. In contrast, wrappers evaluate each combination of features by the predictive accuracy of the calibration model trained on that particular feature subset, measured by statistical resampling or cross-validation of a dataset. Each approach has a number of advantages and disadvantages.[364] The wrapper approach usually achieves better predictive accuracy since the feature subset can be tuned with respect to the particular bias of the calibration model. In addition, the wrapper has a mechanism to avoid overfitting, since the feature subsets are evaluated according to their performance on test data. Wrappers are, however, computationally intensive, since the calibration model must be continuously retrained. Filters usually find a more general feature subset that works well on a wider range of calibration models, and they are computationally attractive,

but it is difficult to design filters that correlate well with the final predictive accuracy of the calibration model. Owing to their respective pros and cons, both wrappers[72,118,264,365−367] and filters[368−372] have been used in different applications in the field of "electronic noses".

Once a measure of performance or "figure of merit" has been designed, an "optimal" subset of features must be found. One may be tempted to exhaustively evaluate all possible combinations of features and to then select the global optimum. However, due to combinatorial explosion, exhaustive search is unfeasible for all but very small problems (see, e.g., ref 118 for an exhaustive evaluation). Thus, several methods have been devised that explore the space of all possible feature combinations in a more efficient fashion.[180,373] These search strategies can be assigned to three categories:[374] (i) exponential, (ii) sequential, and (iii) random strategies. Exponential techniques perform a search whose complexity grows exponentially with the number of states. Among these, branch and bound[375] is guaranteed to find the optimal feature subset of a given size if the evaluation function is monotonic. Monotonicity assumes that the addition of a new feature *always* improves the information content of the subset. This assumption is, however, violated in practical problems, since the addition of features does increase the risk of overfitting. Sequential-search algorithms are strategies that reduce the number of states to be visited during the search by applying local search. The most popular methods include sequential forward selection (SFS) and sequential backward selection (SBS). SFS starts from the empty set and sequentially adds features, whereas SBS starts from the full set and sequentially removes features. These two algorithms, however, have a tendency to become trapped in local minima since they cannot backtrack from there (i.e., SFS cannot remove a feature once it is added, and SBS cannot add a feature once it is removed). More recently, sequential-floating methods with backtracking capabilities have become popular since they do not require monotonicity and often lead to optimal or near-optimal solutions in a fraction of the computation time required by branch and bound. Random search algorithms are an attempt to overcome the computational costs of exponential methods and to avoid the tendency of sequential methods to become trapped in local minima. Among these techniques, simulated annealing[376] and genetic algorithms[377] are most widely used. Simulated annealing (SA) is based on the annealing process of thermal systems. Starting from an initial solution, SA updates the current solution in a local fashion (e.g., adding or removing a feature). If the new solution is better, it is accepted; if it is worse, it can still be chosen with a probability, P, which depends on a global temperature parameter T. The temperature is initially set to a high value, which allows SA to perform a global search, but T is gradually decreased, which allows the algorithm to converge to a final solution. Genetic algorithms (GAs), on the other hand, are inspired by the process of natural selection. Starting from a random population of solutions, a GA will generate a new population of solutions by means of mutation operations (adding or removing features) and crossover operations (combining features from two parent solutions). Members for the new population are selected probabilistically based on their fitness; better solutions have a higher probability of making it to the new population, but "less-fit" solutions are also allowed in order to promote diversity. Because of their ability to perform global optimization and the ever-increasing computational capabilities of personal computers, the tendency in recent years has been to move toward genetic algorithm methods.[261,301,366,368,378−384]

If the number of potential features is large, the selection procedure can be computationally intensive. Therefore, it may be advantageous to initially "weed out" poor features with a filter and then use a wrapper-based selection on a reduced set of features. It must be noted, however, that the prescreening step may remove features that provide limited but complementary information. Gualdron et al.[385] proposed a two-stage selection algorithm, where individual features are first evaluated by their ratio of between-class to within-class variance. A threshold is set, and only those features whose ratio is higher than the threshold are retained for further selection. The results showed that the performance of this two-step method is comparable to that of a one-step selection procedure, in which all features undergo full subset selection, but it requires only 25% of the computation time. On the basis of this work, Llobet et al.[386] developed an improved feature selection procedure for mass-spectrometry-based "electronic nose" instruments. Their method evolves in three stages. During the first stage, every possible pair of features (each being a mass-to-charge ratio) is evaluated according to their Fisher's discriminant ratio (between-class to within-class scattering), and only the top 30% features are selected. Evaluating features in pairs prevents features with low but complementary information from being thrown away. During the second stage, the Pearson's correlation between every pair of features is computed, and a collinearity threshold is set so that only the top 20% of the features (the most uncorrelated) are preserved. During the third stage, stochastic methods (simulated annealing and genetic algorithms) are used to perform a suitable subset selection. The overall method was validated on an experimental database of various kinds of Iberian ham. The three-stage algorithm selected 14 out of 111 m/z ratios as features and yielded 95% classification performance on test data, which compared favorably to the 88% achieved by a classifier trained on the entire feature set.

In addition to these techniques, a high-level view of the information provided by the different sensors/features may be obtained from a loadings plot of, e.g., PCA, LDA, or PLS. In a loadings plot, each feature is displayed as a point, typically in a 2D or 3D representation. The farther a feature is located from the origin, the more information the feature provides for the analysis (e.g., variance in PCA, discrimination in LDA, correlation with the dependent variable in PLS). Boilot et al.[379] performed a sensor fusion from four "electronic nose" instruments, an electronic olfactometer based on a temperature-modulated metal-oxide sensor (INRA), an array of 7 thickness-shear-mode resonators (ROMA), a second array of 8 thickness-shear-mode resonators (UPM), and an array of 32 conductive-polymer sensors (WARWICK). The four instruments were used to measure the headspace of various analyte samples (apple, pear, and peach juices), and a total of 72 features was extracted from the instruments. Figure 42a shows the PCA loadings plot of these features. The analysis of this plot can provide insights on how analyte information is detected by the instruments. First, sensors of the same instrument tend to cluster together, which suggests that they provide correlated information. Second, sensors from the UPM and ROMA instruments also tend to cluster together, a reasonable result since both instruments are based on the same sensor technology. Third, the spread

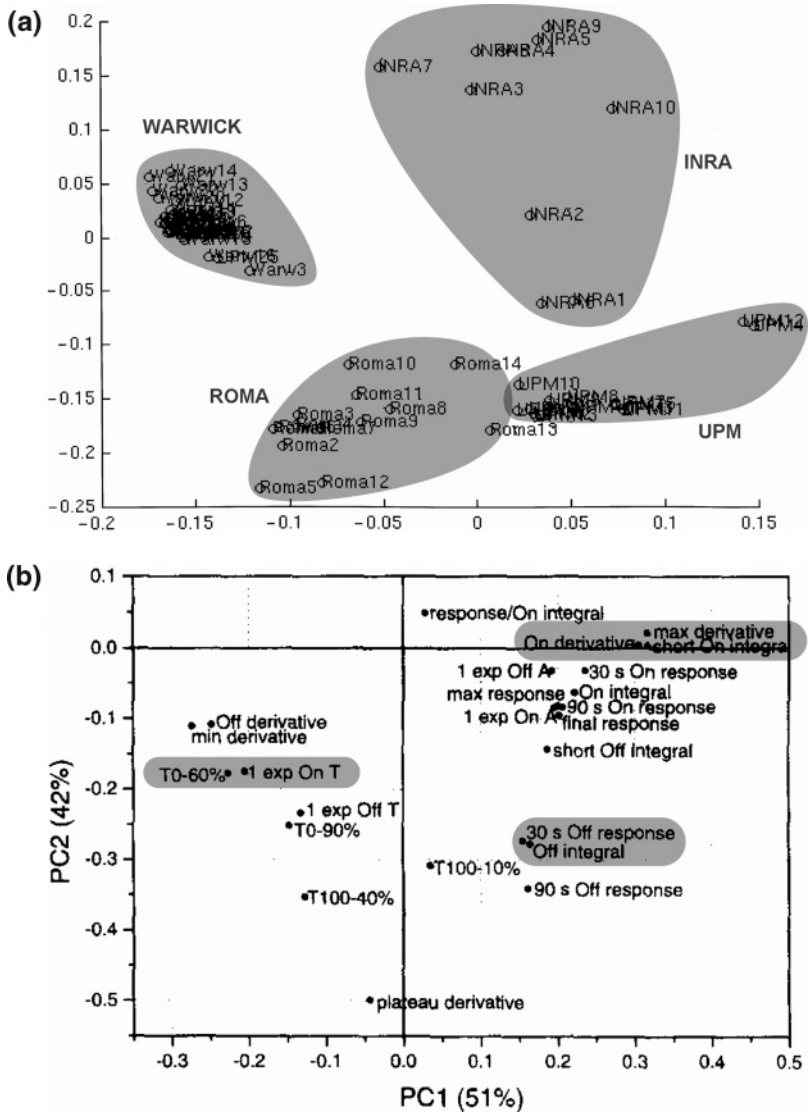

Figure 42. (a) PCA loadings plot of 72 features extracted from four different "electronic-nose" instruments. Reprinted with permission from ref 379. Copyright 2003 Elsevier. (b) PCA loadings plot of the "simple" transient parameters in the study by Eklöv et al.[72] Shadowed areas mark groups of features that provide redundant information. Reprinted with permission from ref 72. Copyright 1997 Elsevier.

of the sensors within each instrument is an indication of the degree of collinearity of the sensors; e.g., the conductive-polymer sensors seem to provide very similar information, possibly due to their large inherent cross-sensitivity to the humidity present in the samples. Figure 42b shows the loadings plot of the "simple" parameters in the study of Eklöv et al.,[72] which was reviewed in section 9.1.4. From this plot, it is possible to identify a number of highly correlated parameters, such as max/on derivative and short-on integral, 1-exp-OnTime constant and TO-60%, off integral and 30s-off response. These features describe the same properties of the response curve, and only one of them is thus needed.

11.3. Optimization of Excitation Profiles

Much less attention has been paid to the optimization of temperature-modulation profiles for metal-oxide sensors. While a number of articles report on empirical studies with various temperature waveforms (e.g., rectangular, sine, sawtooth, and triangular) and stimulus frequencies,[300,304,322] only a handful of studies have approached the problem in a systematic fashion. Kunt et al.[21] developed an optimization method for microhotplate devices that works in two stages. First, a dynamical model of the sensor is developed from experimental data; the model predicts the next conductance value of the sensor (y_{i+1}) from the previous values of the conductance $\{y_k\}_{k=i}^{i-n_y+1}$, as well as from the next and previous values of the temperature set points $\{u_k\}_{k=i+1}^{i-n_u+2}$,

$$y_{i+1} = F(y_i, y_{i-1}, ..., y_{i-n_y+1}, u_{i+1}, u_i, ..., u_{i-n_u+2}) \quad (20)$$

where n_y and n_u represent the model order. A suitable model $F(\,)$ is built from experimental data using a Wavelet network.[387] This model can be used to simulate the sensor response to different temperature programs. In the second stage, an optimization routine is used to find the "optimal" program $\{u_i\}_{i=1}^{T}$ that maximizes the distance between the (simulated) temperature-modulated sensor responses to two target gases:

$$\{u_i\}_{i=1}^{T} = \arg\max_{u_1,u_2,...,u_T} d(y^{gas_1}, y^{gas_2}) \quad (21)$$

This procedure is subject to a continuity constraint ($|u_{i+1} - u_i| \leq 40$ °C) to avoid drastic changes between consecutive

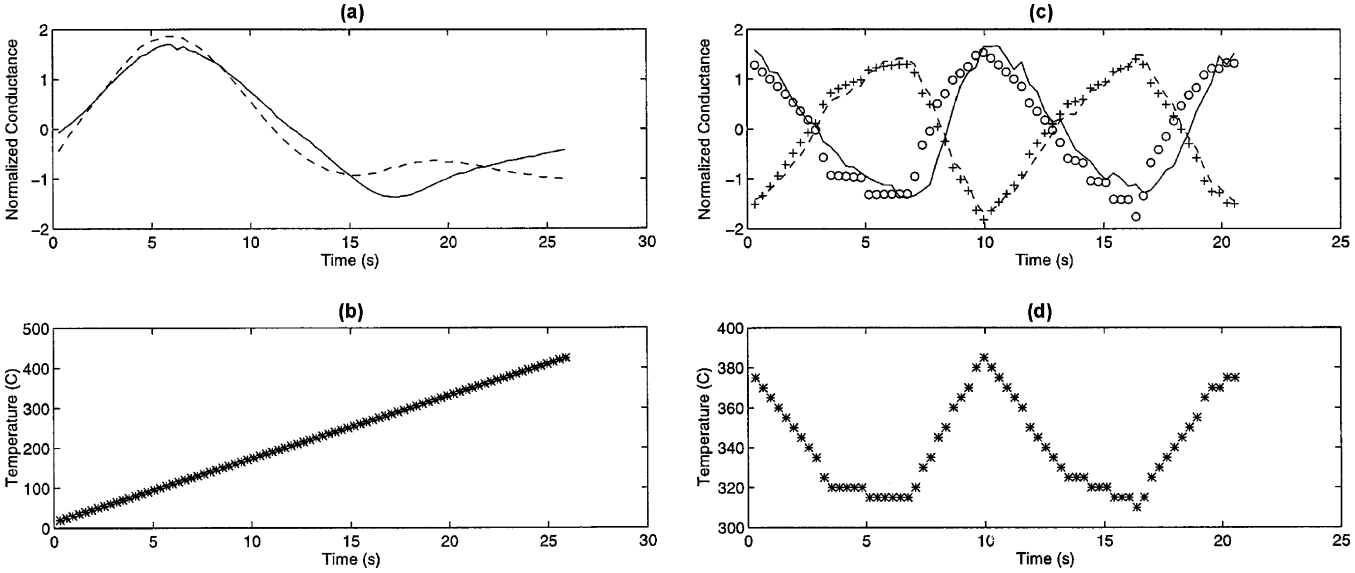

Figure 43. (a) Normalized conductance response to methanol (solid) and ethanol (dashed) upon applying a linear temperature ramp as shown in (b). (c) Normalized conductance response to methanol (solid) and ethanol (dashed) upon application of the "optimal" temperature program shown in (d); predictions from the model in eq 20 are shown as circles (methanol) and crosses (ethanol). Note the dramatic improvement in discrimination between (a) and (c). Reprinted with permission from ref 21. Copyright 1998 Elsevier.

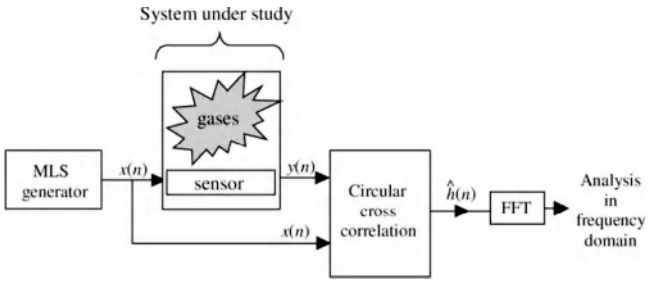

Figure 44. Optimization of the temperature-modulation frequency using pseudo-random binary sequences. Reprinted with permission from ref 333. Copyright 2005 IEEE.

temperatures. Further improvements in smoothness are achieved by means of a wavelet-based distance that uses only the lower scales of the decomposition (lower scales capture the general shape of the sensor response, whereas higher scales capture its details). When applied to the discrimination of methanol and ethanol, the optimization routine of Kunt et al. returned the temperature program shown in parts c and d of Figure 43. Whereas the sensor responses to ethanol and methanol upon applying a simple linear ramp are highly overlapping—see parts a and b of Figure 43—the response patterns upon applying the optimal temperature program are nearly orthogonal.

Vergara et al.[333] have proposed a system-identification method for determining suitable temperature-modulation programs for specific target gases. Their method is based on pseudo-random binary sequences (PRBS) and maximum length sequences (MLSs). PRBS-MLSs are square-wave signals with several interesting properties: (1) they are repeatable, which ensures that the respective results are reproducible, (2) they have a flat power spectrum over a large frequency range, which renders them very suitable for system identification, and (3) they have a maximum length, so that the impulse response of the system can be estimated from the cross-correlation. This method is illustrated in Figure 44 and works as follows. First, a PRBS-MLS is used to drive the sensor heater, while the sensors are exposed to various target compounds (NH_3, NO_2, and mixtures). For each individual target compound, the impulse response $h(t)$ is computed as the cross-correlation between the excitation signal (PRBS) and the sensor response, and the spectral components are computed from the FFT of $h(t)$. Second, each individual frequency is ranked on the basis of its information content (between-class to within-class scatter ratio), and a subset of the most informative frequencies is selected. The authors show that this procedure can be used to discriminate and quantify various gases and their mixtures using one sensor and three modulating frequencies. This method was extended in ref 388 to multilevel pseudo-random sequences (ML-PRS), which are better suited than binary sequences to estimate the linear dynamics of a system with nonlinearities. In a subsequent investigation, Vergara et al.[268] used the dynamic moments of the sensor's phase plot,[266] which we reviewed in section 9.1.2, to extract information from ML-PRS responses. Their results show that similar or better results than those in ref 388 can be obtained with the dynamic moments, while using only a small fraction of the ML-PRS response. Collectively, these studies have demonstrated that temperature profiles with very short time scales can be found that provide a maximum discrimination for a given set of analytes.

12. Conclusion and Outlook

It can be concluded from the contents of this article—and many references herein—that the use of various transducer types or inhomogeneous transducer arrays is, indeed, beneficial with regard to the performance of such sensor arrays. In many cases, the data analysis of sensor-array or "electronic nose" instruments has been limited to an empirical qualitative analysis or the drawing of PCA plots. While useful for rapid visualization purposes, PCA plots are not very representative for higher-dimensional measurement/feature spaces, simply because (i) the data are projected onto a two-dimensional plane irrespective of the original or intrinsic dimensionality and (ii) PCA only captures directions of maximum variance, which do not necessarily contain analytical information. A quantitative indicator of the array performance, such as predictive accuracy (e.g., classification rate or mean-square-

error) on unseen test data, should be used as a figure of merit. A careful selection of sensor arrays, feature subsets, and excitation profiles for a given application can further improve the sensor-array performance.

Another shortcoming of multisensor-array or "electronic nose" papers is that many of the studies have been performed on food samples or their headspaces, the analyte composition of which has been rather complex, hardly known, and highly variable. Moreover, the qualitative sensor results have not been scientifically explained or substantiated by a chemical gas-phase or headspace composition analysis. Thus, it is not always clear which compounds or chemical effects lead to a discrimination of the different samples. Moreover, sample-to-sample variability, sample deterioration, and the strong influence of the sample preparation and sampling procedure on the sensor results, in particular for natural products, are often underestimated, and the corresponding information is missing in many papers.

On the technological side, the progress in micro- and nanotechnology, microelectronics, and in data-processing speed and capability will dramatically influence the development of chemical sensors and sensor systems in the near future: rather complex and versatile microsensor and microanalysis systems operable directly through standard interfaces from a laptop or palmtop by means of standard software are emerging, as has been demonstrated in this article. The end-user is interested in reliable, user-friendly, and affordable sensor systems irrespective of the internal system complexity, which, in most cases, will not be evident to the user anyway. Therefore, we think that a concept of versatile *adaptive (micro)sensor systems* can be most successful. *Adaptive sensor systems* may be devices that include various transducer types, auxiliary sensors, eventually separation and preconcentration units, which can respond or adapt their operation to occurring analysis situations or events. In the event that, e.g., a certain target analyte or a major interferent is detected, the sensor selection, sensor operation mode, feature extraction, and data treatment would be adapted to this situation, and the protocols would be executed in a way that the best-possible target analyte detection is achieved or that the interferent can be recognized and its influence on the sensor system output can be minimized or suppressed. In dealing with interferents, cross-sensitivities, or low signal levels, it may be very effective to purposefully select or deselect sensors or to use signal ratios or differential values instead of merely increasing the array size or the transducer diversity.

13. References

(1) *Sensors, A Comprehensive Survey*; Göpel, W., Hesse, J., Zemel, J. N., Eds.; VCH Verlagsgesellschaft mbH: Weinheim, Germany 1991; Vol. 2

(2) Janata, J. *Principles of Chemical Sensors*; Plenum Press: New York, 1989.

(3) Janata, J. *Anal. Chem.* **2001**, *73*, 150A.

(4) Janata, J.; Josowicz, M.; Devaney, D. M. *Anal. Chem.* **1994**, *66*, R207.

(5) Edmonds, T. E. *Chemical sensors*; Chapman and Hall: New York, 1988.

(6) Gardner, J. W.; Bartlett, P. N. *Electronic noses: principles and applications;* Oxford University Press: Oxford, U.K., 1999.

(7) Kress-Rogers, E. *Handbook of biosensors and electronic noses: Medicine, food, and the environment*; CRC Press: Boca Raton, FL, 1997.

(8) Madou, M. J.; Morrison, S. R. *Chemical sensing with solid state devices*; Academic Press: Boston, MA, 1989.

(9) Janata, J.; Josowicz, M.; Vanysek, P.; DeVaney, D. M. *Anal. Chem.* **1998**, *70*, 179.

(10) Massart, D. L.; Vandeginste, B. G. M.; Deming, S. N.; Michotte, Y.; Kaufman, L. *Chemometrics: A Textbook*; Elsevier: Amsterdam, The Netherlands, 1988.

(11) Hierlemann, A.; Schweizer-Berberich, M.; Weimar, U.; Kraus, G.; Pfau, A.; Göpel, W. In *Sensors Update*; Baltes, H., Göpel, W., Hesse, J., Eds.; VCH: Weinheim, Germany, 1996; Vol. 2, p 119.

(12) Brereton, R. G. *Multivariate Pattern Recognition in Chemometrics*; Elsevier: Amsterdam, The Netherlands, 1992.

(13) Weimar, U.; Göpel, W. *Sens. Actuators, B* **1998**, *52*, 143.

(14) Lorber, A.; Kowalski, B. R. *J. Chemom.* **1988**, *2*, 67.

(15) Lemmo, A. V.; Jörgenson, J. W. *Anal. Chem.* **1993**, *65*, 1576.

(16) Takatera, K.; Watanabe, T. *Anal. Chem.* **1993**, *65*, 759.

(17) Lin, Z. H.; Booksh, K. S.; Burgess, L. W.; Kowalski, B. R. *Anal. Chem.* **1994**, *66*, 2552.

(18) Fort, A.; Gregorkiewitz, M.; Machetti, N.; Rocchi, S.; Serrano, B.; Tondi, L.; Ulivieri, N.; Vignoli, V.; Faglia, G.; Comini, E. *Thin Solid Films* **2002**, *418*, 2.

(19) Heilig, A.; Barsan, N.; Weimar, U.; Schweizer-Berberich, M.; Gardner, J. W.; Göpel, W. *Sens. Actuators, B* **1997**, *43*, 45.

(20) Janata, J. *Proc. IEEE* **2003**, *91*, 864.

(21) Kunt, T. A.; McAvoy, T. J.; Cavicchi, R. E.; Semancik, S. *Sens. Actuators, B* **1998**, *53*, 24.

(22) Lee, A. P.; Reedy, B. J. *Sens. Actuators, B* **1999**, *60*, 35.

(23) Booksh, K. S.; Kowalski, B. R. *Anal. Chem.* **1994**, *66*, 782A.

(24) Smilde, A. K.; Tauler, R.; Saurina, J.; Bro, R. *Anal. Chim. Acta* **1999**, *398*, 237.

(25) Göpel, W. *Sens. Actuators, B* **1998**, *52*, 125.

(26) Elwenspoek, M.; Jansen, H. V. *Silicon micromachining*; Cambridge University Press: Cambridge, U.K., 1998.

(27) Gad-el-Hak, M. *The MEMS handbook*; CRC Press: Boca Raton, FL, 2002.

(28) Kovacs, G. T. A. *Micromachined transducers sourcebook*; WCB: New York, 1998.

(29) Madou, M. *Fundamentals of microfabrication*; CRC Press: Boca Raton, FL, 1997.

(30) Sze, S. M. *Semiconductor Sensors*; Wiley & Sons: New York, 1994.

(31) Hierlemann, A.; Brand, O.; Hagleitner, C.; Baltes, H. *Proc. IEEE* **2003**, *91*, 839.

(32) Brand, O. *Proc. IEEE* **2006**, *94*, 1160.

(33) Hagleitner, C.; Hierlemann, A.; Baltes, H. In *Sensors Update, Vol. 12*; Baltes, H., Korvink, J., Fedder, G., Eds.; Wiley VCH: Weinheim, New York, 2003; pp 51−120.

(34) Hagleitner, C.; Hierlemann, A.; Brand, O.; Baltes, H. In *Sensors Update, Vol. 11*; Baltes, H., Korvink, J., Fedder, G., Eds.: Wiley VCH: Weinheim, New York, 2002; pp 101−155.

(35) Lemmerhirt, D. F.; Wise, K. D. *Proc. IEEE* **2006**, *94*, 1138.

(36) Gardner, J. W.; Bartlett, P. N. *Sens. Actuators, B* **1994**, *18*, 211.

(37) Gardner, J. W.; Bartlett, P. N. *Sens. Actuators, B* **1996**, *33*, 60.

(38) Röck, F.; Barsan, N; Weimar, U. *Chem. Rev.* in press (cr068121q).

(39) Weimar, U.; Göpel, W. *Sens. Actuators, B* **1998**, *52*, 143.

(40) Lee, A. P.; Reedy, B. J. *Sens. Actuators, B* **1999**, *60*, 35.

(41) Demarne, V.; Grisel, A. *Sens. Actuators* **1988**, *13*, 301.

(42) Benkstein, K. D.; Semancik, S. *Chem. Rev.* in press.

(43) Nakamoto, T.; Ishida, H. *Chem. Rev.* in press (cr068117e).

(44) Demarne, V.; Balkanova, S.; Grisel, A.; Rosenfeld, D.; Levy, F. *Sens. Actuators, B* **1993**, *B14*, 497.

(45) Graf, M.; Barrettino, D.; Taschini, S.; Hagleitner, C.; Hierlemann, A.; Baltes, H. *Anal. Chem.* **2004**, *76*, 4437.

(46) Graf, M.; Jurischka, R.; Barrettino, D.; Hierlemann, A. *J. Micromech. Microeng.* **2005**, *15*, 190.

(47) Heilig, A.; Barsan, N.; Weimar, U.; Schweizer-Berberich, M.; Gardner, J. W.; Göpel, W. *Sens. Actuators, B* **1997**, *43*, 45.

(48) Cavicchi, R. E.; Suehle, J. S.; Kreider, K. G.; Gaitan, M.; Chaparala, P. *IEEE Electron Device Lett.* **1995**, *16*, 286.

(49) Cavicchi, R. E.; Suehle, J. S.; Kreider, K. G.; Gaitan, M.; Chaparala, P. *Sens. Actuators, B* **1996**, *33*, 142.

(50) Kunt, T. A.; McAvoy, T. J.; Cavicchi, R. E.; Semancik, S. *Sens. Actuators, B* **1998**, *53*, 24.

(51) Semancik, S.; Cavicchi, R. *Acc. Chem. Res.* **1998**, *31*, 279.

(52) Müller, G.; Friedberger, A.; Kreisl, P.; Ahlers, S.; Schulz, O.; Becker, T. *Thin Solid Films* **2003**, *436*, 345.

(53) Graf, M.; Frey, U.; Taschini, S.; Hierlemann, A. *Anal. Chem.* **2006**, *78*, 6801.

(54) Graf, M.; Müller, S. K.; Barrettino, D.; Hierlemann, A. *IEEE Electron Device Lett.* **2005**, *26*, 295.

(55) Althainz, P.; Goschnick, J.; Ehrmann, S.; Ache, H. J. *Sens. Actuators, B* **1996**, *33*, 72.

(56) Menzel, R.; Goschnick, J. *Sens. Actuators, B* **2000**, *68*, 115.

(57) Sysoev, V. V.; Kiselev, I.; Frietsch, M.; Goschnick, J. *Sensors* **2004**, *4*, 37.

(58) Barsan, N.; Stetter, J. R.; Findlay, M.; Göpel, W. *Sens. Actuators, B* **2000**, *66*, 31.

(59) Cavicchi, R. E.; Semancik, S.; Walton, R. M.; Panchapakesan, B.; DeVoe, D. L.; Aquino, Class, M.; Allen, J. D.; Suehle, J. S. *Proc. SPIE* **1999**, *3857*, 38.
(60) Cavicchi, R. E.; Suehle, J. S.; Chaparala, P.; Kreider, K. G.; Gaitan, M.; Semancik, S. *Technical Digest Solid-State Sensor and Actuator Workshop*; Hilton Head Island, SC, 1994; p 53.
(61) Geistlinger, H. *Sens. Actuators, B* **1993**, *B17*, 47.
(62) Semancik, S.; Cavicchi, R. E.; Wheeler, M. C.; Tiffany, J. E.; Poirier, G. E.; Walton, R. M.; Suehle, J. S.; Panchapakesan, B.; DeVoe, D. L. *Sens. Actuators, B* **2001**, *B77*, 579.
(63) Wlodek, S.; Colbow, K.; Consadori, F. *Sens. Actuators, B* **1991**, *3*, 63.
(64) Wlodek, S.; Colbow, K.; Consadori, F. *Sens. Actuators, B* **1991**, *3*, 123.
(65) Clifford, P. K.; Tuma, D. T. *Sens. Actuators* **1982**, *3*, 255.
(66) Simon, T.; Barsan, N.; Bauer, M.; Weimar, U. *Sens. Actuators, B* **2001**, *73*, 1.
(67) Schweizer-Berberich, M.; Vaihinger, S.; Göpel, W. *Sens. Actuators, B* **1994**, *18*−*19*, 282.
(68) (a)Stetter, J. R.; Zaromb, S.; Findlay, M. W. *Sens. Actuators* **1984**, *6*, 269. (b) Otagawa, T.; Stetter, J. R. *Sens. Actuators* **1987**, *11*, 251.
(69) Vaihinger, S.; Göpel, W.; Stetter, J. R. *Sens. Actuators, B* **1991**, *4*, 337.
(70) Kummer, A. M.; Burg, T. P.; Hierlemann, A. *Anal. Chem.* **2006**, *78*, 279.
(71) Gouws, G. J.; Gouws, D. J. *Sens. Actuators, B* **2003**, *91*, 326.
(72) Eklöv, T.; Martensson, P.; Lundström, I. *Anal. Chim. Acta* **1997**, *353*, 291.
(73) Gardner, J. W. *Sens. Actuators, B* **1990**, *1*, 166.
(74) Fort, A.; Machetti, N.; Rocchi, S.; Santos, M. B. S.; Tondi, L.; Ulivieri, N.; Vignoli, V.; Sberveglieri, G. *IEEE Trans. Instrum. Meas.* **2003**, *52*, 921.
(75) Llobet, E.; Brezmes, J.; Vilanova, X.; Sueiras, J. E.; Correig, X. *Sens. Actuators, B* **1997**, *41*, 13.
(76) Llobet, E.; Vilanova, X.; Brezmes, J.; Sueiras, J. E.; Correig, X. *Sens. Actuators, B* **1998**, *47*, 104.
(77) Yamanaka, T.; Ishida, H.; Nakamoto, T.; Moriizumi, T. *Sens. Actuators, A* **1998**, *69*, 77.
(78) Di Nucci, C.; Fort, A.; Rocchi, S.; Tondi, L.; Vignoli, V.; Di Francesco, F.; Santos, M. B. S. *IEEE Trans. Instrum. Meas.* **2003**, *52*, 1079.
(79) Islam, A.; Ismail, Z.; Ahmad, M. N.; Saad, B.; Othman, A. R.; Shakaff, A. Y. M.; Daud, A.; Ishak, Z. *Sens. Actuators, B* **2005**, *109*, 238.
(80) Nanto, H.; Kondo, K.; Habara, M.; Douguchi, Y.; Waite, R. I.; Nakazumi, H. *Sens. Actuators, B* **1996**, *35*, 183.
(81) Hagleitner, C.; Lange, D.; Hierlemann, A.; Brand, O.; Baltes, H. *IEEE J. Solid State Circuits* **2002**, *37*, 1867.
(82) Langereis, G. R.; Olthuis, W.; Bergveld, P. *Sens. Actuators, B* **1998**, *53*, 197.
(83) Poghossian, A.; Berndsen, L.; Schultze, J. W.; Lüth, H.; Schöning, M. J. *Proceedings of the Meeting of the Electrochemical Society*, San Francisco, CA, 2001; p 143.
(84) Poghossian, A.; Lüth, H.; Schultze, J. W.; Schöning, M. J. *Electrochim. Acta* **2001**, *47*, 243.
(85) Poghossian, A.; Schöning, M. I. *Electroanalysis* **2004**, *16*, 1863.
(86) Poghossian, A.; Schultze, J. W.; Schöning, M. J. *Sens. Actuators, B* **2003**, *91*, 83.
(87) Schöning, M. J.; Poghossian, A. *Electroanalysis* **2006**, *18*, 1893.
(88) Hagleitner, C.; Hierlemann, A.; Lange, D.; Kummer, A.; Kerness, N.; Brand, O.; Baltes, H. *Nature* **2001**, *414*, 293.
(89) Liu, W. L.; Ma, W. C.; Li, L.; Li, J. M. *Sens. Actuators, B* **2000**, *66*, 222.
(90) Takada, T. *Sens. Actuators, B* **2000**, *66*, 1.
(91) Heilig, A.; Barsan, N.; Weimar, U.; Göpel, W. *Sens. Actuators, B* **1999**, *58*, 302.
(92) Mizsei, J.; Lantto, V. *Sens. Actuators, B* **1991**, *4*, 163.
(93) Schierbaum, K. D.; Weimar, U.; Göpel, W.; Kowalkowski, R. *Sens. Actuators, B* **1991**, *3*, 205.
(94) Weimar, U.; Schierbaum, K. D.; Göpel, W.; Kowalkowski, R. *Sens. Actuators, B* **1990**, *1*, 93.
(95) Cardinali, G. C.; Dori, L.; Fiorini, M.; Sayago, I.; Faglia, G.; Perego, C.; Sberveglieri, G.; Liberali, V.; Maloberti, F.; Tonietto, D. *Analog Integ. Circuits Signal Process.* **1997**, *14*, 2756.
(96) Hughes, K. L.; Miller, S. L.; Rodriguez, J. L.; McWhorter, P. J. *Sens. Actuators, B* **1996**, *37*, 75.
(97) Rodriguez, J. L.; Hughes, R. C.; Corbett, W. T.; McWhorter, P. J. *Technical Digest of IEEE International Electron Devices Meeting*, San Francisco, CA, 1992; p 521.
(98) Topart, P.; Josowicz, M. *J. Phys. Chem.* **1992**, *96*, 8662.
(99) Kunugi, Y.; Nigorikawa, K.; Harima, Y.; Yamashita, K. *J. Chem. Soc., Chem. Commun.* **1994**, 873.
(100) Polk, B. J.; Smith, J. A.; DeWeerth, S. P.; Zhou, Z. P.; Janata, J.; Domansky, K. *Electroanalysis* **1999**, *11*, 707−711.
(101) Penza, M.; Cassano, G.; Aversa, P.; Antolini, F.; Cusano, A.; Consales, M.; Giordano, M.; Nicolais, L. *Sens. Actuators, B* **2005**, *111*−*112*, 171.
(102) Penza, M.; Cassano, G.; Aversa, P.; Cusano, A.; Cutolo, A.; Giordano, M.; Nicolais, L. *Nanotechnology* **2005**, *16*, 2536.
(103) Endres, H. E.; Mickle, L. D.; Köstlinger, C.; Drost, S.; Hutter, F. *Sens. Actuators, B* **1992**, *6*, 285.
(104) Haug, M.; Schierbaum, K. D.; Gauglitz, G.; Göpel, W. *Sens. Actuators, B* **1993**, *11*, 383.
(105) Schierbaum, K. D.; Gerlach, A.; Haug, M.; Göpel, W. *Sens. Actuators, A* **1992**, *31*, 130.
(106) Zhou, R.; Hierlemann, A.; Weimar, U.; Göpel, W. *Sens. Actuators, B* **1996**, *34*, 356.
(107) Kurzawski, P.; Hagleitner, C.; Hierlemann, A. *Anal. Chem.* **2006**, *78*, 6910.
(108) Kummer, A. M.; Hierlemann, A.; Baltes, H. *Anal. Chem.* **2004**, *76*, 2470.
(109) Kummer, A. Ph.D. Thesis, ETH Zürich, Switzerland, 2004.
(110) Hagleitner, C.; Hierlemann, A.; Brand, O.; Baltes, H. In *Sensors Update, Vol 11*; Baltes, H., Fedder, G. K., Korvink, J. G., Eds.; Wiley VCH: Weinheim, Germany, 2002; pp 101−155.
(111) Hierlemann, A.; Ricco, A. J.; Bodenhöfer, K.; Dominik, A.; Göpel, W. *Anal. Chem.* **2000**, *72*, 3696.
(112) Bodenhöfer, K.; Hierlemann, A.; Seemann, J.; Gauglitz, G.; Christian, B.; Koppenhoefer, B.; Göpel, W. *Anal. Chem.* **1997**, *69*, 3058.
(113) Bodenhöfer, K.; Hierlemann, A.; Seemann, J.; Gauglitz, G.; Koppenhoefer, B.; Göpel, W. *Nature* **1997**, *387*, 577.
(114) Lerchner, J.; Kirchner, R.; Seidel, J.; Wahlisch, D.; Wolf, G.; Konig, W. A. *Thermochim. Acta* **2006**, *445*, 98.
(115) Holmberg, M.; Winquist, F.; Lundström, I.; Gardner, J. W.; Hines, E. L. *Sens. Actuators, B* **1995**, *27*, 246.
(116) Ulmer, H.; Mitrovics, J.; Noetzel, G.; Weimar, U.; Göpel, W. *Sens. Actuators, B* **1997**, *43*, 24.
(117) Ulmer, H.; Mitrovics, J.; Weimar, U.; Göpel, W. *Sens. Actuators, B* **2000**, *65*, 79.
(118) Pardo, M.; Kwong, L. G.; Sberveglieri, G.; Brubaker, K.; Schneider, J. F.; Penrose, W. R.; Stetter, J. R. *Sens. Actuators, B* **2005**, *106*, 136−143.
(119) Mitrovics, J.; Ulmer, H.; Weimar, U.; Göpel, W. *Acc. Chem. Res.* **1998**, *31*, 307.
(120) http://www.alpha-mos.com/en/index.php.
(121) http://www.appliedsensor.com/.
(122) Li, Y.; Vancura, C.; Barrettino, D.; Graf, M.; Hagleitner, C.; Kummer, A.; Zimmermann, M.; Kirstein, K. U.; Hierlemann, A. *Sens. Actuators, B* **2007**, *126*, 431−440.
(123) Vancura, C.; Ruegg, M.; Li, Y.; Hagleitner, C.; Hierlemann, A. *Anal. Chem.* **2005**, *77*, 2690.
(124) Hierlemann, A.; Baltes, H. *Analyst* **2003**, *128*, 15.
(125) Hierlemann, A.; Brand, O.; Hagleitner, C.; Baltes, H. *Proc. IEEE* **2003**, *91*, 839.
(126) Cole, M.; Ulivieri, N.; Garcia-Guzman, J.; Gardner, J. W. *Microelectron. J.* **2003**, *34*, 865.
(127) Garcia-Guzman, J.; Ulivieri, N.; Cole, M.; Gardner, J. W. *Sens. Actuators, B* **2003**, *95*, 232.
(128) Mielle, P.; Marquis, F. *Sens. Actuators, B* **1999**, *58*, 526.
(129) Mielle, P.; Souchaud, M.; Landy, P.; Guichard, E. *Sens. Actuators, B* **2006**, *116*, 161.
(130) http://www.gsg-analytical.com/english/moses2.htm.
(131) http://www.airsense.com.
(132) http://www.alpha-mos.com.
(133) http://microsensorsystems.com.
(134) http://www.raesystems.com/global.
(135) Norlin, P.; Öhman, O.; Ekström, B.; Forssen, L. *Sens. Actuators, B* **1998**, *49*, 34.
(136) Götz, A.; Gracia, I.; Cane, C.; Morrissey, A.; Alderman, J. *J. Microelectromech. Syst.* **2001**, *10*, 569.
(137) Kloock, J. P.; Moreno, L.; Bratov, A.; Huachupoma, S.; Xu, J.; Wagner, T.; Yoshinobu, T.; Ermolenko, Y.; Vlasov, Y. G.; Schöning, M. J. *Sens. Actuators, B* **2006**, *118*, 149.
(138) Lauwers, E.; Suls, J.; Gumbrecht, W.; Maes, D.; Gielen, G.; Sansen, W. *IEEE J. Solid State Circuits* **2001**, *36*, 2030.
(139) Gumbrecht, W.; Peters, D.; Schelter, W.; Erhardt, W.; Henke, J.; Steil, J.; Sykora, U. *Sens. Actuators, B* **1994**, *19*, 704.
(140) Schelter, W.; Gumbrecht, W.; Montag, B.; Sykora, U.; Erhardt, W. *Sens. Actuators, B* **1992**, *6*, 91.
(141) http://www.abbottpointofcare.com/istat/www/products/cartridges-family.htm.
(142) Baumann, W. H.; Lehmann, M.; Schwinde, A.; Ehret, R.; Brischwein, M.; Wolf, B. *Sens. Actuators, B* **1999**, *55*, 77.

(143) (a) Gross, G.; Rhoades, B. K.; Azzazy, H. M. E.; Ming, Chi, W. *Biosens. Bioelectron.* **1995**, *10*, 553. (b) Gross, G. W.; Rhoades, B.; Jordan, R. *Sens. Actuators, B* **1992**, *B6*, 1.
(144) Gross, G. W.; Harsch, A.; Rhoades, B. K.; Göpel, W. *Biosens. Bioelectron.* **1997**, *12*, 373.
(145) McConnell, H. M.; Owicki, J. C.; Parce, J. W.; Miller, D. L.; Baxter, G. T.; Wada, H. G.; Pitchford, S. *Science* **1992**, *257*, 1906.
(146) Kovacs, G. T. A. *Proc. IEEE* **2003**, *91*, 915.
(147) Pancrazio, J. J.; Bey, P. P., Jr.; Cuttino, D. S.; Kusel, J. K.; Borkholder, D. A.; Shaffer, K. M.; Kovacs, G. T. A.; Stenger, D. A. *Sens. Actuators, B* **1998**, *B53*, 179.
(148) Pancrazio, J. J.; Whelan, J. P.; Borkholder, D. A.; Ma, W.; Stenger, D. A. *Ann. Biomed. Eng.* **1999**, *27*, 687.
(149) Baumann, W.; Schreiber, E.; Krause, G.; Stüwe, S. *Proc. Eurosensors XVI, Prag* **2002**, 4.
(150) Ehret, R.; Baumann, W.; Brischwein, M.; Lehmann, M.; Henning, T.; Freund, I.; Drechsler, S.; Friedrich, U.; Hubert, M. L.; Motrescu, E.; Kob, A.; Palzer, H.; Grothe, H.; Wolf, B. *Fresenius J. Anal. Chem.* **2001**, *369*, 30.
(151) Lehmann, M.; Baumann, W.; Brischwein, M.; Ehret, R.; Kraus, M.; Schwinde, A.; Bitzenhofer, M.; Freund, I.; Wolf, B. *Biosens. Bioelectron.* **2000**, *15*, 117. (b) Ehret, R.; Baumann, W.; Brischwein, M.; Schwinde, A.; Wolf, B. *Med. Biol. Eng. Comput.* **1998**, *36*, 365.
(152) Ziegler, C. *Fresenius J. Anal. Chem.* **2000**, *366*, 552.
(153) Martin, S. J.; Ricco, A. J.; Ginley, D. S.; Zipperian, T. E. *IEEE Trans. UFFC* **1987**, *34* (2), 142.
(154) Grate, J. W.; Egorov, O. B.; O'Hara, M. J.; DeVol, T. A. *Chem. Rev.* in press (cr068115u).
(155) Potkay, J. A.; Driscoll, J. A.; Agah, M.; Sacks, R. D.; Wise, K. D. *Proc. IEEE Micro Electro Mechanical Systems MEMS, 2003, Kyoto, Japan* **2003**, 395−398.
(156) Tian, W. C.; Chan, H. K. L.; Lu, C. J.; Pang, S. W.; Zellers, E. T. *J. Microelectromech. Syst.* **2005**, *14*, 498.
(157) Tian, W. C.; Pang, S. W.; Lu, C. J.; Zellers, E. T. *J. Microelectromech. Syst.* **2003**, *12*, 264.
(158) Lewis, P. R.; Manginell, R. P.; Adkins, D. R.; Kottenstette, R. J.; Wheeler, D. R.; Sokolowski, S. S.; Trudell, D. E.; Byrnes, J. E.; Okandan, M.; Bauer, J. M.; Manley, R. G.; Frye-Mason, G. C. *IEEE Sens. J.* **2006**, *6*, 784.
(159) Lu, C. J.; Jin, C. G.; Zellers, E. T. *J. Environ. Monit.* **2006**, *8*, 270.
(160) Lu, C. J.; Steinecker, W. H.; Tian, W. C.; Oborny, M. C.; Nichols, J. M.; Agah, M.; Potkay, J. A.; Chan, H. K. L.; Driscoll, J.; Sacks, R. D.; Wise, K. D.; Pang, S. W.; Zellers, E. T. *Lab Chip* **2005**, *5*, 1123.
(161) Bender, F.; Barie, N.; Romoudis, G.; Voigt, A.; Rapp, A. *Sens. Actuators, B* **2003**, *93*, 135.
(162) Cho, S. M.; Kim, Y. J.; Heo, G. S.; Shin, S.-M. *Sens. Actuators, B* **2006**, *117*, 50.
(163) Lu, C. J.; Whiting, J.; Sacks, R. D.; Zellers, E. T. *Anal. Chem.* **2003**, *75*, 1400.
(164) Nakamoto, T.; Sukegawa, K.; Sumitomo, E. *IEEE Sens. J.* **2005**, *5*, 68.
(165) Rock, F.; Gurlo, A.; Weimar, U. *Anal. Chem.* **2005**, *77*, 2762.
(166) Wanekaya, A. K.; Uematsu, M.; Breimer, M.; Sadik, O. A. *Sens. Actuators, B* **2005**, *110*, 41.
(167) Pillonel, L.; Bosset, J. O.; Tabacchi, R. *Lebensm.-Wiss. Technol.* **2002**, *35*, 1.
(168) Hossein-Babaei, F.; Hemmati, M.; Dehmobed, M. *Sens. Actuators, B* **2005**, *107*, 461.
(169) Terry, S. C.; Jerman, J. H.; Angell, J. B. *IEEE Trans. Electron Devices* **1979**, *26*, 1880.
(170) Reston, R. R.; Kolesar, E. S. *J. Microelectromech. Syst.* **1994**, *3*, 134.
(171) Cai, Q. Y.; Zellers, E. T. *Anal. Chem.* **2002**, *74*, 3533.
(172) Wohltjen, H.; Snow, A. W. *Anal. Chem.* **1998**, *70*, 2856.
(173) Mowry, C. D.; Morgan, C. H.; Manginell, R. P.; Kottenstette, R. J.; Lewis, P. R.; Frye-Mason, G. C.; Baca, Q. In *Chemical and Biological Early Warning Monitoring for Water, Food, and Ground; Jensen, J. L., Burggraf, L. W., Eds.*; 2002; Vol. 4575, p 83.
(174) (a) Wilson, D. M.; Gaffod, S. D. *IEEE Sens. J.* **2002**, *2*, 169. (b) Zubritsky, E. *Anal. Chem.* **2000**, *72*, 421A.
(175) Pearce, T. C.; Sanchez-Montanes, M. In *Handbook of Machine Olfaction*; Pierce, T. C., Schiffman, S., Nagle, H. T., Gardner, J. W., Eds.; Wiley VCH: Weinheim, New York, 2003; pp 347−375.
(176) Li, J.; Hermann, B.; Hobbs, S.; Severin, E. In *7th International Symposium on Olfaction and Electronic Nose (ISOEN)*, Brighton, U.K., 2000; p 81.
(177) Stetter, J. R.; Penrose, W. R. *Sensors Update, Vol. 10*; Baltes, H., Korvink, J., Fedder, G., Eds.; Wiley VCH: Weinheim, New York, 2002; p 189.
(178) Jimenez, L. O.; Landgrebe, D. A. *IEEE Trans. Syst. Man Cybern. C* **1998**, *28*, 39.
(179) Kendall, M. G. *A course in the geometry of n dimensions*; Hafner Pub. Co.: New York, 1961.
(180) Fukunaga, K. *Introduction to statistical pattern recognition*, 2nd ed.; Academic Press: Boston, MA, 1990.
(181) Hwang, J.-N.; Lay, S.-R.; Lippman, A. *IEEE Trans. Signal Process.* **1994**, *42*, 2795−2810.
(182) Hughes, G. *IEEE Trans. Inf. Theory* **1968**, *14*, 55.
(183) (a) Ulmer, H.; Mitrovics, J.; Weimar, U.; Göpel, W. *Sens. Actuators, B* **2000**, *65*, 79. (b) Ricco, A. J.; Crooks, R. M.; Osbourn, G. C. *Acc. Chem. Res.* **1998**, *31*, 289.
(184) Pearce, T. C. *Neurocomputing* **2000**, *32*−*33*, 941.
(185) Brown, W. M.; Bäcker, A. *Neural Comput.* **2006**, *18*, 1511.
(186) Alkasab, T. K.; White, J.; Kauer, J. S. *Chem. Senses* **2002**, *27*, 261.
(187) Sanchez-Montanes, M. A.; Pearce, T. C. *Biosystems* **2002**, *67*, 229.
(188) Wilke, S. D.; Eurich, C. W. *Neural Comput.* **2002**, *14*, 155.
(189) Ciosek, P.; Wroblewski, W. *Talanta* **2007**, *71*, 738.
(190) Firestein, S. *Nature* **2001**, *413*, 211.
(191) Pearce, T. C.; Verschure, P. F. M. J.; White, J.; Kauer, J. S. In *Neural Computation Architectures Based on Neuroscience*; Wermter, S. A. J., Willshaw, D., Eds.; Springer-Verlag: New York, 2001; p 461.
(192) Wilson, D. M.; Garrod, S.; Hoyt, S.; McKennoch, S.; Booksh, K. S. In *Sensors Update, Vol. 10*; Wiley VCH: Weinheim, New York, 2002; p 77.
(193) Gardner, J. W.; Craven, M.; Dow, C.; Hines, E. L. *Meas. Sci. Technol.* **1998**, *9*, 120.
(194) Gutierrez-Osuna, R.; Nagle, H. T.; Kermani, B.; Schiffman, S. S. In *Handbook of Machine Olfaction: Electronic Nose Technology*; Pearce, T. C., Schiffman, S. S., Nagle, H. T., Gardner, J. W., Eds.; VCH: Weinheim, Germany, 2002; pp 105−132.
(195) Jurs, P. C.; Bakken, G. A.; McClelland, H. E. *Chem. Rev.* **2000**, *100*, 2649.
(196) Gutierrez-Osuna, R.; Nagle, H. T. *IEEE Trans. Syst. Man Cybern. B* **1999**, *29*, 626.
(197) Skov, T.; Bro, R. *Sens. Actuators, B* **2005**, *106*, 719.
(198) Padilla, M.; Montoliu, I.; Pardo, A.; Perera, A.; Marco, S. *Sens. Actuators, B* **2006**, *116*, 145.
(199) Scott, S. M.; James, D.; Ali, Z. *Microchim. Acta* **2007**, *V156*, 183.
(200) Vaihinger, S.; Göpel, W. In *Sensors: A Comprehensive Survey*; Göpel, W., Hesse, J., Zemel, J. N., Eds.; VCH Publishers: Weinheim, Germany, 1991; Vol. 2.
(201) Hierlemann, A.; Schweizer-Berberich, M.; Weimar, U.; Kraus, G.; Pfau, A.; Göpel, W. In *Sensors Update, Vol. 2*; Baltes, H., Göpel, W., Hesse, J., Eds.; VCH: Weinheim, Germany, 1996; pp 119−180.
(202) Gardner, J. W. *Sens. Actuators, B* **1991**, *4*, 109.
(203) Hierlemann, A.; Weimar, U.; Kraus, G.; Schweizer-Berberich, M.; Göpel, W. *Sens. Actuators, B* **1995**, *26*, 126.
(204) Grate, J. W.; Martin, S. J.; White, R. M. *Anal. Chem.* **1993**, *65*, 940A.
(205) Sundgren, H.; Winquist, F.; Lukkari, I.; Lundström, I. *Meas. Sci. Technol.* **1991**, *2*, 464.
(206) Gardner, J. W.; Bartlett, P. N. *Electronic noses: principles and applications*; Oxford University Press: Oxford, New York, 1999.
(207) Persaud, K. C.; Khaffaf, S. M.; Payne, J. S.; Pisanelli, A. M.; Lee, D.-H.; Byun, H.-G. *Sens. Actuators, B* **1996**, *36*, 267.
(208) Severin, E. J.; Doleman, B. J.; Lewis, N. S. *Anal. Chem.* **2000**, *72*, 658.
(209) Geladi, P.; MacDougall, D.; Martens, H. *Appl. Spectrosc.* **1985**, *39*, 491.
(210) Isaksson, T.; Naes, T. *Appl. Spectrosc.* **1988**, *42*, 1273.
(211) Naes, T.; Isaksson, T.; Kowalski, B. *Anal. Chem.* **1990**, *62*, 664.
(212) Zeaiter, M.; Roger, J. M.; Bellon-Maurel, V. *Trends Anal. Chem.* **2005**, *24*, 437.
(213) Trihaas, J.; Nielsen, P. V. *J. Food Sci.* **2005**, *70*, E44.
(214) Daszykowski, M.; Kaczmarek, K.; Vander Heyden, Y.; Walczak, B. *Chemom. Intell. Lab. Syst.* **2007**, *85*, 203.
(215) Duda, R. O.; Hart, P. E.; Stork, D. G. *Pattern classification*, 2nd ed.; Wiley: New York, 2001.
(216) Bishop, C. M. *Pattern recognition and machine learning*; Springer: New York, 2006.
(217) Gutierrez-Osuna, R. *IEEE Sens. J.* **2002**, *2*, 189.
(218) Goschnick, J.; Magapu, V.; Kiselev, I.; Koronczi, I. *Sens. Actuators, B* **2006**, *116*, 85.
(219) Barnes, R. J.; Dhanoa, M. S.; Lister, S. J. *Appl. Spectrosc.* **1989**, *43*, 772.
(220) Johansson, E.; Wold, S.; Sjoedin, K. *Anal. Chem.* **1984**, *56*, 1685.
(221) Khalheim, O. M. *Anal. Chim. Acta* **1985**, *177*, 71.
(222) Guo, Q.; Wu, W.; Massart, D. L. *Anal. Chim. Acta* **1999**, *382*, 87.
(223) Box, G. E. P.; Cox, D. R. *J. R. Stat. Soc. B* **1964**, *26*, 211.
(224) Horner, G.; Hierold, C. *Sens. Actuators, B* **1990**, *2*, 173.
(225) Holmberg, M.; Artursson, T. In *Handbook of Machine Olfaction: Electronic Nose Technology*; Pearce, T. C., Schiffman, S. S., Nagle, H. T. Gardner, J. W., Eds.; 2002; pp 325−346.

(226) Roth, M.; Hartinger, R.; Faul, R.; Endres, H. E. *Sens. Actuators, B* **1996**, *36*, 358.
(227) Aigner, R.; Auerbach, F.; Huber, P.; Müller, R.; Scheller, G. *Sens. Actuators, B* **1994**, *18*, 143.
(228) Fryder, M.; Holmberg, M.; Winquist, F.; Lündstrom, I. *Proc. Transducers' 95 and Eurosensors IX*, Stockholm, Sweden, 1995; p 683.
(229) Haugen, J.-E.; Tomic, O.; Kvaal, K. *Anal. Chim. Acta* **2000**, *407*, 23.
(230) Sisk, B. C.; Lewis, N. S. *Sens. Actuators, B* **2005**, *104*, 249.
(231) Holmberg, M.; Winquist, F.; Lundström, I.; Davide, F.; DiNatale, C.; D'Amico, A. *Sens. Actuators, B* **1996**, *36*, 528.
(232) Kohonen, T. *Biol. Cybern.* **1982**, *43*, 59.
(233) Davide, F. A. M.; Di Natale, C.; D'Amico, A. *Sens. Actuators, B* **1994**, *18*, 244.
(234) Marco, S.; Ortega, A.; Pardo, A.; Samitier, J. *IEEE Trans. Instrum. Meas.* **1998**, *47*, 316.
(235) Marco, S.; Pardo, A.; Ortega, A.; Samitier, J. *Proc. IEEE Instrumentation and Measurement Technology Conference*, Ottawa, Canada, 1995; p 904.
(236) Zuppa, M.; Distante, C.; Siciliano, P.; Persaud, K. C. *Sens. Actuators, B* **2004**, *98*, 305.
(237) Distante, C.; Siciliano, P.; Persaud, K. C. *Pattern Anal. Appl.* **2002**, *5*, 306.
(238) Holmberg, M.; Davide, F. A. M.; Di, Natale, C.; D'Amico, A.; Winquist, F.; Lundström, I. *Sens. Actuators, B* **1997**, *42*, 185.
(239) Davide, F. A. M.; Natale, C. D.; D'Amico, A.; Hierlemann, A.; Mitrovics, J.; Schweizer, M.; Weimar, U.; Göpel, W.; Marco, S.; Pardo, A. *Sens. Actuators, B* **1995**, *27*, 275.
(240) Marco, S.; Pardo, A.; Davide, F. A. M.; Natale, C. D.; D'Amico, A.; Hierlemann, A.; Mitrovics, J.; Schweizer, M.; Weimar, U.; Göpel, W. *Sens. Actuators, B* **1996**, *34*, 213.
(241) Pardo, A.; Marco, S.; Samitier, J. *IEEE Trans. Instrum. Meas.* **1998**, *47*, 644.
(242) Perera, A.; Papamichail, N.; Barsan, N.; Weimar, U.; Marco, S. *IEEE Sens. J.* **2006**, *6*, 770.
(243) Ku, W.; Storer, R. H.; Georgakis, C. *Chemom. Intell. Lab. Syst.* **1995**, *30*, 179.
(244) Russell, E. L.; Chiang, L. H.; Braatz, R. D. *Chemom. Intell. Lab. Syst.* **2000**, *51*, 81.
(245) Wold, S.; Antti, H.; Lindgren, F.; Ohman, J. *Chemom. Intell. Lab. Syst.* **1998**, *44*, 175.
(246) Artursson, T.; Eklöv, T.; Lundström, I.; Mårtensson, P.; Sjöström, M.; Holmberg, M. *J. Chemom.* **2000**, *14*, 711.
(247) Gutierrez-Osuna, R. *Proc. 7th International Symposium On Olfaction & Electronic Noses (ISOEN)*, Brighton, U.K., 2000; p 137.
(248) Esbensen, K.; Lindqvist, L.; Lundholm, I.; Nisca, D.; Wold, S. *Chemom. Intell. Lab. Syst.* **1987**, *2*, 161.
(249) Kermit, M.; Tomic, O. *IEEE Sens. J.* **2003**, *3*, 218.
(250) Hyvarinen, A. *IEEE Trans. Neural Networks* **1999**, *10*, 626.
(251) Weimar, U.; Göpel, W. *Sens. Actuators, B* **1998**, *52*, 143.
(252) Müller, R.; Lange, E. *Sens. Actuators* **1986**, *9*, 39.
(253) Vilanova, X.; Llobet, E.; Alcubilla, R.; Sueiras, J. E.; Correig, X. *Sens. Actuators, B* **1996**, *31*, 175.
(254) Llobet, E.; Brezmes, J.; Vilanova, X.; Sueiras, J. E.; Correig, X. *Sens. Actuators, B* **1997**, *41*, 13.
(255) Di Natale, C.; Marco, S.; Davide, F.; D'Amico, A. *Sens. Actuators, B* **1995**, *25*, 578.
(256) Nakamoto, T.; Iguchi, A.; Moriizumi, T. *Sens. Actuators, B* **2000**, *71*, 155.
(257) Nanto, H.; Tsubakino, S.; Ikeda, M.; Endo, F. *Sens. Actuators, B* **1995**, *25*, 794.
(258) Saunders, B. W.; Thiel, D. V.; Mackay-Sim, A. *Analyst* **1995**, *120*, 1013.
(259) Hongmei, W.; Lishi, W.; Wanli, X.; Baogui, Z.; Chengjun, L.; Jianxing, F. *Anal. Chem.* **1997**, *69*, 699.
(260) White, J.; Kauer, J. S.; Dickinson, T. A.; Walt, D. R. *Anal. Chem.* **1996**, *68*, 2191.
(261) Kermani, B. G.; Schiffman, S. S.; Nagle, H. T. *IEEE Trans. Biomed. Eng.* **1999**, *46*, 429.
(262) Brahim-Belhouari, S.; Bermak, A.; Guangfen, W.; Chan, P. C. H. *2004 IEEE Region 10 Conference (TENCON 2004)*, 2004; Vol. 1, p 693.
(263) Roussel, S.; Forsberg, G.; Steinmetz, V.; Grenier, P.; Bellon-Maurel, V. *J. Food Eng.* **1998**, *37*, 207.
(264) Paulsson, N.; Larsson, E.; Winquist, F. *Sens. Actuators, A* **2000**, *84*, 187.
(265) Martinelli, E.; Falconi, C.; D'Amico, A.; Di Natale, C. *Sens. Actuators, B* **2003**, *95*, 132.
(266) Martinelli, E.; Pennazza, G.; Natale, C. D.; D'Amico, A. *Sens. Actuators, B* **2004**, *101*, 346.
(267) Schalkoff, R. J. *Pattern recognition: Statistical, structural, and neural approaches*; J. Wiley: New York, 1992.
(268) Vergara, A.; Llobet, E.; Martinelli, E.; Di Natale, C.; D'Amico, A.; Correig, X. *Sens. Actuators, B* **2007**, *122*, 219.
(269) Pardo, M.; Sberveglieri, G. *Sens. Actuators, B* **2007**, *123*, 437.
(270) Lanczos, C. *Applied analysis*; Prentice Hall: Englewood Cliffs, NJ, 1956.
(271) Samitier, J.; Lopez-Villegas, J. M.; Marco, S.; Camara, L.; Pardo, A.; Ruiz, O.; Morante, J. R. *Sens. Actuators, B* **1994**, *18*, 308.
(272) Claverie, P.; Denis, A.; Yeramian, E. *Comput. Phys. Rep.* **1989**, *9*, 247.
(273) Sobol, W. T. *Comput. Methods Programs Biomed.* **1993**, *39*, 243.
(274) Gardner, D. G.; Gardner, J. C.; Laush, G.; Meinke, W. W. *J. Chem. Phys.* **1959**, *31*, 978.
(275) Marco, S.; Samitier, J.; Morante, J. R. *Meas. Sci. Technol.* **1995**, *6*, 135.
(276) Yeramian, E.; Claverie, P. *Nature* **1987**, *326*, 169.
(277) Llobet, E.; Vilanova, X.; Brezmes, J.; Sueiras, J. E.; Correig, X. *Sens. Actuators, B* **1998**, *47*, 104.
(278) Galdikas, A.; Mironas, A.; Senuliene, D.; Strazdiene, V.; Setkus, A.; Zelenin, D. *Sens. Actuators, B* **2000**, *69*, 258.
(279) Di Nucci, C.; Fort, A.; Rocchi, S.; Tondi, L.; Vignoli, V.; Di Francesco, F.; Santos, M. B. S. *IEEE Trans. Instrum. Meas.* **2003**, *52*, 1079.
(280) Baumbach, M.; Kammerer, T.; Sossong, A.; Schütze, A. *Proc, IEEE Sensors* **2004**, *3*, 1388.
(281) Nakamura, M.; Sugimoto, I.; Kuwano, H.; Lemos, R. *Sens. Actuators, B* **1994**, *20*, 231.
(282) Artursson, T.; Spangeus, P.; Holmberg, M. *Anal. Chim. Acta* **2002**, *452*, 255.
(283) Gutierrez-Osuna, R.; Nagle, H. T.; Schiffman, S. S. *Sens. Actuators, B* **1999**, *61*, 170.
(284) Siemiarczuk, A.; Wagner, B. D.; Ware, W. R. *J. Phys. Chem.* **1990**, *94*, 1661.
(285) Ware, W. R.; Doemeny, L. J.; Nemzek, T. L. *J. Phys. Chem.* **1973**, *77*, 2038.
(286) Gutierrez-Osuna, R.; Gutierrez-Galvez, A.; Powar, N. *Sens. Actuators, B* **2003**, *93*, 57.
(287) Carmel, L.; Levy, S.; Lancet, D.; Harel, D. *Sens. Actuators, B* **2003**, *93*, 67.
(288) Hillier, F. S.; Lieberman, G. J. *Introduction to operations research*, 8th ed.; McGraw-Hill: Boston, MA, 2005.
(289) Carmel, L. *Sens. Actuators, B* **2005**, *106*, 95.
(290) Haddad, R.; Carmel, L.; Harel, D. *Sens. Actuators, B* **2007**, *120*, 467.
(291) Eklöv, T.; Martensson, P.; Lundström, I. *Anal. Chim. Acta* **1999**, *381*, 221.
(292) Delpha, C.; Siadat, M.; Lumbreras, M. *Sens. Actuators, B* **2001**, *77*, 517.
(293) Distante, C.; Leo, M.; Siciliano, P.; Persaud, K. C. *Sens. Actuators, B* **2002**, *87*, 274.
(294) Cortes, C.; Haffner, P.; Mohri, M. *J. Mach. Learn. Res.* **2004**, *5*, 1035.
(295) Shafiqul Islam, A. K. M.; Ismail, Z.; Ahmad, M. N.; Saad, B.; Othman, A. R.; Shakaff, A. Y. M.; Daud, A.; Ishak, Z. *Sens. Actuators, B* **2005**, *109*, 238.
(296) Madou, M. J.; Morrison, S. R. *Chemical sensing with solid state devices*; Academic Press: Boston, MA, 1989.
(297) Le Vine, H. D. U.S. Patent 3,906,473, 1975.
(298) Sears, W. M.; Colbow, K.; Consadori, F. *Sens. Actuators* **1989**, *19*, 333.
(299) Sears, W. M.; Colbow, K.; Consadori, F. *Semicond. Sci. Technol.* **1989**, *4*, 351.
(300) Gutierrez-Osuna, R.; Korah, S.; Perera, A. In *Proceedings of the 8th International Symposium on Olfaction and Electronic Noses*, Washington, DC, 2001; p 212.
(301) Corcoran, P.; Lowery, P.; Anglesea, J. *Sens. Actuators, B* **1998**, *48*, 448.
(302) Gramm, A.; Schütze, A. *Sens. Actuators, B* **2003**, *95*, 58.
(303) Schütze, A.; Gramm, A.; Ruhl, T. *IEEE Sens. J.* **2004**, *4*, 857.
(304) Ortega, A.; Marco, S.; Perera, A.; Sundic, T.; Pardo, A.; Samitier, J. *Sens. Actuators, B* **2001**, *78*, 32.
(305) Cai, K.; Maekawa, T.; Takada, T. *IEEE Sens. J.* **2002**, *2*, 230.
(306) Kato, Y.; Mukai, T. *Sens. Actuators, B* **2007**, *120*, 514.
(307) Yea, B.; Osaki, T.; Sugahara, K.; Konishi, R. *Sens. Actuators, B* **1997**, *41*, 121.
(308) Kato, K.; Kato, Y.; Takamatsu, K.; Udaka, T.; Nakahara, T.; Matsuura, Y.; Yoshikawa, K. *Sens. Actuators, B* **2000**, *71*, 192.
(309) Nason, G. P. *IEE Colloquium on Applied Statistical Pattern Recognition*, Brimingham, U.K., 1999; p 1.
(310) Strang, G.; Nguyen, T. *Wavelets and filter banks*; Wellesley-Cambridge Press: Wellesley, MA, 1996.
(311) Nakata, S.; Yoshikawa, K.; Kawakami, H. *Physica D* **1992**, *59*, 169.
(312) Nakata, S.; Nakamura, H.; Yoshikawa, K. *Sens. Actuators, B* **1992**, *8*, 187.

(313) Yoshikawa, K.; Yoshinaga, T.; Kawakami, H.; Nakata, S. *Physica A* **1992**, *188*, 243.
(314) Nakata, S.; Yoshikawa, K.; Shoji, M.; Kawakami, H.; Ishii, T. *Biophys. Chem.* **1989**, *34*, 201.
(315) Nakata, S.; Akakabe, S.; Nakasuji, M.; Yoshikawa, K. *Anal. Chem.* **1996**, *68*, 2067.
(316) Nakata, S.; Ozaki, E.; Ojima, N. *Anal. Chim. Acta* **1998**, *361*, 93−100.
(317) Nakata, S.; Nakasuji, M.; Ojima, N.; Kitora, M. *Appl. Surf. Sci.* **1998**, *135*, 285.
(318) Nakata, S.; Ojima, N. *Sens. Actuators, B* **1999**, *56*, 79.
(319) Nakata, S.; Okunishi, H.; Nakashima, Y. *Sens. Actuators, B* **2006**, *119* (2), 556.
(320) Nakata, S.; Okunishi, H.; Inooka, S. *Anal. Chim. Acta* **2004**, *517*, 153.
(321) Fort, A.; Machetti, N.; Rocchi, S.; Serrano Santos, M. B.; Tondi, L.; Ulivieri, N.; Vignoli, V.; Sberveglieri, G. *IEEE Trans. Instrum. Meas.* **2003**, *52*, 921.
(322) Huang, X.; Meng, F.; Pi, Z.; Xu, W.; Liu, J. *Sens. Actuators, B.* **2004**, *99*, 444.
(323) Meier, D. C.; Evju, J. K.; Boger, Z.; Raman, B.; Benkstein, K. D.; Martinez, C. J.; Montgomery, C. B.; Semancik, S. *Sens. Actuators, B* **2007**, *121* (1), 282.
(324) Dable, B. K.; Booksh, K. S.; Cavicchi, R.; Semancik, S. *Sens. Actuators, B* **2004**, *101*, 284.
(325) Semancik, S.; Cavicchi, R. E.; Gaitan, M.; Suehle, J. U.S. Patent 5,345,213, 1994.
(326) Cavicchi, R. E.; Suehle, J. S.; Chaparala, P.; Poirier, G. E.; Kreider, K. G.; Gaitan, M.; Semancik, S. *Proc. 5th International Meeting on Chemical Sensors*, Rome, Italy, 1994; p 1136
(327) Cavicchi, R. E.; Suehle, J. S.; Kreider, K. G.; Gaitan, M.; Chaparala, P. *IEEE Electron Device Lett.* **1995**, *16*, 286.
(328) Semancik, S.; Cavicchi, R. E.; Gaitan, M.; Suehle, J. S. U.S. Patent 5345213, 1995.
(329) Ionescu, R.; Llobet, E.; Al-Khalifa, S.; Gardner, J. W.; Vilanova, X.; Brezmes, J.; Correig, X. *Sens. Actuators, B* **2003**, *95*, 203.
(330) Ionescu, R.; Llobet, E. *Sens. Actuators, B* **2002**, *81*, 289.
(331) Llobet, E.; Vilanova, X.; Brezmes, J.; Lopez, D.; Correig, X. *Sens. Actuators, B* **2001**, *77*, 275.
(332) Vergara, A.; Llobet, E.; Brezmes, J.; Ivanov, P.; Cane, C.; Gracia, I.; Vilanova, X.; Correig, X. I. *Sens. Actuators, B* **2007**, *123* (2), 1002.
(333) Vergara, A.; Llobet, E.; Brezmes, J.; Vilanova, X.; Ivanov, P.; Gracia, I.; Cane, C.; Correig, X. *IEEE Sens. J.* **2005**, *5*, 1369.
(334) Llobet, E.; Brezmes, J.; Ionescu, R.; Vilanova, X.; Al-Khalifa, S.; Gardner, J. W.; Barsan, N.; Correig, X. *Sens. Actuators, B* **2002**, *83*, 238.
(335) Llobet, E.; Ionescu, R.; Al-Khalifa, S.; Brezmes, J.; Vilanova, X.; Correig, X.; Barsan, N.; Gardner, J. W. *IEEE Sens. J.* **2001**, *1*, 207.
(336) Ding, H.; Ge, H.; Liu, J. *Sens. Actuators, B* **2005**, *107*, 749−755.
(337) Bermak, A.; Belhouari, S.; Shi, M.; Martinez, D. In *The Encyclopedia of Sensors*; Grimes, C. A., Dickey, E. C., Pishko, M. V., Eds.; American Scientific Publishers: Valencia, CA, 2006; p 1.
(338) Hines, E. L.; Boilot, P.; Gardner, J. W.; Gongora, M. A. In *Handbook of Machine Olfaction: Electronic Nose Technology*; Pearce, T. C., Schiffman, S. S., Nagle, H. T., Gardner, J. W., Eds.; 2002; pp 133−160.
(339) Bro, R. *Chemom. Intell. Lab. Syst.* **1997**, *38*, 149.
(340) Bro, R. *Anal. Chim. Acta* **2003**, *500*, 185.
(341) Harshman, R. A. *UCLA Working Papers in Phonetics* **1970**, *16*.
(342) Carroll, J. D.; Chang, J. *Psychometrika* **1970**, *35*, 283.
(343) Kroonenburg, P. M. *Three-Mode Principal Component Analysis: Theory and Applications*; DSWO Press: Leiden, The Netherlands, 1983.
(344) Gurden, S. P.; Westerhuis, J. A.; Bro, R.; Smilde, A. K. *Chemom. Intell. Lab. Syst.* **2001**, *59*, 121.
(345) Tucker, L. *Psychometrika* **1966**, *31*, 279.
(346) Kiers, H. A. L. K. *Psychometrika* **1991**, *56*, 449.
(347) de Juan, A.; Tauler, R. *J. Chemom.* **2001**, *15*, 749.
(348) Harshman, R. A. *UCLA Working Papers in Phonetics* **1972**, *22*, 30.
(349) Shaffer, R. E.; Rose Pehrsson, S. L.; McGill, A. *NRL Formal Report 6110-98-9879*; 1998.
(350) Shaffer, R. E.; Rose-Pehrsson, S. L.; McGill, A. *Anal. Chim. Acta* **1999**, *384*, 305.
(351) Shaffer, R. E.; Rose-Pehrsson, S. L.; Mcgill, R. A. *Field Anal. Chem. Technol.* **1998**, *2*, 179.
(352) Bro, R.; Kiers, H. A. L. *J. Chemom.* **2003**, *17*, 274.
(353) Elman, J. L. *Cognit. Sci.* **1990**, *14*, 179.
(354) Roppel, T.; Dunman, K.; Padgett, M.; Wilson, D.; Lindblad, T. *23rd International Conference on Industrial Electronics, Control and Instrumentation IECON 97*, 1997; Vol. 1, p 218.
(355) Tan, G.; Wilson, D. *Proc. IEEE Sensors* **2003**, *1*, 139.
(356) Rabiner, L. R. *Proc. IEEE* **1989**, *77*, 257.
(357) Zhang, H.; Balaban, M. O.; Principe, J. C. *Sens. Actuators, B* **2003**, *96*, 385.
(358) de Vries, B.; Principe, J. C. *Neural Networks* **1992**, *5*, 565.
(359) Zaromb, S.; Stetter, J. R. *Sens. Actuators* **1984**, *6*, 225.
(360) Niebling, G.; Müller, R. *Sens. Actuators, B* **1995**, *25*, 781.
(361) Di Natale, C.; D'Amico, A.; Davide, F. A. M. *Sens. Actuators, A* **1993**, *37*−*38*, 612.
(362) Wilson, D. M.; Gaffod, S. D. *IEEE Sens. J.* **2002**, *2*, 169.
(363) John, G.; Kohavi, R.; Pfleger, K. *Proceedings of the Eleventh International Conference on Machine Learning (ICML-94)*, 1994; p 121.
(364) Hall, M. A.; Smith, L. A. *Proceedings of the 1997 International Conference on Neural Information Processing and Intelligent Information Systems*, 1997; p 855.
(365) Pardo, A.; Marco, S.; Ortega, A.; Perera, A.; Sundic, T.; Samitier, J. *Proceedings of International Symposium on Olfaction and Electronic Noses (ISOEN*), Brighton, U.K., 2000; p 83.
(366) Gardner, J. W.; Boilot, P.; Hines, E. L. *Sens. Actuators, B* **2005**, *106*, 114.
(367) Pardo, M.; Sberveglieri, G. *Sens. Actuators, B* **2007**, *123* (1), 437.
(368) Corcoran, P.; Anglesea, J.; Elshaw, M. *Sens. Actuators, A* **1999**, *76*, 57.
(369) Kermani, B. G.; Schiffman, S. S.; Nagle, H. T. *IEEE Trans. Instrum. Meas.* **1998**, *47*, 728.
(370) Stella, R.; Barisci, J. N.; Serra, G.; Wallace, G. G.; De Rossi, D. *Sens. Actuators, B* **2000**, *63*, 1.
(371) Xiao-bo, Z.; Jiewen, Z.; Shou-yi, W. *Sens. Actuators, B* **2002**, *87*, 437.
(372) (a) Chaudry, A. N.; Hawkins, T. M.; Travers, P. J. *Sens. Actuators, B* **2000**, *69*, 236. (b) Osbourn, G. C.; Bartholomew, J. W.; Ricco, A. J.; Frye, G. C. *Acc. Chem. Res.* **1998**, *31*, 297.
(373) Devijver, P. A.; Kittler, J. *Pattern recognition: A statistical approach*; Prentice/Hall International: Englewood Cliffs, NJ, 1982.
(374) Doak, J. *An evaluation of feature selection methods and their application to Computer Security*; Tech Report CSE-92-18; University of California at Davis: Davis, CA, 1992.
(375) Narendra, P. M.; Fukunaga, K. *IEEE Trans. Comput.* **1977**, *26*, 917.
(376) Kirkpatrick, S.; Gelatt, C. D.; Vecchi, M. P. *Science* **1983**, *220*, 671.
(377) Michalewicz, Z. *Genetic algorithms + data structures = evolution programs*, 3rd rev. and extended ed.; Springer-Verlag: Berlin, New York, 1996.
(378) Llobet, E.; Brezmes, J.; Gualdron, O.; Vilanova, X.; Correig, X. *Sens. Actuators, B* **2004**, *99*, 267.
(379) Boilot, P.; Hines, E. L.; Gongora, M. A.; Folland, R. S. *Sens. Actuators, B* **2003**, *88*, 80.
(380) Marth, M.; Maier, D.; Stahl, U.; Rapp, M.; Wessa, T.; Honerkamp, J. *Sens. Actuators, B* **1999**, *61*, 191.
(381) Buratti, S.; Ballabio, D.; Benedetti, S.; Cosio, M. S. *Food Chem.* **2007**, *100*, 211.
(382) Roussel, S.; Bellon-Maurel, V.; Roger, J.-M.; Grenier, P. *J. Food Eng.* **2003**, *60*, 407.
(383) Pavlou, A. K.; Magan, N.; Sharp, D.; Brown, J.; Barr, H.; Turner, A. P. F. *Biosens. Bioelectron.* **2000**, *15*, 333.
(384) Srivastava, A. K.; Shukla, K. K.; Srivastava, S. K. *Microelectron. J.* **1998**, *29*, 921.
(385) Gualdron, O.; Llobet, E.; Brezmes, J.; Vilanova, X.; Correig, X. *Sens. Actuators, B* **2006**, *114*, 522.
(386) Llobet, E.; Gualdron, O.; Vinaixa, M.; El-Barbri, N.; Brezmes, J.; Vilanova, X.; Bouchikhi, B.; Gomez, R.; Carrasco, J. A.; Correig, X. *Chemom. Intell. Lab. Syst.* **2007**, *85*, 253.
(387) Zhang, Q.; Benveniste, A. *IEEE Trans. Neural Networks* **1992**, *3*, 889.
(388) Vergara, A.; Llobet, E.; Brezmes, J.; Ivanov, P.; Vilanova, X.; Gracia, I.; Cane, C.; Correig, X. *Sens. Actuators, B* **2005**, *111*−*112*, 271.

CR068116M